DOE/ET/34203-38
NEDC-23856-3
MARCH 1979

OXYGEN SUPPRESSION IN BOILING-WATER REACTORS

QUARTERLY REPORT 4
JULY 1 TO SEPTEMBER 30, 1978

E. L. BURLEY

CONTRACT DE-AC02-76ET34203
COMMONWEALTH RESEARCH CORPORATION
U.S. DEPARTMENT OF ENERGY

GENERAL ELECTRIC

DISCLAIMER

DOE/ET/34203-38
NEDC-23856-3
March 1979

OXYGEN SUPPRESSION IN BOILING-WATER REACTORS

QUARTERLY REPORT 4

July 1 to September 30, 1978

Under Contract DE-AC02-76ET34203

Prepared by E. L. Burley

for the Commonwealth Research Corp.

and the U.S. Department of Energy

Reviewed: M. Siegler
M. Siegler, Manager
Chemical Testing

Reviewed: W. R. DeHollander
W. R. DeHollander, Manager
Chemical and Radiological
Engineering

Approved: D. R. Wilkins
D. R. Wilkins, Manager
Plant Design and Analysis

Program Manager for Commonwealth Research Corp.: J. C. Blomgren
Program Manager for the U.S. Department of Energy: P. M. Lang

NUCLEAR ENGINEERING DIVISION • GENERAL ELECTRIC COMPANY
SAN JOSE, CALIFORNIA 95125

GENERAL ELECTRIC

LEGAL NOTICE

This report was prepared by the General Electric Company (GE) as an account of work sponsored by the Department of Energy (DOE). Neither DOE, members of DOE, nor GE, nor any person acting on behalf of either, including Commonwealth Research Corporation:

a. *Makes any warranty or representation, express or implied, with respect to the accuracy, completeness, or usefulness of the information contained in this report, or that the use of any information, apparatus, method, or process disclosed in this report may not infringe privately owned rights; or*

b. *Assumes any liabilities with respect to the use of, or for damages resulting from the use of, any information, apparatus, method, or process disclosed in this report.*

CONTENTS

CONTENTS (Continued)

ILLUSTRATIONS

ILLUSTRATIONS (Continued)

TABLES

TABLES (Continued)

ACKNOWLEDGEMENTS

The information and insights contributed to this program by the management and scientists of the Chalk River Laboratories of Atomic Energy of Canada Limited are gratefully acknowledged. Their willingness to share their thoughts and experience in so many areas pertinent to this Alternate Water Chemistry study has been of great assistance and is deeply appreciated by the program investigators and sponsors.

1. INTRODUCTION

Boiling water reactors (BWR's) generally use high purity, no-additive feedwater. The primary recirculating coolant is neutral pH, and contains 100 to 300 ppb oxygen with stoichiometrically related dissolved hydrogen. However, this oxygen concentration increases the susceptibility of austenitic stainless steel to intergranular stress-corrosion cracking (IGSCC) when the other requisite factors, stress and sensitization, are present. Thus, reduction or elimination of the oxygen in BWR water may preclude cracking incidents. One approach to such a reduction of the BWR coolant oxygen concentration is to adopt alternate water chemistry (AWC) conditions using an additive(s) to suppress or reverse radiolytic oxygen formation. Several additives are available to do this but they have seen only limited and specialized application in BWR's. The objective of this program is to perform an in-depth engineering evaluation of the potential suppression additives supported by critical experiments where required to resolve substantive uncertainties. On the basis of the engineering evaluation, the optimum oxygen suppression approach will be selected and a specific BWR plant recommended for an extended plant demonstration experiment.

The program is funded by the U. S. Department of Energy and managed by Commonwealth Research Corporation. The preliminary engineering evaluations and related test work are being done by the General Electric Co.

2. SUMMARY

2.1 MASS BALANCE FLOW SHEETS

New data on additive concentrations have been received from independent investigators overseas. These data were analyzed with respect to possible impact on the material balance flow sheets prepared earlier in this program.[1] No revisions to the methods or results are considered to be justified.

2.2 TURBINE BUILDING RADIATION LEVELS

Various points in the Dresden 2 and a typical BWR/6 turbine building have been modeled to facilitate calculation of dose rates at various AWC conditions. These calculations agree reasonably well with actual measurements when compared at identical power levels or exceed them by as much as a factor of two depending on the difficulty of modeling any particular location.

2.3 STEAM ACTIVITY

It is expected that by using a hydrogen-addition flow sheet, N-16 activity in the steam will increase eightfold. The C-15 activity in the steam will not be changed significantly.

2.4 OFF-GAS IMPURITIES

Off-gas sampling and analysis were completed at Nine Mile Point 1. Trace impurity levels were:

Component	Concentration (ppm by volume)
Kr	1.1
Xe	<0.2
CO	1.1
CO_2	700

Component	Concentration (ppm by volume)
CH_4	2.8
Higher Hydrocarbons	<0.1
NO	6
NO_2	<0.2
O_3	<0.03

2.5 OFF-GAS SYSTEM MODIFICATIONS

An off-gas system is proposed in which oxygen is added just upstream of the recombiner in an amount sufficient to oxidize all of the hydrogen present. The system downstream of the recombiner then operates at essentially normal flow rates and compositions. System modifications would cost an estimated $440,000. Oxygen cost would be about $3,000/month.

2.6 CONDENSER COOLANT LEAKAGE MONITORING

In-line specific-ion sodium and chloride monitors have been tested in the laboratory in the 0 to 5 ppb range. With only minor modifications the sodium monitor is accurate and stable enough that it is suitable for routine in-plant use. The chloride monitor is very flow sensitive and requires major improvements before it would be ready for routine, in-plant use.

2.7 CONSTANT EXTENSION RATE TESTS

The resistance of Type-304 stainless steel constant extension rate test (CERT) specimens to IGSCC at 288°C in BWR coolant was increased by reduction of dissolved oxygen concentration. Addition of 220 ppm ammonia had no effect on failure mechanism, crack propagation rate or ductility characteristics.

2.8 STRAINING ELECTRODE TESTS

Straining Electrode Tests (SET), using hydrogen additions to depress the specimen potential, showed that 100 ppb added hydrogen altered the failure

of as-welded-plus-low-temperature-sensitized Type-304 stainless steel specimens from IGSCC to ductile failure.

2.9 DEMINERALIZER PERFORMANCE

Because of the overwhelming adverse impact that the use of ammonia additives is predicted to have on demineralizer system performance and radwaste volume, confirming tests will be made. A test system is being assembled to actually measure both deep bed and filter-demineralizer performance at the high ammonia concentration and pH which are necessary for successful use of an ammonia flow sheet.

2.10 RADWASTE SYSTEM IMPACT

The minimum effect of the use of ammonia additives on the radwaste system is to increase radwaste volumes and required system capacity a factor of six. With cooling water leakage into the condenser, this may become as high as a 200-fold increase.

2.11 ADDITIVE INJECTION SYSTEM

Four different methods for injecting and dissolving hydrogen gas into reactor feedwater were studied: (a) counter-current, continuous gas-phase absorption in a packed column; (b) cocurrent, discontinuous gas-phase absorption in a packed column; (c) cocurrent absorption in a bubble column; and, (d) cocurrent absorption in a bubble column containing static mixing elements. The bubble column with the static mixers was the preferred method and will operate with a hydrogen solution efficiency of 99.95% of initial feed (30 lb/hr) when 14 feet of mixing units are used at final feedwater conditions. A preliminary estimate of the installed cost is $450,000.

2.12 EMERGENCY CORE COOLING SYSTEM AND LOSS-OF-COOLANT ACCIDENT ANALYSES

Since there is no change in suppression-pool hydrogen or oxygen level, use of the hydrogen additive does not modify existing emergency core cooling

system (ECCS) conditions. Increased drywell inventories of hydrogen cause less than 0.1% increase in post-loss-of-coolant accident (LOCA) drywell hydrogen concentrations. Hydrogen concentration does not reach the 4.0% lower explosive limit for hydrogen in air.

2.13 RADIOACTIVITY TRANSPORT

Data from a boiling, in-reactor loop with hydrogen addition operated by Atomic Energy of Canada Limited (AECL) show that the effects of the hydrogen-rich environment on a normal BWR system will be minimal with respect to corrosion product transport and radiation buildup.

2.14 ADDITIVE CONSUMPTION AND SOURCE

The use of hydrogen separating membranes and sponges is being considered as a means of recycling hydrogen thereby reducing additive cost. Technology exists for several separation schemes.

3. DISCUSSION

3.1 TASK A. O_2 CONTROL — MASS BALANCE FLOW SHEETS (T. L. Wong)

Objective. This task establishes the basic primary system flow sheets for the additives being considered. Optimum additive levels will be selected to allow a reasonable operating control range, prevent excessive and wasteful use of the chemical, and yet assure that minimum concentration requirements are always met.

Existing test information on the addition of hydrogen, ammonia and hydrazine to suppress oxygen formation has been used to predict mass balances for the GE BWR. Since the results reported in the literature cannot be applied directly because the test equipment and conditions were significantly different from those for the BWR, the results from several different tests have been used to develop methods to extrapolate the test data to BWR conditions.

3.1.1 Additional Flow Sheet Considerations

Mass balance flow sheets for the addition of hydrogen, ammonia, and hydrazine have been calculated and are presented in previous quarterly reports for this program.[1,2] These flow sheets are still tentative and are constantly being reviewed and improved as applicable new data are discovered.

3.1.2 Hydrogen Addition

An unpublished Japanese paper[3] describing a study on the use of hydrogen and hydrazine addition to control dissolved oxygen in the reactor water was reviewed. In the study, a hydrogen concentration of 3 ppm at the reactor core inlet was considered necessary to reduce the oxygen concentration to one-tenth its current value (to 20 ppb). This is a factor of twenty higher than calculated in Reference 1 and is based solely on experimental results from the EBWR (Experimental Boiling Water Reactor). The hydrogen models already prepared for this program which are based on several different reactor tests (including the EBWR data) were not modified.

Further support is lent to the hydrogen flow sheet presented in Reference 1 by independent Swedish studies[4] in which predicted oxygen levels and corresponding hydrogen concentrations are essentially identical.

3.1.3 Hydrazine Addition

In terms of hydrazine addition, the Japanese study states that a hydrazine addition rate of 7 kg/h (1.54 lb/h) at the inlet of the recirculation line is required to reduce the oxygen concentration by a factor of approximately two. This hydrazine addition value is very low compared to Reference 1 but is based only on replacing losses due to thermal decomposition. Radiolytic decomposition is not considered. In addition, the quantity and location of the hydrazine injection are directed toward decreasing the oxygen concentration in the recirculation piping, not the entire primary system.

The thermal decomposition data referenced in the Japanese study (Figure 3-1) show that the hydrazine thermal decomposition rates are about two orders of magnitude lower than those discussed and used in Reference 1. Based on these decomposition rates, the hydrazine addition requirements for the hydrazine-controlling and the ammonia-controlling cases were recalculated using previously determined values for the radiolytic decomposition effects. A hydrazine addition rate of approximately 6000 kg/h (13,000 lb/h) was required to obtain a 25 ppb hydrazine concentration in the core exit flow. The mass balance flow sheet for the hydrazine-controlling case at the lower thermal decomposition rate is shown in Figure 3-2. Although this value is only about 5% of that previously calculated to be necessary[1] the amount of hydrazine required is still excessive. In the case where only enough hydrazine is required to decompose to give 10 ppm ammonia in the core exit water, the flow sheets are identical, regardless of which thermal decomposition rate is accepted.

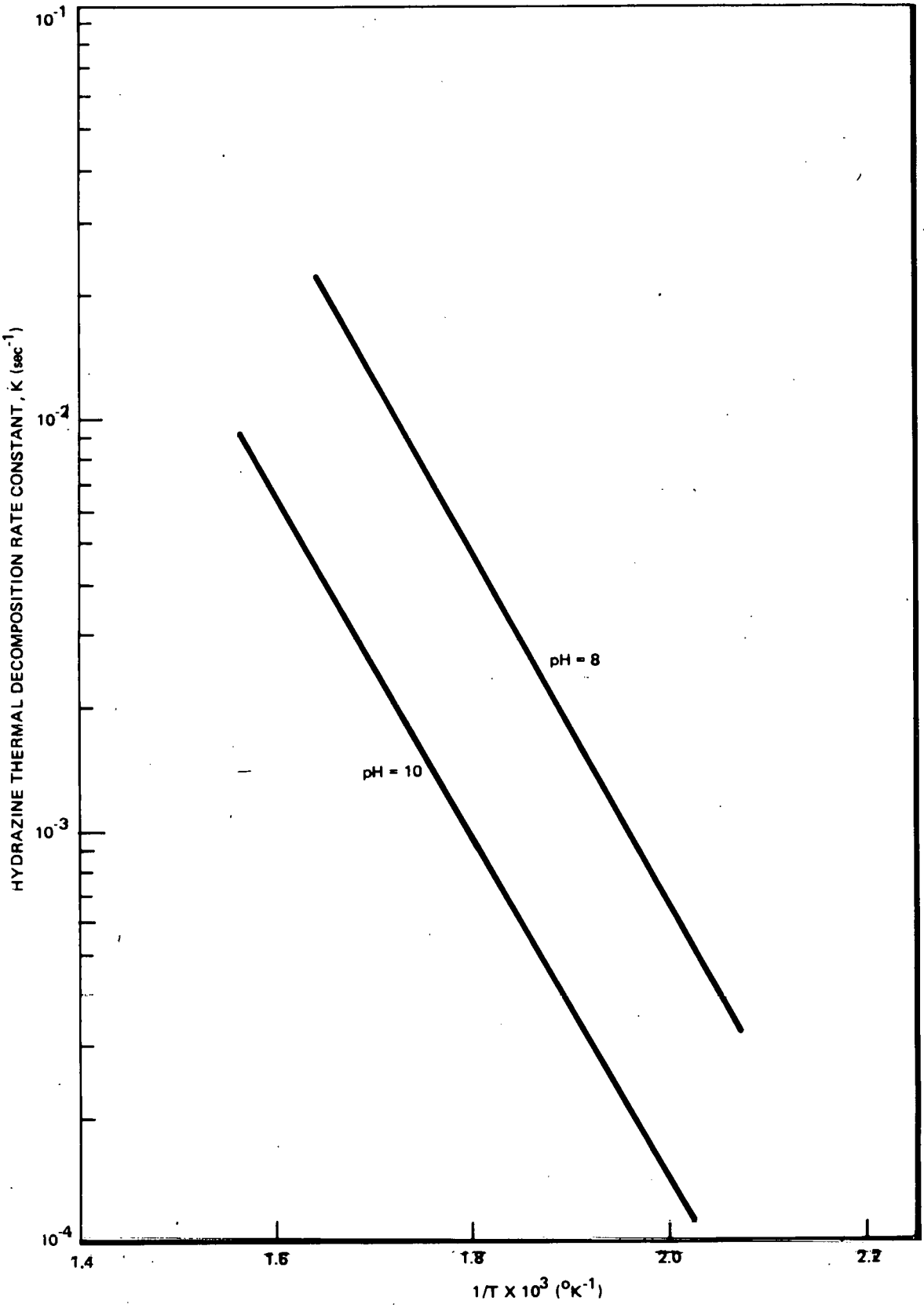

Figure 3-1. Hydrazine Decomposition Rates versus Temperature
[From: H. Hartmann, G. Resch, Mit. VGB52 54, 1958]

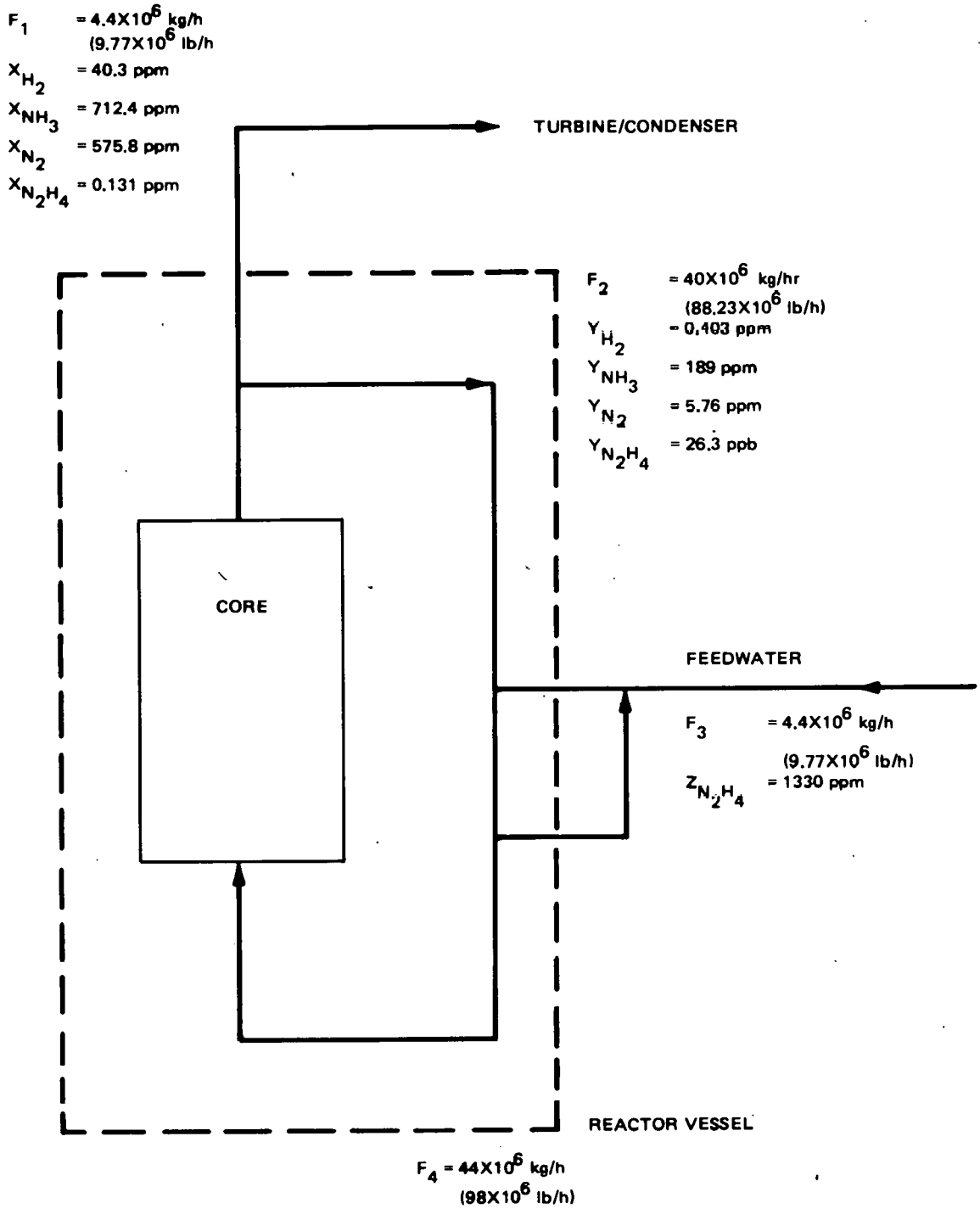

Figure 3-2. Hydrazine Addition - Hydrazine Controlling Case (Using Japanese[3] thermal decomposition data)

3.2 TASK B-1. N-16 DOSE RATE (H. H. Paustian, G. F. Palino)

Objective. The primary source of radioactivity in the steam from a BWR is N-16 from the O-16 (n,p) reaction. The N-16 is formed in the liquid phase within the reactor core and then partitioned between the reactor water and steam during the phase separation. With standard BWR water chemistry, the bulk of the N-16 formed is quickly converted to relatively non-volatile anionic species, primarily NO_2^- or NO_3^-. Only a small amount of the N-16 goes into the steam. As the oxidizing potential of the coolant is reduced by oxygen suppression additives, the proportion of the N-16 converted to relatively volatile, cationic (NH_4^+) species markedly increases and the fraction released to the steam rises commensurately. All three potential additives, i.e., H_2, NH_3, and N_2H_4, appear to act similarly in increasing the N-16 activity in the steam; however, the exact relationships need to be verified quantitatively so that the impact on turbine building shielding and/or operator-environment dose rates can be evaluated.

3.2.1 Dose Rate Calculations

Models have been prepared to calculate dose rates on the turbine operating floor and in the environment surrounding the turbine building. These calculations were done for the Dresden 2 and for a typical BWR/6 arrangement. The isotopes considered were N-16 having a 7.3 sec half-life and C-15 having a 2.45-sec half-life. For results to be applicable to a number of AWC's, the calculations were done assuming concentrations in the steam of 1.0 μCi/g of N-16 or 1.0 μCi/g of C-15 at the outlet of the reactor pressure vessel (RPV) nozzles. Thus, to estimate the radiation levels for a selected water chemistry, one would multiply these results by actual RPV nozzle concentrations of N-16 and C-15 and add them to get a total radiation level at a particular location. The results of these calculations are reported in subsequent sections.

3.2.1.1 Main Steam Line Calculations for Dresden 2

A number of steam line dose rate measurements have been made at Dresden 2 as a part of this program. These measurements are reported in Table 3-1 and Figure 3-3.

Table 3-1

"C" STEAM LINE DOSE RATE MEASUREMENTS

A. Victoreen 470A Panoramic Survey Meter Measurements:

Distance[a] (cm)	Exposure Rate (R/h)	Comments
14.7	1.05	Side Measurement
14.7	1.20	Face Measurement
45.2	0.80	Face Measurement
75.7	0.64	Face Measurement
106.2	0.57	Face Measurement

B. LiF Thermal Luminescense Dosimeter Measurements:

Distance[a] (cm)	Exposure Rate (R/h)	Comments
9.0	1.19	Side Measurement
9.0	1.31	Face Measurement
24.2	1.03	Face Measurement
54.7	0.67	Face Measurement
100.4	0.49	Face Measurement

[a]Distance is from outer metal surface of the "C" steam line to the effective center of the detector system.

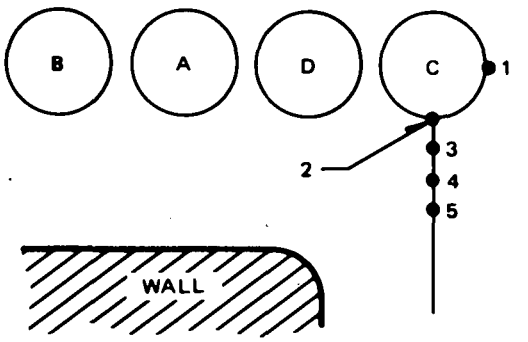

A STEAMLINE SEPARATION (INSULATION EXTERIOR-TO-INSULATION EXTERIOR) = 1.02m. INSULATION THICKNESS ~9 cm. STEAMLINES ARE 24-inch SCHEDULE 80 PIPE

Figure 3-3. Configuration of Steam Lines[a] (pictorial)

This measurement program also included a Ge(Li) gamma scan of the "C" steam line at the point where the dose rate measurements were made. The radionuclides of N-16, C-15 and O-19 were identified in the spectra. The ratio of their concentrations in the steam was 10.6/5.2/1.0, respectively.

The information on the ratio of isotopes and the steam line geometry, as shown in Figures 3-3 and 3-4, was used in the QAD-F computer code to calculate exposure rates based on an assumed concentration of 1.0 μCi/g of N-16 in the steam at the measurement location. By then determining the ratio of the measured exposures rates to the QAD-F calculated exposure rates, the actual N-16 and C-15 concentrations could be determined. The contribution from each line and the total QAD-F exposure rates are shown in Table 3-2.

Table 3-2

QAD-F CALCULATED EXPOSURE RATES

Detector[a] No.	Contribution From Line C (mR/hr)	Contribution From Line D (mR/hr)	Contribution From Line A (mR/hr)	Contribution From Line B (mR/hr)	Total (mR/hr)
1	42.7	1.57	1.185	-	44.5
2	42.7	7.77	0.788	-	51.3
3	23.7	7.27	2.51	0.665	34.1
4	15.9	6.65	2.95	1.13	26.6
5	11.6	6.00	2.84	1.53	22.0

[a]These correspond to the measurement locations of the Victoreen 470V Panoramic Survey Meter per Figure 3-3.

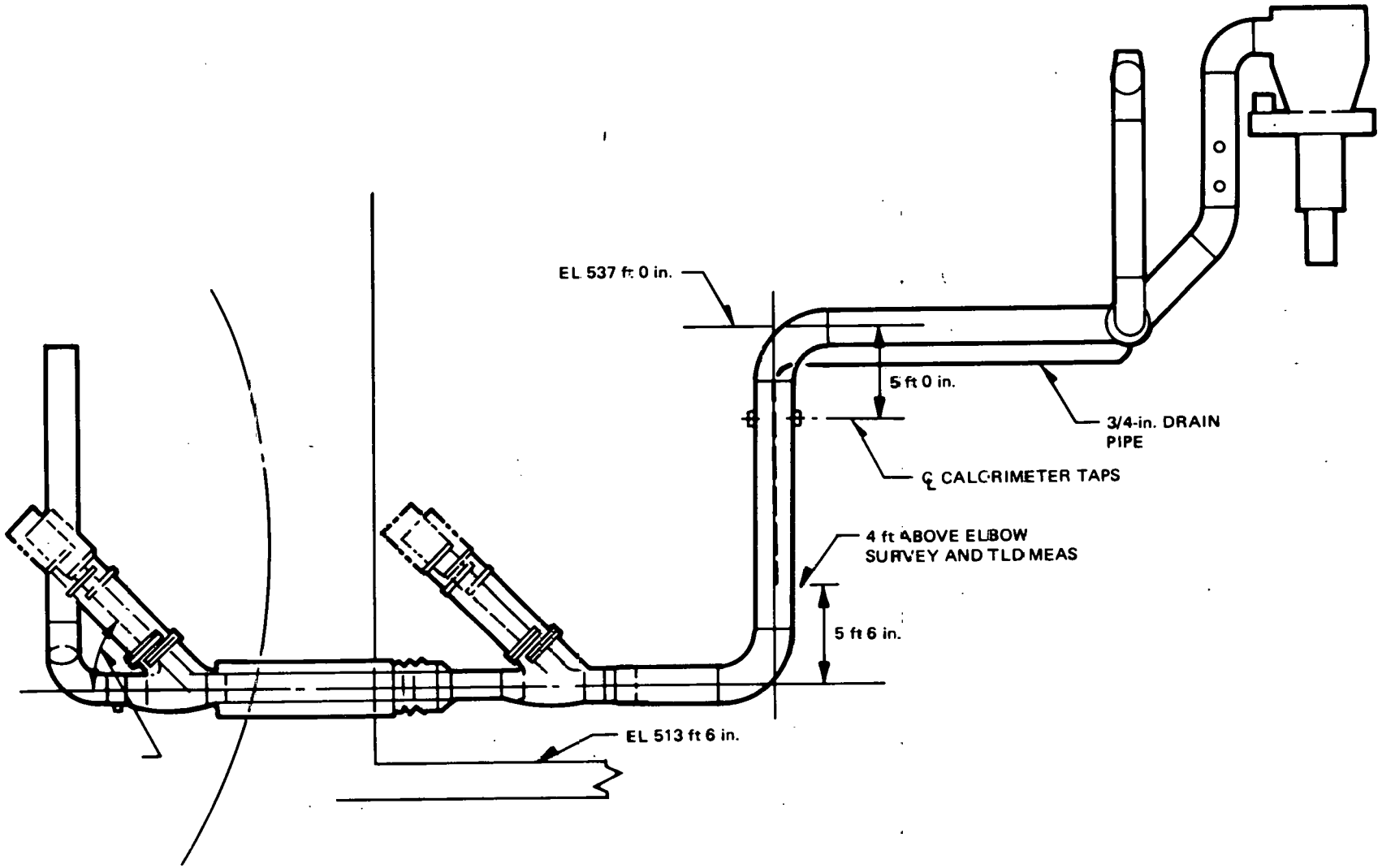

Figure 3-4. Dresden 2 Steam Line Geometry

Table 3-3 shows the ratio of measured exposure rates to calculated exposure rates.

The average ratio was 24.1. Because results from the first three locations are somewhat more accurate, a value of 23.5 was selected. This means that at the measurement location, the N-16 concentration in the steam was 23.5 μCi/g and the C-15 concentration was (5.2/10.6)(23.5 μCi/g) = 11.5 μCi/g. A check of this value was made using the third measurement for the LiF Thermal Luminescense Dosimeter (TLD) data. In this case, a measured-to-calculated ratio of 22.6 was obtained. This information is useful for base line data in understanding N-16/C-15 behavior in a BWR power plant. The measured-to-calculated ratio for the several detector locations showed quite good consistency, thereby giving added confidence in its validity.

3.2.1.2 Turbine Operating Floor Dose Rates at Dresden 2

The Dresden 2 turbine operating floor arrangement is shown in Figure 3-5. It is a relatively simple arrangement with only the following turbine equipment above the floor containing significant inventories of N-16 or C-15: (a) the high pressure turbine; (b) the three low pressure turbines; (c) the six combined intermediate valves (CIV's); (d) the piping located above the floor entering the CIV's and going from the CIV's to the low pressure turbines; and (e) portions of two of the four main steam lines that rise above the operating floor before entering the high pressure turbine.

Table 3-3

RATIO OF MEASURED EXPOSURE RATES TO QAD-F CALCULATED EXPOSURE RATES

Detector No.	Measured Exposure Rate (mR/hr)	QAD-F Exposure Rate (mR/hr)	Ratio
1	1050	44.5	23.6
2	1200	51.3	23.4
3	800	34.1	23.5
4	640	26.6	24.1
5	570	22.0	25.9

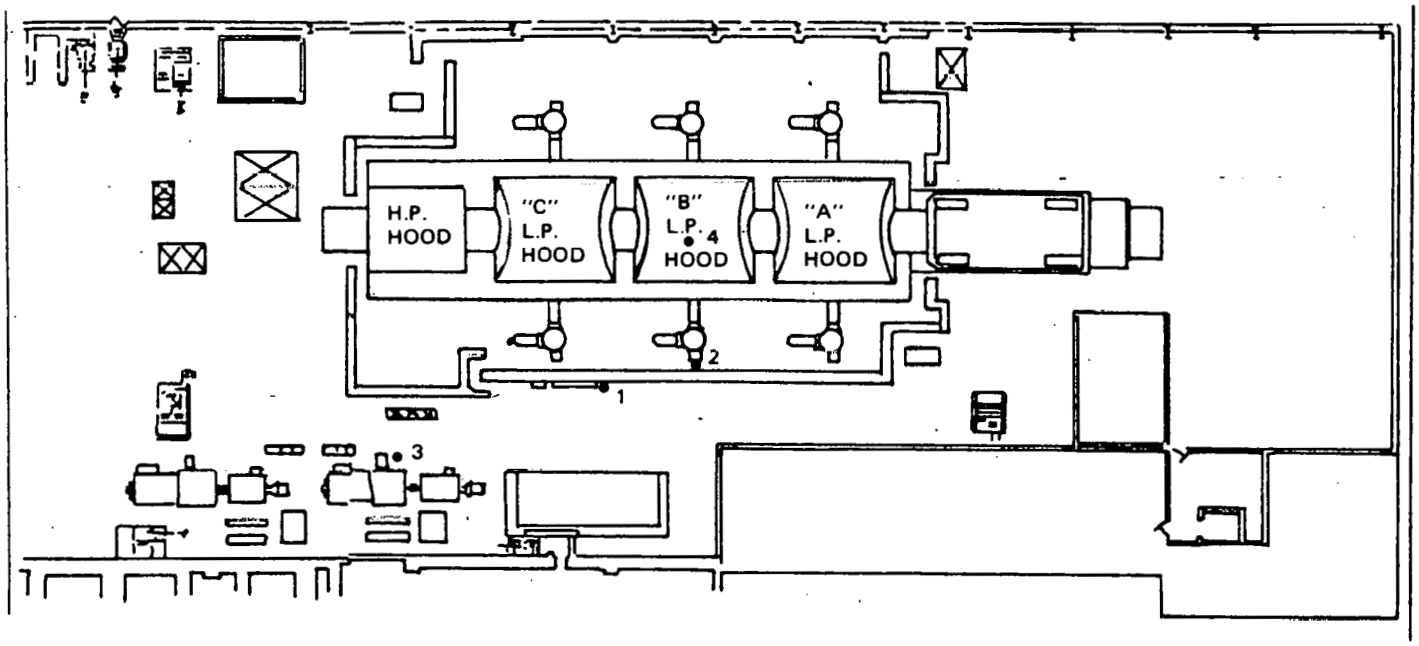

DETECTOR 1 – OUTSIDE SHIELDING, DIRECTLY OPPOSITE CIV-4, 4 ft ABOVE FLOOR
DETECTOR 2 – INSIDE SHIELDING, DIRECTLY OPPOSITE CIV-5, 4 ft ABOVE FLOOR
DETECTOR 3 – NEAR M-G SET, 4 ft ABOVE FLOOR
DETECTOR 4 – DIRECTLY ABOVE CENTER OF LP HOOD "B", 4 ft ABOVE ROOF OF TURBINE BUILDING

Figure 3-5. Dresden 2 Turbine Operating Floor

To calculate the inventory of either N-16 or C-15 in the above components, the mass inventory of steam or water in the component must be known, the mass flow rate through the component must be known, and the "age" (time since it left the RPV nozzle) of the entering steam must be known. The inventory of the isotope is then calculated from:

$$A = a_o \dot{M} e^{-\lambda t_{in}} (1-e^{-\lambda \Delta t})/\lambda, \qquad (3\text{-}1)$$

where

A = contained inventory

a_o = specific activity at RPV nozzle

$\dot{M}$ = mass flow rate through component

t_{in} = age of steam entering component

Δt = transit time through component = mass inventory/mass flow rate (slug flow assumed)

λ = decay constant = 0.693/t-1/2

$t_{1/2}$ = half-life

Now even though only inventories above the operating floor are of interest, the mass inventories of <u>all</u> components between the RPV nozzle and the turbine must be estimated to calculate the age of the steam entering the components on the floor. Thus, the mass of steam in the main steam line between the reactor and the turbine and the mass in the moisture separators must be estimated to calculate the time delay through each. Table 3-4 shows the mass inventories, mass flow rates, and age of entering steam for the turbine components on the floor, all at full power conditions. These values will change for lower power levels.

Table 3-5 then shows the contained inventories calculated for each component based on 1.0 μCi/g of either N-16 or C-15 at the RPV nozzle. These were calculated with time-share routines which are based on Equation (3-1).

Table 3-4

MASS FLOW CONDITIONS IN TURBINE COMPONENTS ON DRESDEN 2 OPERATING FLOOR AT 100% POWER

Component	Mass Inventory (kg)	Mass Flow Rate (kg/h x 10^6)	Age of Entering Steam (sec)
11.6 m of 20-in. o.d. steam line entering high pressure turbine	65	4.42	1.7
High pressure turbine	205	4.42	1.8
Intermediate piping (36-in o.d.):			
Upstream of CIV's - 18.2 m	90	3.93	5.4
Downstream of CIV's - 31.7 m	157	3.93	5.6
CIVs	147	3.93	5.5
Low pressure turbines	431	3.93	5.7

Table 3-5

CONTAINED INVENTORIES IN D-2 TURBINE EQUIPMENT (BASED ON 1.0 μCi/g of N-16 OR OF C-15 AT RPV NOZZLE)

Component	N-16 Inventory (Ci)	C-15 Inventory (Ci)
11.6 m of 20-in. o.d. steam line	0.0548	0.0394
High pressure turbine	0.172	0.121
Intermediate piping (36-in. 1.d.):		
Upstream of CIV's - 18.2 m	0.0538	0.0194
Downstream of CIV's - 31.7 m	0.0915	0.0315
CIV's	0.0871	0.0308
Low pressure turbines	0.245	0.0804
	0.704	0.323

The difference between the N-16 inventories and the C-15 inventories is caused by the C-15's more rapid decay. The inventories listed in Table 3-5 were the basis for calculating both the operating floor dose rates as well as the air-scattered dose rates to receivers outside the Dresden 2 turbine building.

To calculate operating floor dose rates, the QAD-F computer code was again utilized. Three detector locations on the operating floor and one detector on the roof were selected. Models of each of the turbine components in Table 3-5 were set up in the QAD-F geometry and dose rates calculated based on the inventories shown. Figure 3-5 shows the three detector locations on the floor and the fourth detector on the roof directly above the center of low pressure turbine hood "B". Note that one would expect Detector 2 to be one of the highest locations inside the shield wall without being in direct contact with any of the components, while Detectors 1 and 4 would be expected to be representative of comparatively high readings outside the shield walls. All detectors were 1.3 m above the floor or roof, respectively. Tables 3-6 and 3-7 show the dose rate contribution from each component at the selected detector locations with everything still based on 1.0 μCi/g of either N-16 or C-15 at the RPV nozzle.

Note that the contributions from CIV's 1, 2, and 3 and associated piping to the dose rates at Detectors 1, 2, and 3 were neglected because the line-of-sight between these sources and those detectors is heavily shielded by the turbine itself. Their contribution to the dose rate at Detector 4, however, is accounted for. Because CIV's 1, 2, and 3 and CIV's 4, 5, and 6 are symmetric with respect to Detector 4, the contributions from the CIV's on either side of the turbine are the same for that detector location. The inventory in the steam lines entering the high pressure turbine was treated conservatively by assuming it all to be in the pipe on the same side of the turbine as the detector position. The information in Tables 3-6 and 3-7 may be used to estimate what dose rates on the operating floor of Dresden 2 would be for any given N-16 and C-15 concentrations at the RPV nozzle.

Table 3-6

N-16 OPERATING FLOOR DOSE RATES
(FOR 1 μCi N-16 Gm STEAM)

Component	Detector 1 (mR/hr)	Detector 2 (mR/hr)	Detector 3 (mR/hr)	Detector 4 (mR/hr)
11.6 m of 20-in. l.d. steam line	1.16-4[a]	8.15-2	4.29-3	5.19-2
High pressure turbine	2.04-4	2.83-2	8.98-4	9.20-3
DIV-4 and piping	4.52-2	2.99-1	6.16-4	7.35-2
CIV-5 and piping	3.73-5	6.33+0	1.61-5	1.15 1
CIV-6 and piping	3.50-0	2.63-1	4.57-7	7.35-2
Low pressure turbine "A"	1.74-3	2.48-2	1.31-4	3.26-2
Low pressure turbine "B"	1.32-4	1.11-1	1.79-5	6.21-2
Low pressure turbine "C"	6.42-6	2.48-2	2.16-6	3.26-2
Total	4.74-2	7.16+0	5.97-3	4.50-1

[a]Note 1.16-4 = 1.16×10^{-4}

$$\left(\begin{array}{c}+2.62\text{-}1 \\ \text{for CIV-1,2,3}\end{array}\right) \over 7.12\text{-}1$$

Table 3-7

C-15 OPERATING FLOOR DOSE RATES
(FOR 1 μCi C-15/Gm STEAM)

Component	Detector 1 (mR/hr)	Detector 2 (mR/hr)	Detector 3 (mR/hr)	Detector 4 (mR/hr)
11.6 m of 20-in. o.d. steam line	4.86-5[a]	4.78-2	2.17-3	3.04-2
High pressure turbine	9.04-5	1.62-2	4.28-4	5.24-3
CIV-4 and piping	1.09-2	8.52-2	1.41-4	2.10-2
CIV-5 and piping	7.54-6	1.83+0	3.20-6	3.29-2
CIV-6 and piping	5.45-9	1.15-1	7.92-8	2.10-2
Low pressure turbine "A"	9.97-4	9.50-3	5.04-5	1.96-2
Low pressure turbine "B"	5.84-5	7.74-2	3.52-6	4.37-2
Low pressure turbine "C"	9.63-7	9.50-3	3.26-7	1.96-2
Total	1.21-2	2.19+0	2.80-3	1.93-1

[a]Note $4.86\text{-}5 = 4.86 \times 10^{-5}$

$$+ \frac{\left(\begin{array}{c}7.49\text{-}2 \\ \text{for CIV-1,2,3}\end{array}\right)}{2.68\text{-}1}$$

3.2.1.3 Environmental Gamma Radiation Levels at Dresden 2

A large number of sources contribute to the environmental gamma radiation levels on the Dresden site. In addition to inventories on the turbine operating floor of both Dresden 2 and Dresden 3, there are contributions from waste and surge tanks located outside the plant building, contributions from natural background (both terrestrial and cosmic) and fallout, and a contribution from the Dresden 1 turbine, which has no shielding surrounding it. The contribution from the Dresden 1 turbine is the major portion of current site gamma radiation levels.[1] Thus, there would have to be a quite significant increase in N-16 and C-15 concentrations at Dresden 2 before the total site gamma radiation levels would be substantially changed.

This section reports on calculations done to estimate the contribution to the total gamma radiation level from the inventories in turbine equipment above the operating floor for Dresden 2 at a large number of detector locations in several directions about the Dresden 2 turbine building. Only air-scattering was considered; building-scattered and direct line-of-sight contributions from Dresden 2 should be negligible. The starting point for the air-scattering calculation is the contained inventories in Table 3-5. These contained inventories are then each multiplied by a self-shielding factor to obtain equivalent point sources. The self-shielding factors are a measure of how much shielding is provided by the very material making up the turbine component containing the inventory of interest and are derived from data in appropriate QAD-F runs. Self-shielding factors for the turbine components modeled here are taken from Reference 5. The same self-shielding factors are used for N-16 and C-15 inventories. Table 3-8 shows the self-shielding factors used and the resulting equivalent point source strengths. Note that the equivalent point sources are considered to be isotopic. Self-shielding actually is a strong function of the angle at which the source to detector ray emerges from the turbine component. For this calculation, self-shielding factors are generally conservatively selected for a direction or angle having the least amount of self-shielding by the actual turbine component itself. For example, this might be a direction ray perpendicular to the high pressure turbine axis.

The computerized data-handling procedure SKREEN[5] was used to calculate estimated air-scatter dose rates for the equivalent point sources shown in Table 3-8. Table 3-9 shows the coordinates of the detector positions selected, where the X axis is coincident with the turbine-generator axis and the Y axis is perpendicular to it and an extension of the common wall of units 2 and 3. Table 3-10 lists the N-16 and C-15 air-scatter dose rates at each detector location. All of the values are still normalized to unit activities of N-16 and C-15 at the RPV nozzle.

Table 3-8

EQUIVALENT POINT SOURCES FOR D-2 AIR-SCATTERING CALCULATION
(BASED ON UNIT STEAM ACTIVITIES)

Component	Self-Shielding Factor	N-16 Equivalent Point Source Inventory (Ci)	C-15 Equivalent Point Source Inventory (Ci)
11.6 m of 20-in o.d. steam line (2.6 cm wall)	0.45	0.0247	0.0177
High pressure turbine	0.042	0.00722	0.00508
Intermediate piping:			
Upstream of CIV's - 18.2 m (1.27 cm wall)	0.661	0.0356	0.0128
Downstream of CIV's - 31.7 m (1.27 cm wall)	0.661	0.0605	0.0208
CIV's	0.237	0.0206	0.00730
Low pressure turbines	0.052	0.0127	0.00418
		0.161	0.0679

Table 3-9

DETECTOR LOCATIONS FOR DRESDEN 2 AIR-SCATTER CALCULATION
(BASED ON UNIT STEAM ACTIVITIES)

Detector	x, m	y, m	Description
1	152	43	152 m North of Dresden 2 LPT "B"
2	305		305 m North of Dresden 2 LPT "B"
3	457		457 m North of Dresden 2 LPT "B"
4	609		609 m North of Dresden 2 LPT "B"
5	762		762 m North of Dresden 2 LPT "B"
6	914		914 m North of Dresden 2 LPT "B"
7	1067		1067 m North of Dresden 2 LPT "B"
8	0	152	152 m West of Dresden 2
9	0	305	305 m
10	0	457	457 m
11	0	609	609
12	0	762	762
13	0	914	914
14	0	1067	1067
15	-52	86	Southwest corner of Administration Building
16	-90	90	Northwest corner of Visitors Center
17	-133	67	Parking Lot "Center"
18	67	58	South corner of 2/3 Crib House
19	145	39	Southeast corner of 34 Kv Relay House

Table 3-10

AIR-SCATTER EXPOSURE RATES FROM DRESDEN 2 TURBINE COMPONENTS ABOVE TURBINE OPERATING FLOOR (BASED ON UNIT STEAM ACTIVITIES)

Detector	Location	N-16 Air-Scatter Exposure Rate (mR/yr)	C-15 Air-Scatter Exposure Rate (mR/yr)
1	152 m north	2.902+0*	9.565-1
2	305 m north	9.455-1	3.046-1
3	457 m north	2.961-1	9.294-2
4	609 m north	1.112-1	3.466-2
5	762 m north	5.090-2	1.569-2
6	914 m north	2.403-2	7.369-3
7	1067 m north	1.292-2	3.941-3
8	152 m west	1.794+0	5.840-1
9	305 m west	5.903-1	1.878-1
10	457 m west	1.903-1	6.023-2
11	609 m west	7.958-2	2.504-2
12	762 m west	3.655-2	1.138-2
13	914 m west	1.829-2	5.635-3
14	1067 m west	9.431-3	2.893-3
15	Admin. Building	6.982+0	2.402+0
16	Visitor's center	3.960+0	1.390+0
17	Parking lot center	2.557+0	9.118-1
18	2/3 crib house	9.325+0	3.082+0
19	34 Kv relay house	3.104+0	1.027+0

*2.902+0 = $2.902 \times 10^{+0}$ etc.

3.2.1.4 Operating Floor Dose Rate Calcuations for Typical BWR/6 Arrangement

These calculations were carried out in a very similar fashion to those done for Dresden 2 with the following exceptions:

a. The BWR/6 turbine operating floor arrangement was considered to have four moisture separator-reheaters (MSR's) located on the operating floor.

b. Experience gained from the Dresden 2 calculations indicated that for most detector locations on the operating floor, the nearest (or largest) sources were the major contributors to the total dose rate. This effect will be even stronger for the BWR/6 operating floor arrangement that was used. Thus, dose rates near the "hottest" components (with shielding included where appropriate) were calculated individually for each important component. Past experience with measurements at operating plants was also drawn upon in deciding what sources to consider in doing these calculations.

c. The presence of MSR's on the operating floor means there also is crossover piping from the MSR's to the CIV's. This crossover piping, plus the MSR's themselves, are the major contributors to the air-scattered dose rates outside the turbine building.

Figure 3-6 shows the modified turbine operating floor arrangement used for these BWR/6 calculations. The original arrangement from the C. F. Braun standard SAR was modified by shortening the original two MSR's and adding an additional two MSR's for a total of four. Crossover piping for the second pair of MSR's was also added. The MSR's were considered to each have an active length of 16m. Only the turbine components on the operating floor shown in Figure 3-6 were considered. The air-scattering calculation was done both with and without shielding lid slabs over the MSR's and crossover piping. Also, for the air-scattering calculation, all shielding was considered to be infinitely thick or "black." This operating floor arrangement is a good representation of what will be found at BWR/6 plants.

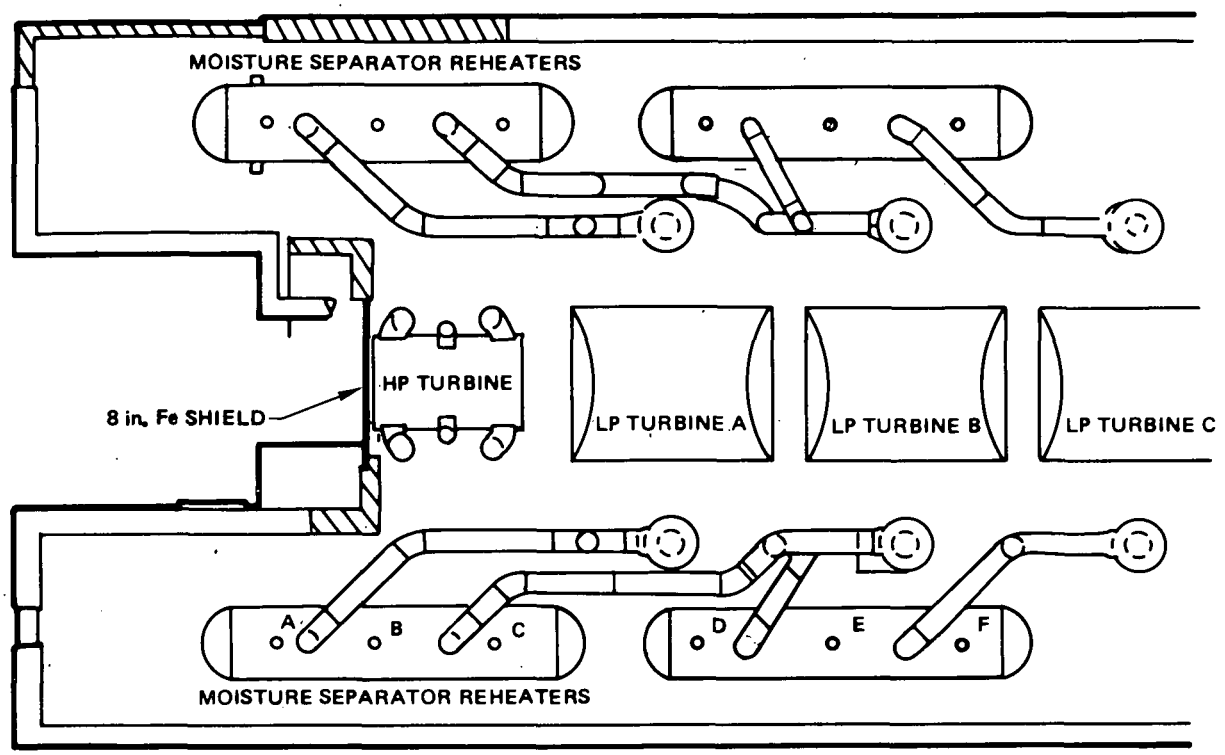

Figure 3-6. Turbine Operating Floor Arrangement For BWR/6 Calculations

Table 3-11 shows the mass flow conditions and the mass inventories in these turbine components at full power. Again, these values all vary with power level. Also note that both in Table 3-11 and in Table 3-5, the piping downstream of the CIV's is actually somewhat smaller than the upstream piping. Because of the difficulty in documenting this, however, they are both assumed to have the larger diameter. This is slightly conservative. Note also that Reference 7 was used for estimated lengths of piping beneath the operating floor and for main steam line lengths needed to calculate time delays before the steam entered the components on the operating floor. These piping lengths are not exact values from a particular plant design, but are representative for BWR/6 plants.

The contained N-16 and C-15 inventories in the BWR/6 components on the operating floor are shown in Table 3-12. These are the inventories used both in the air-scattering calculation and in the operating floor dose rate calculations. For the operating floor dose rates calculations, the highest dose rates inside the access shielding will occur in the vicinity of the high

Table 3-11

MASS FLOW CONDITIONS IN TURBINE COMPONENTS ON BWR/6 OPERATING FLOOR AT 100% POWER

Component	Total Mass Inventory, kg	Mass Flow Rate (10^6 kg/hr)	Age of Entering Steam (sec)
11m of 28-in. o.d. steam line entering high pressure turbine (2 lines)	122	6.69	3.111
High pressure turbine	172	6.69	3.177
20m of 42-in. o.d. piping (above floor) going from high pressure turbine to MSRs (4 lines)	120	5.97	3.3
MSRs			
1) Shell side before mositure separation	1048	5.97	4.2
2) Shell side after moisture separation	1425	4.88	4.8
3) Drain trough	2722	1.04	4.7
4) First stage reheater tube bundle	3902	0.32	4.3
5) Second stage reheater tube bundle	4310	0.28	5.4
	13407		
178m of 42-in. o.d. piping from MSR's to CIV's	758	4.88	5.9
CIV's	129	4.88	6.4
31m of 42-in. o.d. piping from CIV's to low pressure turbines	132	4.88	6.5
Low pressure turbines	346	4.88	6.6

Table 3-12

CONTAINED INVENTORIES IN BWR/6 TURBINE EQUIPMENT
(BASED ON 1.0 μCi/g OF N-16 OR C-15 AT RPV NOZZLE)

Component	N-16 Inventory (Ci)	C-15 Inventory (Ci)
11 m of 28-in. o.d. steam line entering high pressure turbine (2 lines)	0.090	0.050
High pressure turbine	0.13	0.069
20 m of 42-in. o.d. piping from high pressure turbine to MSR's (4 lines)	0.089	0.048
MSRs	3.8	1.0
178 m of 42-in. o.d. piping from MSR's to CIV's	0.42	0.13
CIV's	0.070	0.021
31 m of 42-in. o.d. piping from CIV's to low pressure turbine	0.071	0.021
Low pressure turbine	0.18	0.051
	4.83	1.4

pressure turbine and the MSR's. Outside the shield walls, the highest dose rate will occur at the wall surface near the midpoint of an MSR. These are the locations where dose rate calculations were done.

The first operating floor dose rate calculations done were simply for a number of detector locations near an MSR. Figure 3-7 is a simple sketch of the MSR and the detector locations and Table 3-13 shows the QAD-F results.

Note that contact dose rates on the crossover piping leaving the MSR's were calculated to be approximately 12.7 mR/hr for N-16 and 3.27 mR/hr for C-15. This is still based on 1.0 Ci/g of either N-16 or C-15 at the RPV nozzle.

Table 3-14 shows the effect of a concrete shield wall upon the dose rate of a detector lcoated at the MSR midplane 3 m above the floor and 30 cm away from the outer surface of the wall. The inner surface of the shield wall is 4.1 m from the center of the MSR.

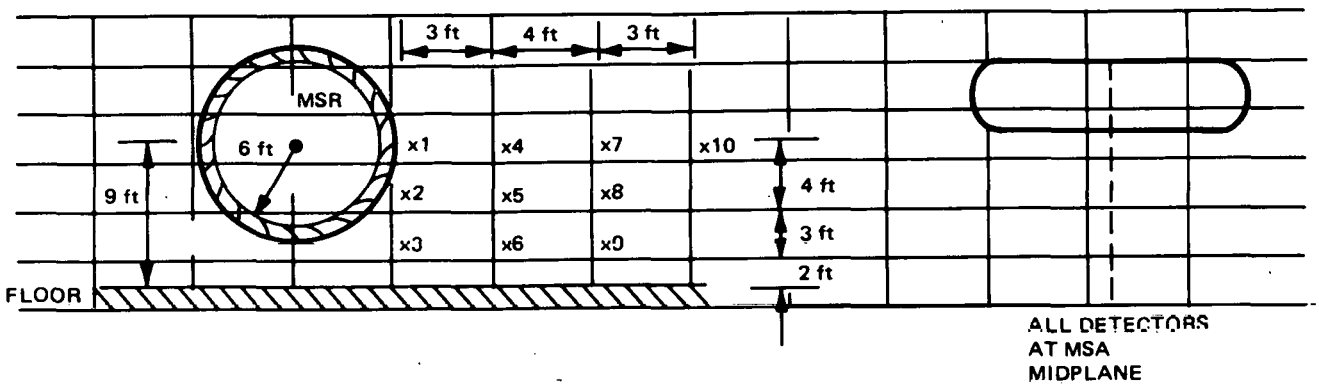

Figure 3-7. Detector Locations Near MSR

Table 3-13

QAD-F CALCULATED DOSE RATES NEAR BWR/6 MSR

Detector	N-16 Dose Rate (mR/hr)	C-15 Dose Rate (mR/hr)
1	11.03	2.64
2	13.02	3.84
3	10.27	3.00
4	7.86	1.97
5	7.79	2.26
6	7.21	2.11
7	5.35	1.39
8	5.05	1.45
9	4.95	1.43
10	4.32	1.14

Table 3-14

QAD-F CALCULATED DOSE RATES ON OTHER SIDE OF SHIELD WALL ADJACENT TO AN MSR

Shield Wall Thickness	N-16 Dose Rate (mR/hr)	C-15 Dose Rate (mR/hr)
0.45 m	0.311	0.0728
0.61 m	0.123	0.0278
0.91 m	0.0195	0.00407
1.22 m	0.00310	0.000595

The other major sources on the BWR/6 operating floor in addition to the MSR's and associated crossover piping are the high pressure turbine, the two segments of main steam line that rise above the floor before entering the turbine, and the four segments of turbine-to-MSR piping that exit the turbine above the floor, but then drop below the operating floor to travel to the MSR's. Table 3-15 shows the QAD-F calculated dose rates for detectors 0.9m, 1.5m, 3.0m, and 6.1m from the outside surface of the 20 cm iron shield immediately west of the high pressure turbine and for detectors 1, 1.5, 3 and 6.1 m from the outside surface of the high pressure turbine along a line perpendicular to the turbine axis passing through the turbine center. All detectors are 1.3 m above the floor. Dose rates in Table 3-15 are caused only by the inventory contained in the high pressure turbine.

Table 3-15

QAD-F CALCULATED DOSE RATES NEAR THE HIGH PRESSURE TURBINE

Detector Location	N-16 Dose Rate (mR/hr)	C-15 Dose Rate (mR/hr)
1m from Fe shield	0.00918	0.00373
1.5m from Fe shield	0.00923	0.00379
3m from Fe shield	0.00605	0.00250
6.1m from Fe shield	0.00255	0.00106
1m on perpendicular	1.29	0.573
1.5m on perpendicular	0.852	0.378
3m on perpendicular	0.388	0.172
6.1m on perpendicular	0.168	0.0745

In reality, the eight detector locations in Table 3-15 will see contributions from the high pressure turbine, the piping entering and exiting the high pressure turbine, and from the nearest MSR. In this case it was conservatively assumed that the location of the MSR was shifted so that the midplane coincided with the midplane of the high pressure turbine. Figure 3-8 shows the simplified shielding geometry that was mocked up.

Tables 3-16 and 3-17 show the dose rate contributions from each source. Contributions from all other sources are considered negligible. The rather sharp increase in the MSR contribution to the dose rate in moving from Detector 7 to Detector 8 occurs because Detector 8 is far enough beyond the west end of the MSR model that there is a significant contribution through the end of the MSR instead of through the side. Self-shielding in the direction of the MSR end is less than it is for the side. Note also that the piping entering and exiting the high pressure turbine contributes more than does the high pressure turbine itself.

Table 3-16

QAD-F CALCULATED N-16 DOSE RATES FOR COMBINED SOURCES NEAR HIGH PRESSURE END OF TURBINE

Detector	High Pressure Turbine (mR/hr)	MSR (mR/hr)	High Pressure Steam Inlet Lines (mR/hr)	Turbine-to MSR Piping (mR/hr)	Total (mR/hr)
1	1.29+0*	2.06+0	4.60+1	6.48+0	5.58+1
2	8.52-1	2.31+0	1.26+1	6.74+0	2.25+1
3	3.88-1	3.12+0	3.38+0	4.92+0	1.18+1
4	1.68-1	7.14+0	9.89-1	1.67+0	9.97+0
5	9.18-3	1.22-3	1.72-2	6.88-2	9.64-2
6	9.23-3	3.51-3	1.50-2	5.62-2	8.39-2
7	6.05-3	4.78-3	1.09-2	3.51-2	5.68-2
8	2.55-3	2.42-1	6.18-3	1.57-2	2.66-1

*1.29+0 = $1.29 \times 10^{+0}$

Table 3-17

QAD-F CALCULATED C-15 DOSE RATES FOR COMBINED SOURCES NEAR HIGH PRESSURE END OF TURBINE

Detector	High Pressure Turbine (mR/hr)	MSR (mR/hr)	High Pressure Steam Inlet Lines (mR/hr)	Turbine-to MSR Piping (mR/hr)	Total (mR/hr)
1	5.73-1	5.84-1	1.99+1	2.85+0	2.39+1
2	3.78-1	6.55-1	5.72+0	2.97+0	9.72+0
3	1.72-1	8.92-1	1.53+0	2.16+0	4.75+0
4	7.45-2	2.11+0	4.48-1	7.34-1	3.37+0
5	3.73-3	2.77-4	7.19-3	2.87-2	3.99-2
6	3.79-3	8.49-4	6.30-3	2.35-2	3.44-2
7	2.50-3	1.24-3	4.58-3	1.47-2	2.30-2
8	1.06-3	6.91-2	2.60-3	6.61-3	7.94-2

*1.29+0 = $1.29 \times 10^{+0}$

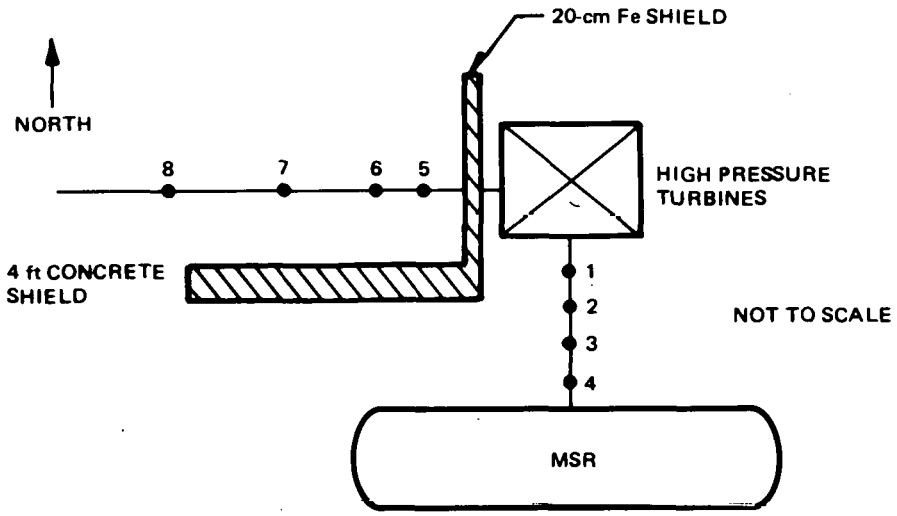

Figure 3-8. Geometry for Combined Source QAD-F Dose Rate Calculation

The dose rates listed in Tables 3-16 and 3-17 are representative of those values which would be encountered in a BWR/6 turbine operating floor arrangement and may be scaled up by the appropriate RPV nozzle concentration factors to evaluate the impact of any particular AWC.

3.2.1.5 Environmental Gamma Radiation Levels for a BWR/6 Plant

This section reports on calculations done to estimate the contribution to the total environmental gamma radiation levels from the inventories in turbine equipment above the operating floor for a BWR/6 turbine operating floor arrangement. Just as was done for Dresden 2, the starting point for this air-scattering calculation was the contained inventories in the turbine equipment that are listed in Table 3-14. The contained inventories were multiplied by self-shielding factors to obtain equivalent point sources. Table 3-18 shows the self-shielding factors used and the resulting equivalent point source strengths. Reference 5 was again used for self-shielding factors. Comments on the variation of self-shielding with direction also apply to the BWR/6 arrangement.

SKREEN was again used to calculate the estimated air-scatter dose rates; the spectral information required was obtained from Reference 7. In the case of the BWR/6, two sets of calculations were run, one including concrete lids over the entire length of the MSR's and crossover piping (but not over the turbine itself and with no inner shield walls between the MSR's and the turbine), and one without such concrete lids. C. F. Braun's Safety Analysis Report (SAR), which was the starting point for this BWR/6 arrangement, included lids over the MSR's and crossover piping.

Table 3-19 shows the N-16 and C-15 air-scatter dose rates at each of 14 detector locations along 2 detector axes for the arrangement with and without MSR lids. Note all these calculations are based on 1.0 μCi/g of either N-16 or C-15 at the RPV nozzle.

The coordinate system origin is on the operating floor at the center of the high pressure turbine. The detector location description "perpendicular" and "parallel" are with respect to the turbine-generator axis. The

Table 3-18

EQUIVALENT POINT SOURCES FOR BWR/6 AIR-SCATTERING CALCULATION

Component	Self-Shielding Factor	N-16 Equivalent Point Source Inventory (Ci)	C-15 Equivalent Point Source Inventory (Ci)
11m of 28-in o.d. steam line entering high pressure turbine (2 lines)	0.348	0.0314	0.0174
High pressure turbine	0.042	0.00533	0.00291
20m of 42-in. o.d. piping from high pressure turbine to MSR's (4 lines)	0.600	0.0532	0.0287
MSR's	0.141	0.533	0.142
178m of 42-in. o.d. piping from MSR's to CIV's	0.600	0.254	0.0800
CIV's	0.237	0.0165	0.00488
31m of 42-in. o.d. piping from CIV's to low pressure turbines	0.600	0.0425	0.0124
Low pressure turbines	0.055	0.0100	0.00282
		0.946	0.291

Table 3-19

AIR-SCATTER EXPOSURE RATES FROM BWR/6 TURBINE COMPONENTS
(FOR STEAM ACTIVITY OF UNITY AT RPV OUTLET)

Detector Number	Location	N-16 Air-Scatter Exposure Rate (mR/yr)		C-15 Air-Scatter Exposure Rate (mR/yr)	
		No MSR Lids	MSR Lids	No MSR Lids	MSR Lids
1	152m, perpendicular	14.0	5.7	3.4	1.4
2	305m, perpendicular	3.3	1.3	0.79	0.32
3	457m, perpendicular	0.92	0.37	0.21	0.09
4	610m, perpendicular	0.33	0.14	0.08	0.03
5	762m, perpendicular	0.14	0.07	0.03	0.02

Table 3-19

AIR-SCATTER EXPOSURE RATES FROM BWR/6 TURBINE COMPONENTS
(FOR STEAM ACTIVITY OF UNITY AT RPV OUTLET) (Continued)

Detector Number	Location	N-16 Air-Scatter Exposure Rate (mR/yr)		C-15 Air-Scatter Exposure Rate (mR/yr)	
		No MSR Lids	MSR Lids	No MSR Lids	MSR Lids
6	914m, perpendicular	0.06	0.03	0.01	0.007
7	1067m, perpendicular	0.03	0.02	0.008	0.004
8	152m, parallel	16.0	6.0	3.7	1.5
9	305m, parallel	4.9	1.8	1.2	0.48
10	457m, parallel	1.4	0.47	0.34	0.13
11	610m, parallel	0.50	0.17	0.12	0.05
12	762m, parallel	0.22	0.07	0.05	0.02
13	914m, parallel	0.10	0.03	0.02	0.009
14	1067m, parallel	0.05	0.02	0.01	0.005

perpendicular direction vector passes through the center of the high pressure turbine. The parallel direction vector is coincident on the turbine-generator axis and passes through the high pressure turbine toward the low pressure end of the turbine-generator. This direction was selected rather than the opposite direction ray 180 deg away from it because the reactor building situated on the high pressure end of the turbine building would cast a large "shadow" for any detectors located behind it.

3.2.2 N-16 Activity Level

Table 3-20 lists five studies in which N-16 steam activity measurements were made during addition of hydrogen to the coolant of a BWR or of a test facility simulating the BWR. These tests occurred on ALPR,[6] BORAX IV,[7] EBWR,[8] HBWR,[9] and in a test loop at R2 in Sweden.[10] Interestingly, the results of all five measurements were quite similar in that the steam line radiation levels increased by factors in the range of 2 to 10. It is recommended that projected dose rate calculations be based on an increase of eightfold for the proposed hydrogen addition flow sheets.

Table 3-20

EFFECT OF HYDROGEN ADDITION ON N-16 STEAM LINE ACTIVITY

Reactor	Reactor Power (MW_t)	Temperature (°C)	Absolute Pressure (M P)	N-16 Steam-Water Dist. Coefficient	Steam Line N-16 Fractional Increase	Feedwater H_2 Addition Rate[a] (mℓSTP/kg)
ALPR	2.7	216	2.17	-	2-6	12-51
BORAX IV	4.0	216	2.17	-	4.3	42.3
EBWR[13]	20.0	254	4.24	0.115	-	no addition
EBWR[8]	20.0	254	4.24	-	∿4	40
EBWR[13]	(?)	-	-	(?)	10.7	(?)
HBWR	10.0	-	2.93	0.06[b]	-	no addition
HBWR	10.0	-	2.93	0.4[b]	∿7	>30
Loop 5 at R2	49.0	277	6.48	0.2 to 0.4	-	no addition
Loop 5 at R2	49.0	277	6.48	1.0 to 4.0	3-10	0.5 to 15

[a] 1 cc H_2(STP)/kg ∿ 0.09 ppm.

[b] Could be low by up to a factor of 4.

3.2.3 Carbon Chemistry

The chemical form of C-15 (2.49s) and C-14 (5692y) in the BWR is of interest due to the primary system radiation fields resulting from C-15 and the long-term environmental impact of the release of C-14. In addition, questions have arisen concerning the expected change in the C-15 carryover upon adoption of an AWC for the BWR.

Of the few fundamental studies of the reactions of hot carbon atoms in aqueous solutions that have been performed, the most extensive and detailed was made by Stenström[11] who studied the reactions of ^{11}C atoms in aqueous solutions.[12] Numerous reaction products were observed and the yield of any one product was found to be dose dependent.

At low doses (160 rad) CO_2(23 ± 1%), CO(32 ± 1%), HCO_2H(17 ± 2%), H_2CO (21 ± 2%), CH_3OH(6 ± 2%) and CH_4(0.2 ± 0.03%) are the observed reaction products. At the higher doses (>14000 rad) the principal product is CO_2. The dose rate in the Dresden 2 core during operation has been estimated to be $\sim 6.6 \times 10^4$ rad/sec (neutron + gamma),[14] and since the in-channel transit time is on the order of 1 second, doses considerably in excess of 14000 rads are expected and $^{15}CO_2$ (or $^{14}CO_2$) should be the principal reaction product released from the core of the BWR.

This prediction is supported by the measurements of Kunz, et al., of the chemical form of C-14 in the offgas of Nine Mile Point.[15] Their measurement yielded an off-gas composition of 95% CO_2, 2.5% CO, and 2.5% hydrocarbons.

If CO_2 is the principal species produced in the BWR coolant, the fraction of the $^{15}CO_2$ carried over in the steam can be calculated if high temperature partitioning and hydrolysis data for CO_2, as well as data for the dissociation of water are available. A recent report by J. W. Cobble of San Diego State tabulated the high temperature free energy of formation for species of interest in the carbonate system,[16] and Sweeton, et al., has published an excellent article on the dissociation of water.[17]

From these data the following reactions were postulated for a BWR operating at a saturated steam pressure of 7.0 M Pa (1015 psia):

$$CO_{2(\ell)} \rightleftharpoons CO_{2(g)} \qquad K = 7.9 \text{ M Pa kg/mole}$$

$$H_2CO_{3(aq)} \rightleftharpoons H^+_{(aq)} + HCO_3^-{}_{(aq)} \qquad K_1 = 7.5 \times 10^{-9} m$$

$$HCO_3^-{}_{(aq)} \rightleftharpoons H^+_{(aq)} + CO_3^{2-}{}_{(aq)} \qquad K_2 = 3.03 \times 10^{-12} m$$

$$H_2O \rightleftharpoons H^+_{(aq)} + OH^-_{(aq)} \qquad k_w = 5.62 \times 10^{-12} \frac{2}{m}$$

Using these equilibrium data, the chemical-species distribution in the aqueous phase was calculated to be 99.685% H_2CO_3, 0.315% HCO_3^-, and 4.0×10^{-7}% CO_3^{2-}. Assuming a Van der Waals gas for CO_2, the distribution coefficient was estimated to be 49.5.

Based upon the Dresden 2 flow and heat balance[2] (2527 MW_t, steam flow 4.33×10^6 kg/h, and core flow 44×10^6 kg/hr, the fraction of CO_2 leaving the core that is carried by the steam is 0.845. The remaining fraction, 0.155, stays with the liquid as H_2CO_3 (chemically identical to $CO_{2(\ell)}$), HCO_3^-, and CO_3^{2-}. The other potential chemical species, CO and CH_4, are more volatile than CO_2 and consequently a greater fraction of these species will be borne by the stream. Since their contribution to the total volatile radiocarbon is minor, it is justifiable to make any engineering projections and estimates based upon only one chemical species, CO_2. This consideration has relevance in the calculations of the inventory of C-15 in the turbine system components, such as the moisture separator drains.

The chemical form of radiocarbon under AWC's is not really relevant in terms of radiation levels in the steam system since the worst case condition is the carryover of the remaining 15.5% of the radiocarbon that had remained with the liquid in the non-additive condition. Therefore, the maximum fractional increase would be 1.18. This increase in radiation level is inconsequential when compared with the expected radiation field increases resulting from N-16.

Stenstrom's thesis sheds only limited light on what might be expected in the BWR. The following selected data represent the expected trend in the product distribution upon the addition of reducing species to the aqueous systems (Table 3-21).

The principal observation is that the addition of the reducing solute (CH_4) decreases the yield of CO_2 while increasing the yield of CO and the aldehydes and alcohols with only minor changes in the yields of the carboxylic acids. Since the formation of aldehydes and alcohols will result in C-15 products that are less volatile than CO_2, there is a real possibility that the steam line C-15 level will be reduced under AWC's.

3.2.4 Expected Dose Rates

Using the normalized dose rate calculations from Subsection 3.2.1 and the predicted changes in N-16 and C-15 activities from Subsections 3.2.2 and 3.2.3, the dose rates expected for a hydrogen addition flow sheet were calculated. They are presented in Table 3-22 which shows the contributions from each major equipment piece on the turbine floor. Locations of the points considered are shown in Figure 3-5. The CIV's are major contributors and the feasibility of controlling radiation levels through the use of localized shielding at these valves is being evaluated. Also these calculated radiation levels may be checked against actual measured dose rates[18] if the numbers are adjusted to comparable power levels. These comparisons show that the calculated values exceed the observed values by as much as a factor of two depending on exact location and modeling difficulty. Recommendations for additional shielding will take these differences into consideration. If additional shielding is added, a foot-thick wall of ordinary concrete will reduce radiation levels by a factor of about six.

Table 3-21

YIELD OF C-11 PRODUCTS IN AQUEOUS SOLUTIONS IRRADIATED
(1.0 k rad) WITH 185 MeV PROTONS

Solution	Concentration (mM)	$^{11}CO_2$	^{11}CO	^{11}C Carboxylic Acids	^{11}C Aldehydes	^{11}C Alcohols	^{11}C Hydrocarbons	Not Identified	Dose Rate (rad/sec)
CH_4	4	11.9	34.8	15.0	28.2	8.6	0.3	1.1	10
None	-	71.1	2.1	17.3	6.4	1.9	0.06	1.2	11
CH_4	4	10.8	34.6	16.2	29.4	8.1	0.22	0.8	13
None	-	64.4	2.6	24.4	5.4	1.8	0.04	1.4	14
CH_4	4	11.0	15.3	22.1	37.3	11.9	0.27	2.1	15

Table 3-22

ESTIMATED DRESDEN 2 TURBINE OPERATING FLOOR DOSE RATES FOR PROPOSED HYDROGEN ADDITIVE FLOW SHEET

Component	Dose Rate at Detector 1 (mR/hr)	Dose Rate at Detector 2 (mR/hr)	Dose Rate at Detector 3 (mR/hr)	Dose Rate at Detector 4 (mR/hr)
11.6 m of 20-in. steam line that enters HP turbine above floor	0.0244	17.3	0.907	11.0
High pressure turbine	0.0429	6.01	0.189	1.95
CIV-4 and piping	9.38	62.2	0.128	15.3
CIV-5 and piping	0.00772	1318.0	0.00333	23.9
CIV-6 and piping	7.38×10^{-6}	55.3	9.44×10^{-5}	15.3
Low pressure turbine "A"	0.370	5.20	0.0275	6.94
Low pressure turbine "B"	0.0278	23.8	0.00370	13.3
Low pressure turbine "C"	0.00132	5.20	4.45×10^{-4}	6.94
Total	9.85	1493.0	1.26	94.6 (154.5 for CIV-1,2,3) 149.1

3.3 TASK B-2. ADDITIVE VOLATILITY/DECOMPOSITION — OFF-GAS SYSTEM MODIFICATION (R. J. Law)

Objective. Each of the potential oxygen suppression additives and its volatile decomposition products will be continuously stripped into the steam phase in the reactor vessel. These volatile components are subsequently extracted from the condenser by the steam jet air ejector (SJAE) and, with any fission product gases present, constitute the inlet flow of the off-gas treatment system. The exact magnitude of the inlet gas flow to the offgas for each additive must be determined. It is possible that the gas flow will be several times larger than that in the current, no-additive situation and will dictate an increase in the size of the system components and piping. In addition, the altered composition (including trace impurities) of the offgas may alter the recombiner performance, affect the hydrogen explosion hazard, and will be of special significance if hydrogen is to be recycled as the feedwater additive.

3.3.1 Off-Gas Base Line Impurity Measurements

The objectives of the base line impurity analysis program were to determine the concentrations of trace gas components (Kr, Xe, CO, CO_2, NO, NO_2, O_3, CH_4, and higher hydrocarbons) in the offgas of a typical BWR. These tests were conducted at Nine Mile Point 1 during July and August of 1978 as a supplementary task to the Alternate Water Chemistry Additive Program. The results will be used to evaluate (a) the potential interaction of the impurities with an additive, and (b) the overall effects of these impurities in the various modifications being postulated for the off-gas system.

Nine-Mile Point 1 was selected as the test site since it has a recombiner typical of present BWR off-gas systems and there existed an approved sampling device in the Improved Noble Gas Retention System (INGR) that was tied into the off-gas system at the proper location. This eliminated the cost and time of installing sample taps, sampling hardware and obtaining subsequent site agreements, approvals, and procedures.

3.3.1.1 Test Location

The test equipment was located on the 250-ft level, southwest corner of the Nine Mile Point 1 turbine building, adjacent to the 30-min holdup pipe. The INGR sampling system was used to supply an off-gas sample for analysis then return it to the main condenser for subsequent off-gas treatment. Figure 3-9 indicates that portion of the system used for these tests.

3.3.1.2 Site Conditions

The Nine Mile Point 1 off-gas flow rate was checked daily during the testing period. One week prior to the initiation of the testing, the off-gas flow rate increased from 5.7 L/S to 8.5 L/S. This higher rate persisted throughout the duration of the analysis program.

The electric output during the test period was approximately 520 MW. The derated output was caused by the loss of one recirculation pump and the end-of-cycle (EOC) coast-down.

3.3.1.3 Test Equipment

The analysis equipment used for these tests is identified in Table 3-23 for each component.

The inlet and outlet tie-ins of the analysis equipment to the INGR sampling system are diagrammed in Figures 3-10 through 3-13 for each of the techniques used.

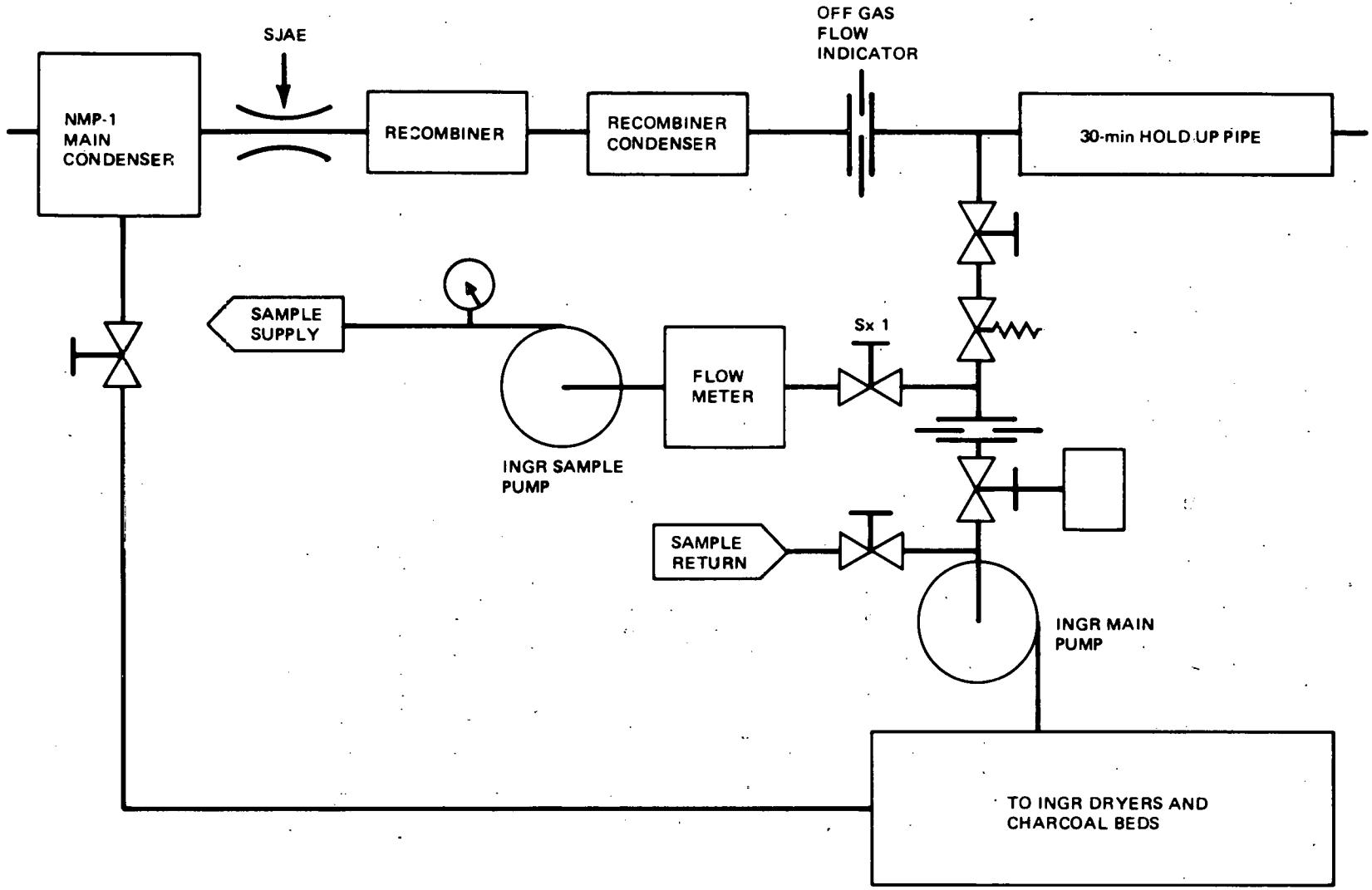

Figure 3-9. Off-Gas Sampling System

Figure 3-10 shows the gas chromatograph (GC) sampling controls and flow paths for the calibration and sample gases. The GC sample loop pressure was maintained by the backpressure regulator, BPR-1, located in the return line. The rotameter, RM-1, was used to verify that the required volume of sample gas (purge) passed through the loop before the next analysis (>5 times the GC loop volume). A schematic diagram of the internal GC flow paths and controls is shown in Figure 3-14.

The mass spectrometer (MS) sample flow path used to measure Kr is shown in Figure 3-11. The MS sample pump (VP-1) was used to draw the sample to the mass spectrometer and reduce the pressure upstream of the first orifice (FO-1). The oil-vacuum pump (VP-2) was used to reduce the pressure upstream of the second orifice (FO-2) and to maintain a low pressure, (<100 mtorr) downstream of the turbo-molecular pump (VP-3). The analysis control point for the mass spectrometer was the internal total-pressure of the analyzer chamber (1.0×10^{-6} torr) measured with an ion gauge (IG). This pressure was maintained for

Table 3-23

INSTRUMENTATION

1.	Tracor Gas Chromatograph, MT-150	Xe, CO, CO_2, CH_4 and higher hydrocarbons
2.	Dasibi Ozone Monitor, Model 8000	O_3
3.	Drager Adsorption Tubes (NO and NO_2)	NO, NO_2, O_3, $C\ell_2$
4.	UTI Mass Spectrometer	Kr
5.	EGG 880 Dew Point Hygrometer	Humidity

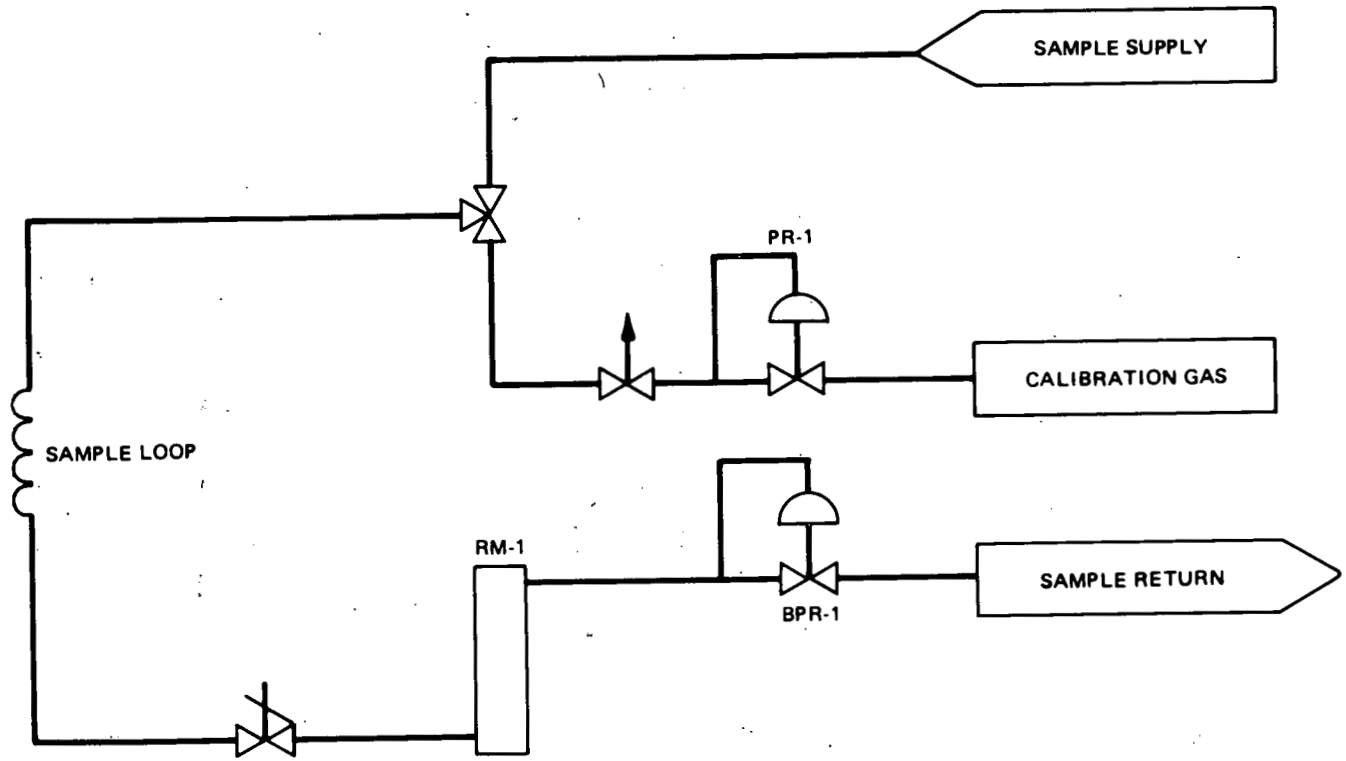

Figure 3-10. Gas Chromatograph Sampling System

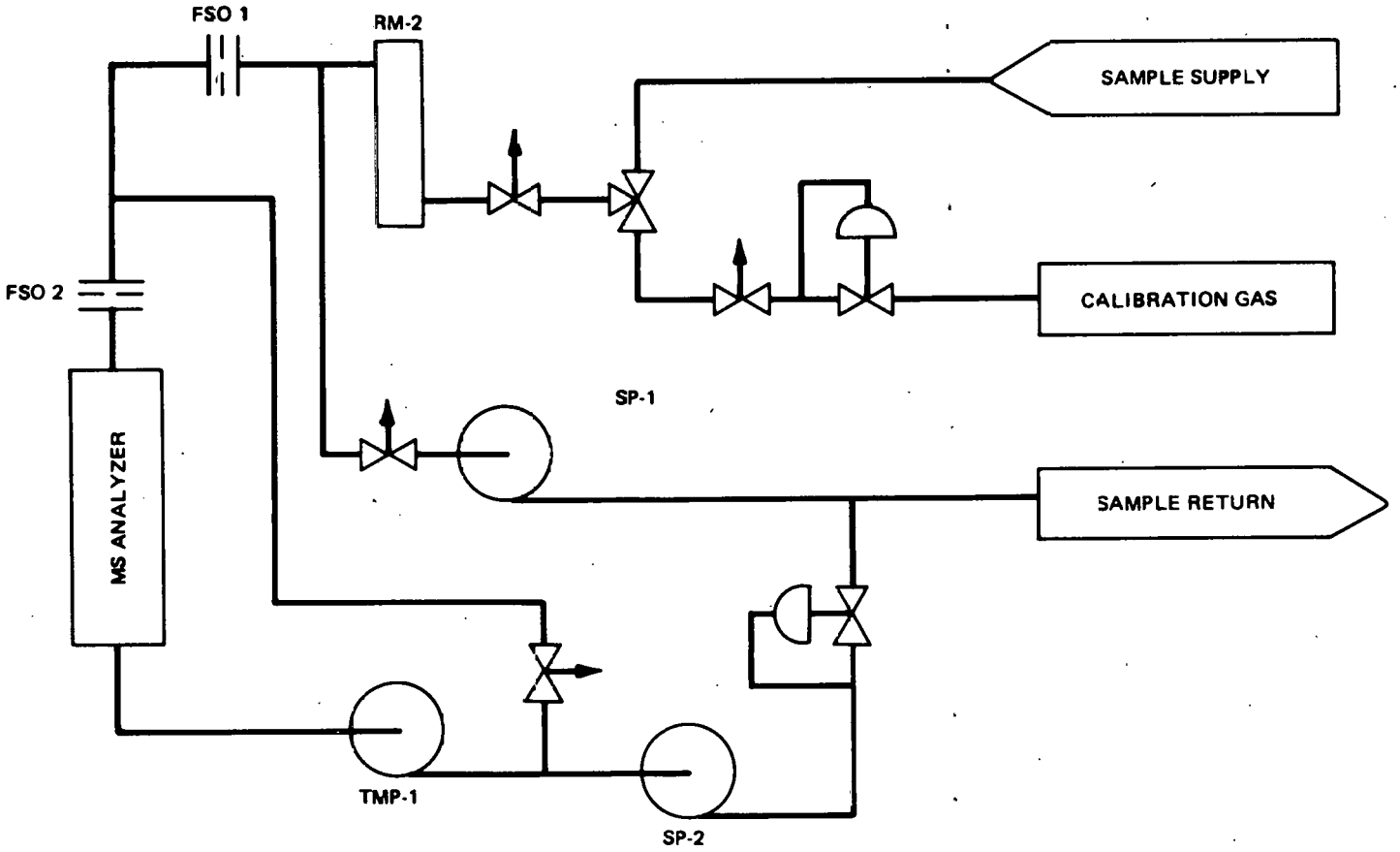

Figure 3-11. Mass Spectrometer Sampling System

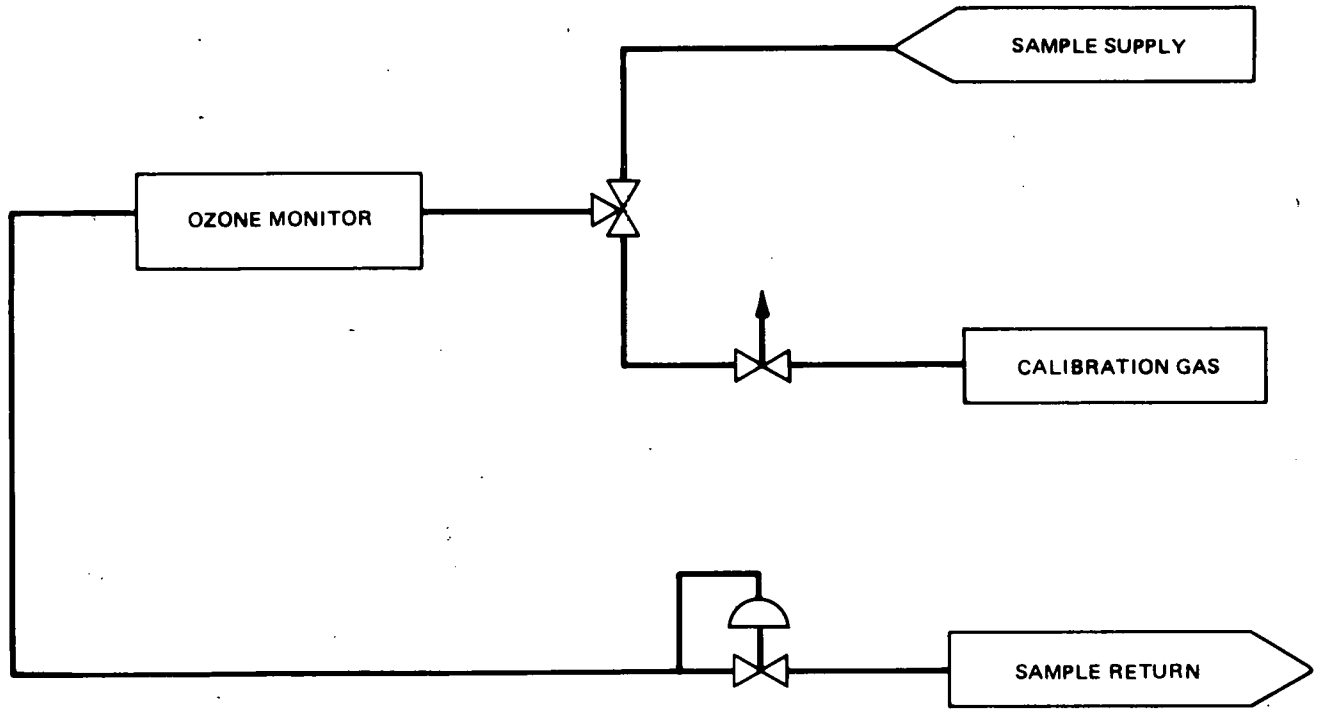

Figure 3-12. Ozone Monitoring Sampling System

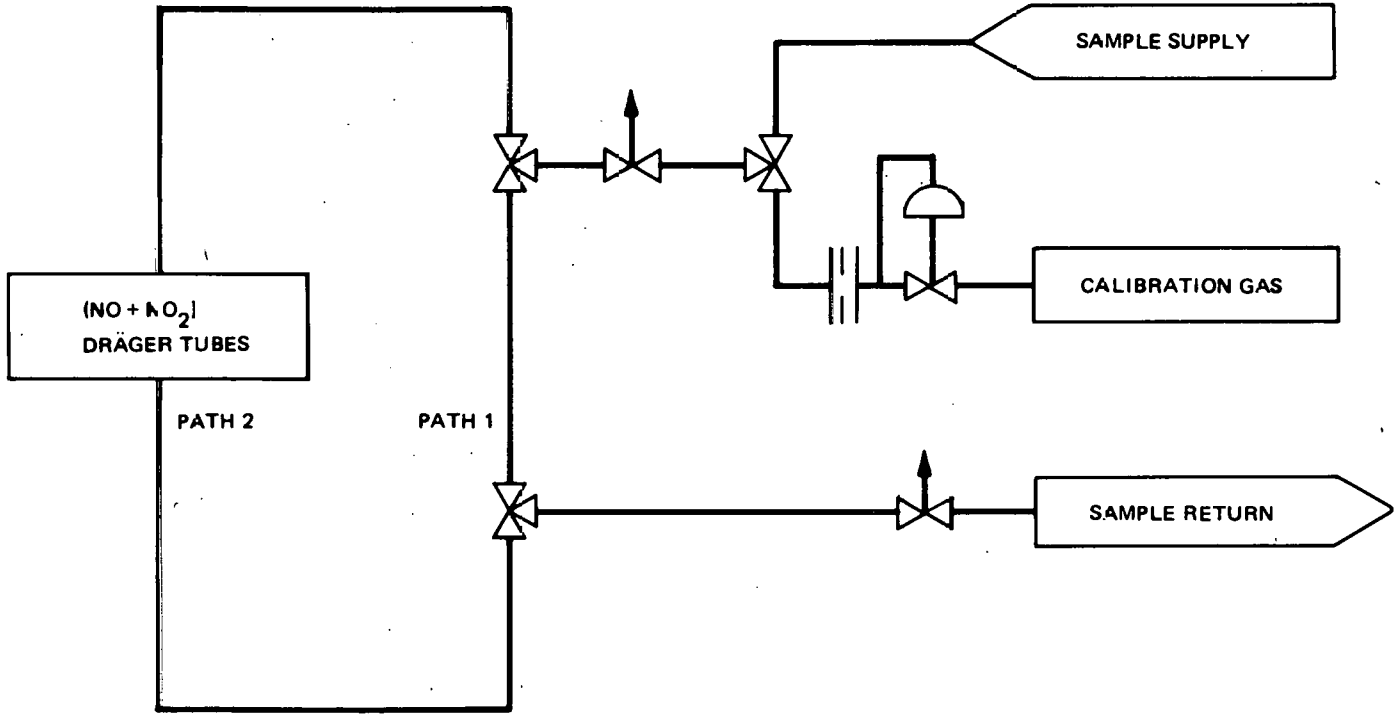

Figure 3-13. (NO+NO_2) Dräger Adsorption Tube Sampling System

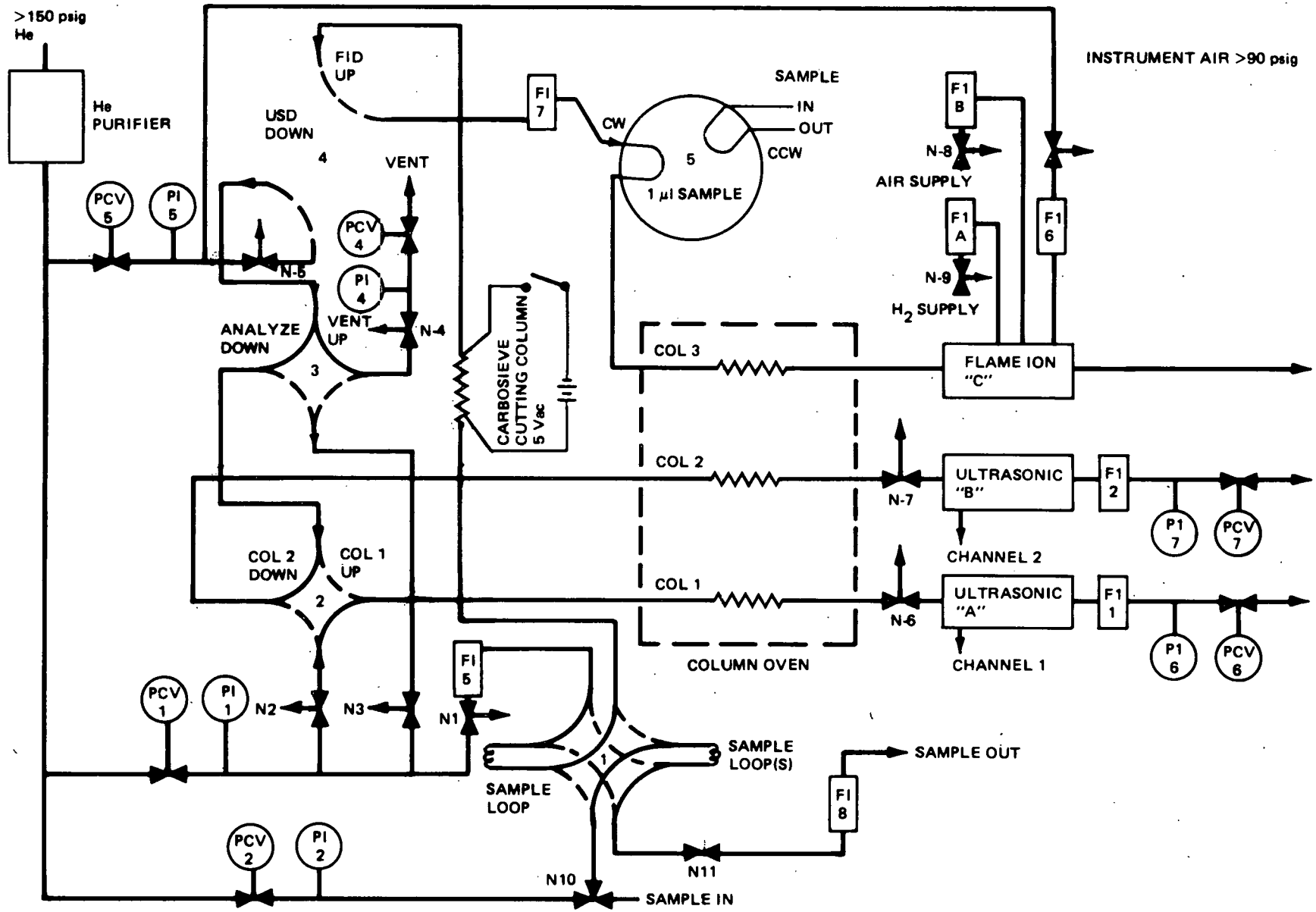

Figure 3-14. Gas Chromatograph Internal Flow Paths

the analysis of both the sample and calibration gases. The MS output signal was, therefore, a direct measurement of the Kr partial pressure.

Figure 3-12 shows the sampler controls required for the specific ozone monitor. Operational details for the above techniques are in the test plan and procedure for this task.

The NO and NO_2 analysis was performed with the backup adsorption tubes due to a malfunction of the primary monitoring system. For low NO_x concentrations, the monitor detection cell contains a very thin membrane which apparently was damaged during shipment. After considerable testing, a second cell was shipped to the site in a neutral pressure container. All precautions were taken to prevent membrane damage. After extensive tests were performed with the new detector, as per discussions with the manufacturer, the exact problem could still not be diagnosed or solved without return of the entire system to the factory.

Both the monitor and adsorption tube measuring techniques were selected for their performance with radioactive gas samples. Other NO and NO_2 analysis techniques have been tested or examined by Gas Technology, e.g., GC, MS, chemiluminescence and wet chemistry. Since the nitrogen oxides are very reactive and are usually present at low concentration in the offgas, GC techniques do not provide the required accuracy and precision. The mass spectrometer was not usable since interference due to high concentrations of mass neighbors N_2 and O_2 for NO and CO_2 for NO_2. Chemiluminescent detectors were tested for the KRB study. This type of detector was too sensitive to radiation emitted from the gas sample. Wet chemistry techniques were not considered for NMP-1 because of the gas release hazards and the expense of special wet chemistry facilities required at the sampling location.

Figure 3-13 shows the sampling schematic used with the adsorption tubes. The exact procedures, tests, and supplementary calibrations required for the adsorption tube method are contained in the test procedures.

3.3.1.4 Analysis and Results

The operational details for each component analysis, except for NO and NO_2, are located in the test procedure and the associated standard operating or calibration procedures. The final concentration results of the measured impurities with the lower measurable limits are listed in Table 3-24.

In general, the detection limit was based on a signal-to-noise ratio of 2:1.

The analysis of $NO+NO_2$ was complicated by the closed-loop approach required to analyze the radioactive gas, versus the normal use of the tubes utilizing the open-exhausted hand-pump. The tube markings are calibrated for a particular number of pump strokes. Although the pump volume (100 cc) was accurate, the flow varies from >1000 cc/min to zero in a nonlinear manner during each stroke. This type of flow characteristic could not be duplicated with the closed-loop sampling system. The response of the detection tube to variations in constant flow rates were measured and are reported in the test file, Section 4.2.2.11. The responses of the tubes tested with off-gas samples are listed in Table 3-25.

Table 3-24

OFFGAS IMPURITY CONCENTRATIONS AT NINE MILE POINT 1, SUMMER OF 1978

Component	Concentration (vppm)[a]	Detection Limit (vppm)
Kr	1.1	0.1
Xe	<(0.2)	0.2
CO	1.1	0.5
CO_2	700	10
CH_4	2.8	0.2
Higher Hydrocarbons	<(0.1)	0.1
NO†	∿6 ±3	2
NO_2	<(0.2)	0.2
O_3	<(0.03)	0.03

[a]vppm = volumetric parts per million

Table 3-25

QUALITATIVE RESULTS OF VARIOUS ADSORPTION TUBES TO OFF-GAS SAMPLES
(at 100 sccm for 5 min)

Tube Type	Response
$NO + NO_2$ (NO catalyzed to NO_2)	Blue color change
Ozone	No change
NO_2	No change

According to the manufacturer, only chlorine (Cl_2) and Ozone (O_3) interfere with the selectivity of the NO_2 detecting agent. The total nitrogen oxides measured with the NO+NO_2 type tube are obtained by oxidizing the NO to NO_2 in the sample gas with a Cr (VI) catalyst located in the tube inlet. The NO_2 type tube does not contain CR (VI) and is not sensitive to NO. No response was observed using the NO_2 or the O_3 type tubes; therefore, only NO and not NO_2, O_3 or Cl_2 was responsible for the color change in the NO+NO_2 tubes. The lack of response with the O_3 detection tubes confirms the result obtained previously with the ozone monitor.

3.3.1.5 Discussion

The Nine Mile Point 1 results were similar to those obtained from previous studies performed at KRB and are also in agreement with values expected from turbine-building air inleakage. Turbine building air analyses were performed for Kr, CO, CO_2 and NO+NO_2. These tests showed a similar amount of Kr, less than half as much CO and very little NO+NO_2 (<0.1 ppm). It appears that CO and NO are generated in the reactor system or recombiner.

Two accidental releases of CO_2 into the 250-ft level from the fire extinguishment system occurred 1 and 2 weeks prior to the CO_2 off-gas analysis. There was no sure way of determining if these releases had any effect on the later CO_2 analysis but measurements of the local turbine building air for CO_2 (300 vppm) agreed with the reported normal air concentration. The 700 vppm

CO_2 value measured in the offgas is similar to the high concentrations obtained at KRB in 1971 (800 to 1000 vppm) and in 1974 (1500 vppm).

The potential interactions of these impurities with the proposed additives and the effects on the off-gas treatment system are being evaluated.

3.3.2 Off-Gas System Mass Balances

The mass balance flow sheets for the single-pass hydrogen addition cases to maintain 10 ppb and 50 ppb O_2 in the core exit water are shown in Figures 3-15 and 3-16, respectively.

3.3.2.1 Potential Problems

For these two cases, the hydrogen in the steam is partially recombined with the condenser inleakage oxygen in the off-gas catalytic recombiner. The excess hydrogen then passes through the off-gas treatment system with the condenser inleakage nitrogen. This single-pass approach is simple but certain questions must be answered before this approach can be utilized. The major concerns are:

a. Operational. The total flow rate through the off-gas treatment system could be 2 to 3 times the design flow rate, depending on the level of hydrogen addition. At the higher flow rates, the operation of the desiccant dryer, used to condition the offgas to an appropriate dew point, would be marginal. The decontamination factor provided by the activated carbon column would be reduced and the pressure drop across the off-gas system would be increased at the higher flow rates.

b. Safety. The off-gas hydrogen concentration downstream of the recombiner would be approximately 80 percent. Any air inleakage into the off-gas system would constitute an explosion hazard. The General Electric supplied off-gas treatment systems operate at a

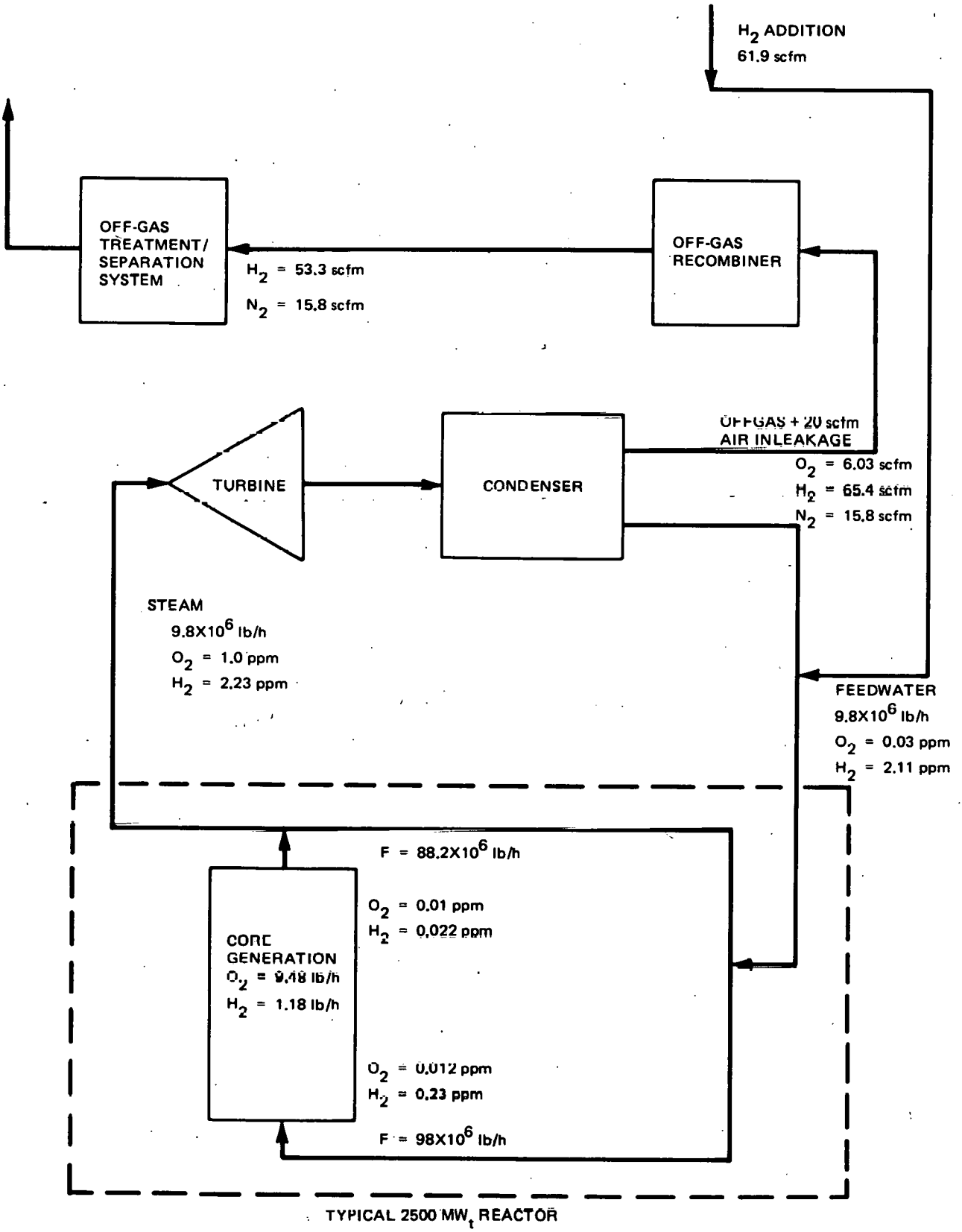

Figure 3-15. Hydrogen Addition-10 ppb Oxygen in Core Exit Water (One Pass for Hydrogen)

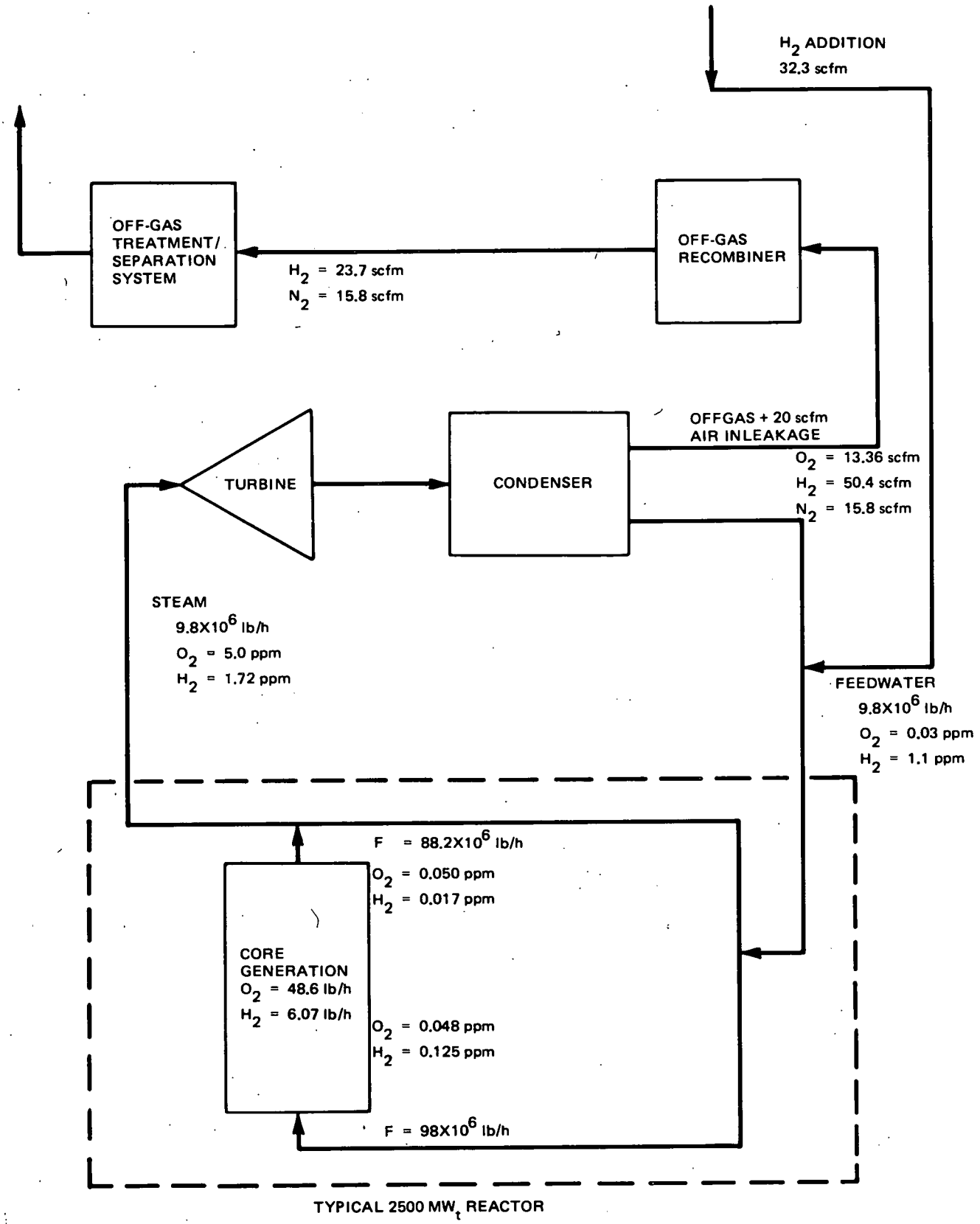

Figure 3-16. Hydrogen Addition-50 ppb Oxygen in Core Exit Water (One Pass for Hydrogen)

slight positive pressure such that air inleakage should not be a problem. However, some off-gas systems supplied by other vendors operate at a negative pressure. Air inleakage into these systems could be a potential problem.

The single-pass hydrogen addition is a simple approach requiring no changes to the present off-gas system if the identified problem areas can be properly addressed.

3.3.2.2 Improved System

One method for resolving these problem areas is to add oxygen immediately upstream of the off-gas recombiner. With oxygen addition, the gas flow rate downstream of the recombiner is reduced and the explosion hazard is eliminated because the hydrogen is totally recombined. Figures 3-17 and 3-18 show the mass balance flow sheets for hydrogen addition to maintain 10 ppb and 50 ppb O_2 in the core exit water and with oxygen addition at the inlet of the off-gas recombiner to oxidize essentially all the hydrogen in the offgas.

With this oxygen addition approach the off-gas flow rate is below the design value of the off-gas treatment system. The composition of the offgas downstream of the recombiner would be essentially only nitrogen; thus eliminating the safety problems.

A preliminary design of an oxygen addition system is shown in Figure 3-19. The equipment and installation costs for the oxygen addition system have been estimated and are shown in Table 3-26. The operating costs for the oxygen would be approximately $6500/mo for the 10 ppb case and $3000/mo for the 50 ppb reactor water oxygen concentration case.

3.3.3 Current Activities

Effort on this task is being directed toward developing the mass balance flow sheets for the other two additives and for the hydrogen addition with hydrogen

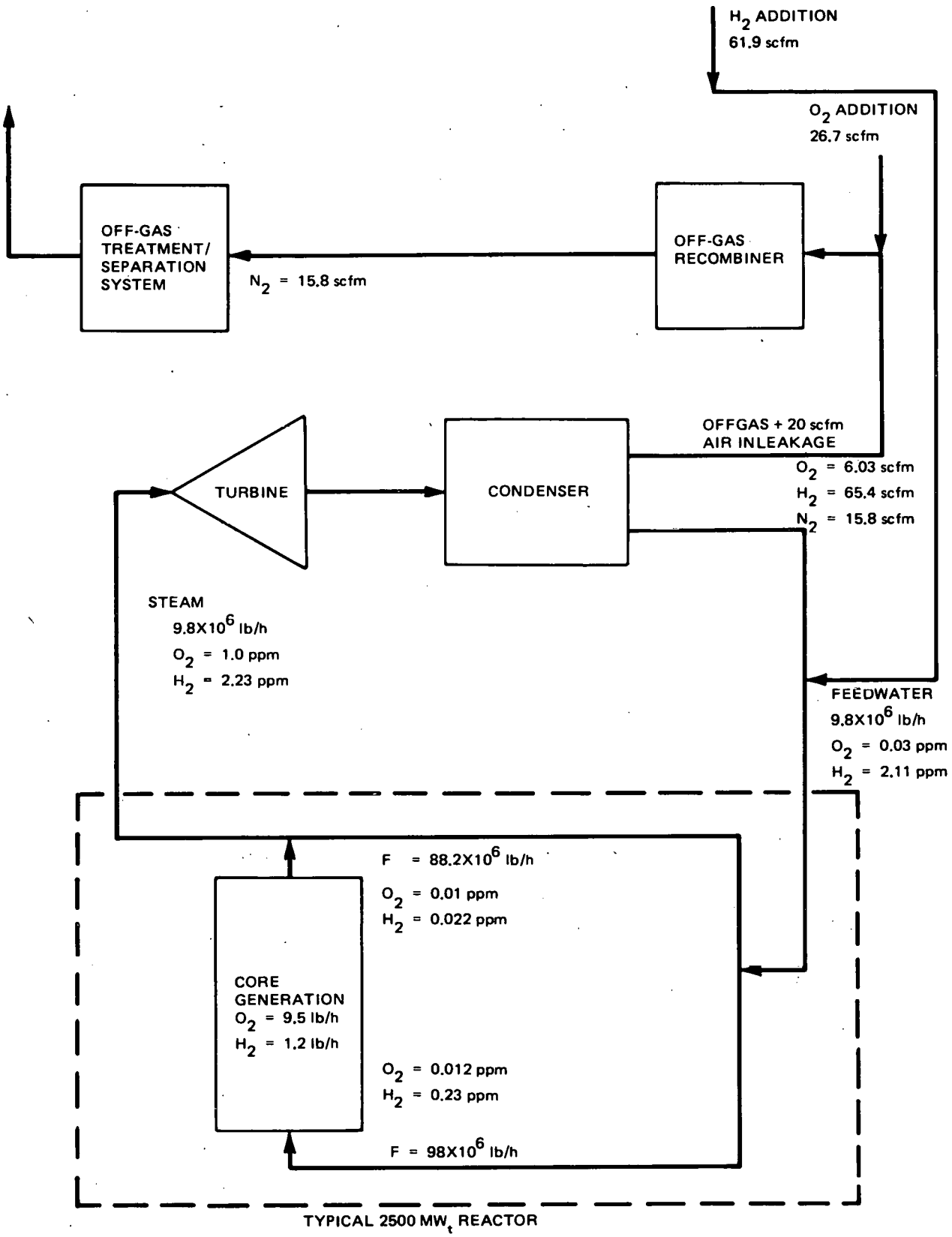

Figure 3-17. Hydrogen Addition-10 ppb Oxygen in Core Exit Water (One Pass for Hydrogen and Oxygen Addition to Recombine Hydrogen)

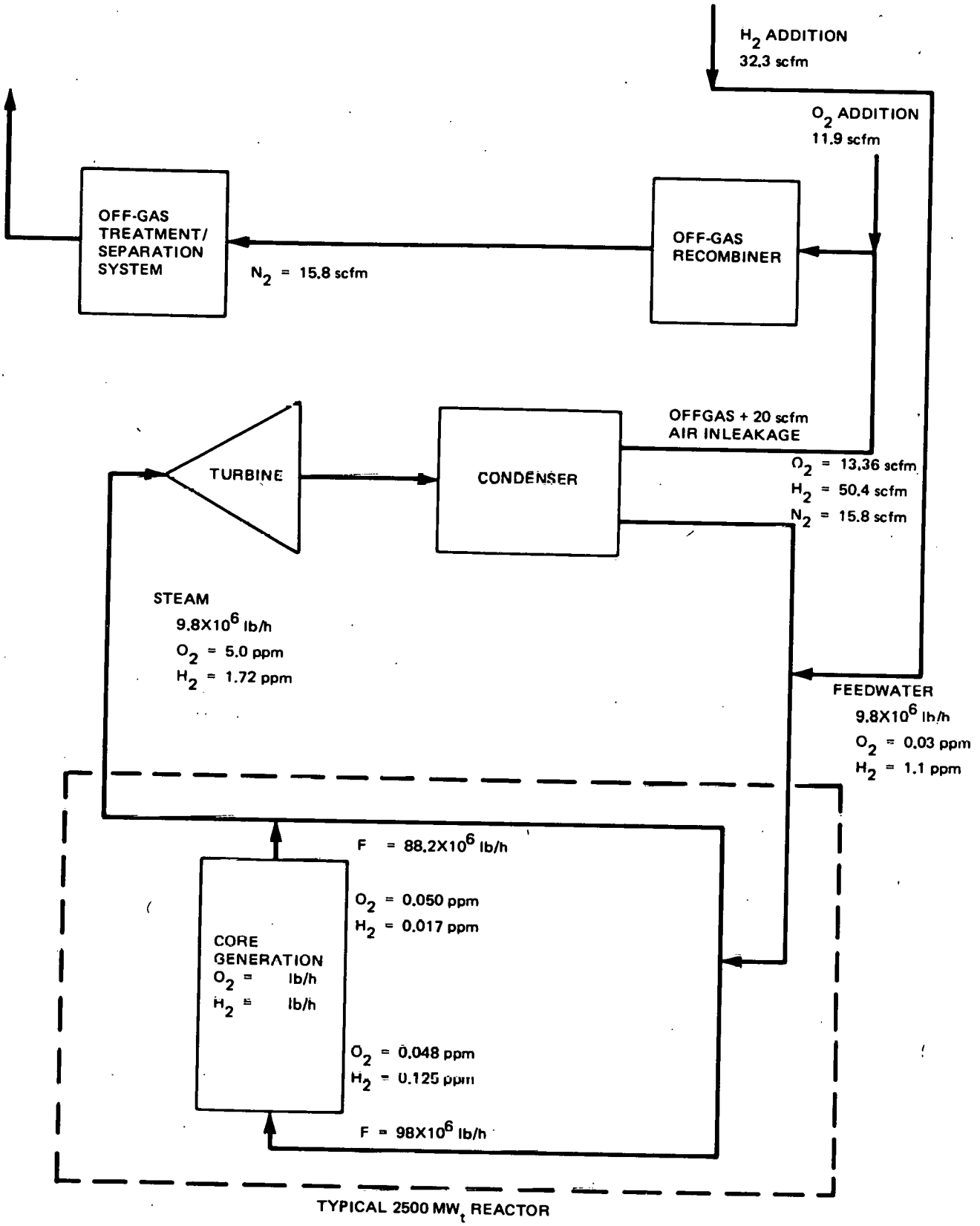

Figure 3-18. Hydrogen Addition-50 ppb Oxygen in Core Exit Water (One Pass for Hydrogen and Oxygen Addition to Recombine Hydrogen)

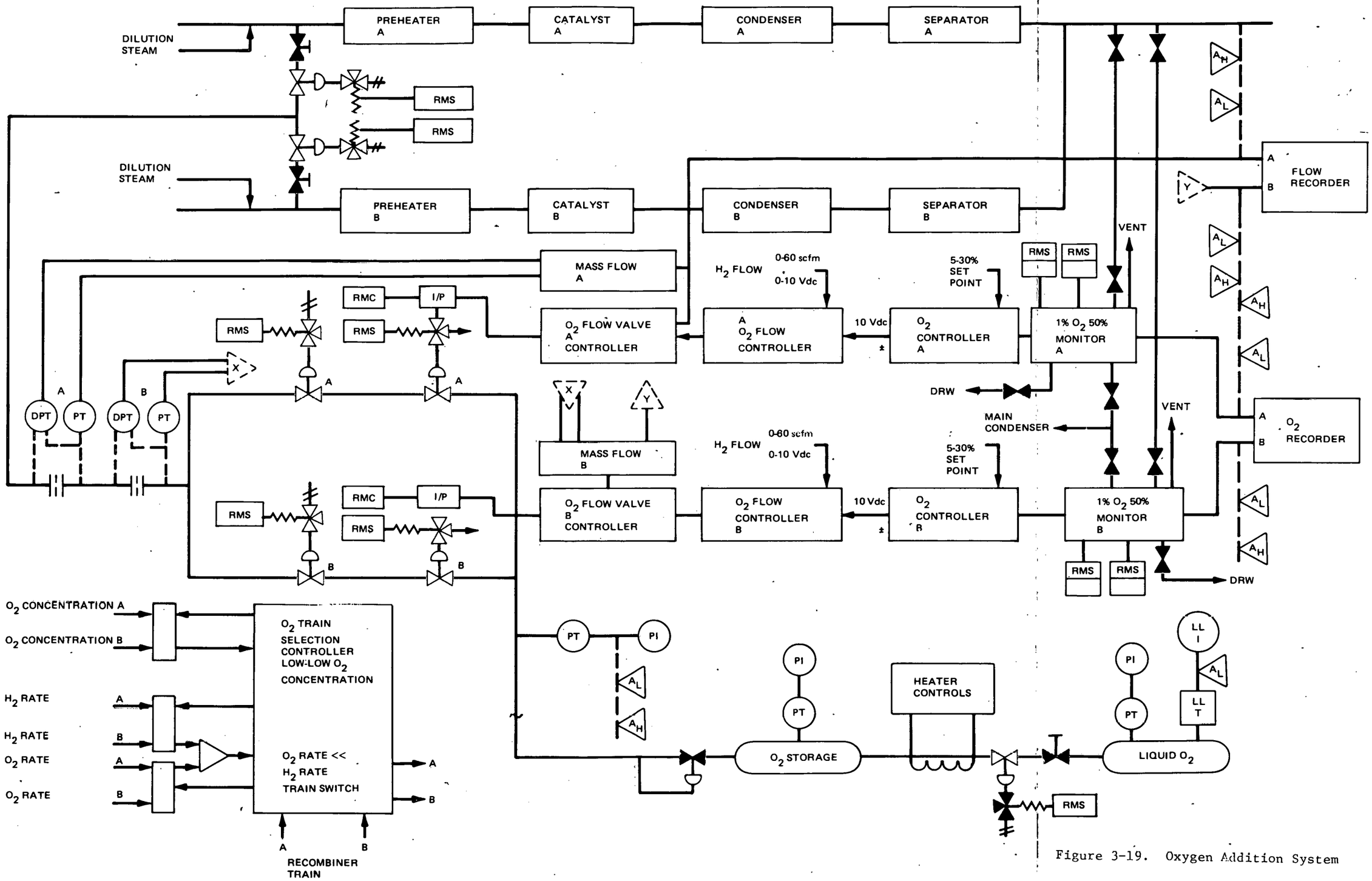

Figure 3-19. Oxygen Addition System

separation downstream of the off-gas recombiner. This task will be completed during the forthcoming quarter.

Table 3-26

O_2 ADDITION SYSTEM EQUIPMENT AND INSTALLATION COST

I.	Liquid oxygen supply system consisting of a 6000-gal vessel and vaporizer and installation	$ 80K
II.	Oxygen addition control system	
	A. Equipment consisting of O_2 analyzers, flow element, controllers, valves and piping	190K
	B. Engineering, installation and testing	170K
	Total	$440K

3.4 TASK B-3. COOLANT LEAKAGE MONITORING (L.L. Sundberg)

Objective. Uncorrected condenser leakage can quickly exhaust the BWR full flow, condensate demineralizers and inject undesirable impurities, including chloride, into the reactor water. With ionic additives such as NH_3 or N_2H_4, the condensate conductivity becomes about 35 μS/cm and simple conductivity is no longer a sensitive leakage monitoring technique. An alternative leakage detection system must be selected and evaluated.

3.4.1 Chloride Monitor

An in-line specific-ion electrode chloride monitor has been received from its vendor, Orion Research Corporation. The unit is very similar to the sodium monitor in many respects. The total size of the package, plumbing, polishing column, and dynamic calibrator are identical. There are, however, two subtle differences. In the chloride analyzer, the process stream passes through 2 feet of diffusion tubing which is immersed in 88% formic acid. Gas phase diffusion of formic acid lowers the pH of the sample stream, thereby decreasing the concentration of OH^- and improving the selectivity of the electrode. The pH of the effluent is roughly 3.0. There is no temperature compensation circuitry in the chloride monitor. The temperature is held constant by a circulating water bath which operates at 4°C (39°F).

3.4.2 Instrument Calibration

The sodium and chloride monitors were installed in the laboratory and calibrated using mechanically driven calibration syringes and standard calibration solutions of NaCl. In spite of the overall simplicity of the syringe calibrators, they were checked and are very accurate. A known standard was injected at various flow rates into the process stream (40 mℓ/min). The calculated standard values and the meter readings are in excellent agreement within the limitations of reading the meter.

Calculated Cl^-	Observed Cl^-
50 ppb	50 ppb (setpoint)
40	40
30	30
20	20
10	10
5	4
2.5	2
25	25
28	30

Calculated Na^+	Observed Na^+
100 ppb	100 ppb (setpoint)
50	50
10	10
5	5
1	1
0	0.15

The calibration of these analyzers requires extremely accurate delivery on the calibrator and rotameters. These devices are calibrated by classical stopwatch/gravimetric techniques. If and when these units go to a site, formal calibration procedures will be generated.

The ability to observe sodium and chloride "free" water appears quite good. After calibration, the building demineralized water was passed through the ion-exchange columns built into the systems. The chloride monitor indeed read 0 ppb, in the absence of flow perturbations. The base line sodium value was 0.15 ppb (lowest scale reading 0.1 ppb, zero undefined on logarithmic scale). The mixed bed resin column is manufactured by Barnsted. The particular resins are HCR (cation) and SBR-P (anion). These acronyms are from Nalco Chemical Co. (Nalcite), the material distributor. Thus, the cation resin could be Duolite C-20 (Diamond Alkali), Dowex 50 (Dow), C-240 (Ionac), or

Amberlite IR-120 (Rohm & Haas); the anion could be Duolite A-101D, Dowex 1, Ionac A-540 or Amberlite IRA-402. The nominal mesh size is 30-50. For consistency, it would be worthwhile to purchase resins and fabricate columns. Since the direction of flow through the column is upward, a finer mesh size could be tolerated for better polishing.

3.4.3 Instrument Stability and Sensitivity Testing

The systems were run for approximately 1 month on laboratory demineralized water, from the same outlet. Chloride levels ranged from 1 to 4 ppb, sodium from 0.4 to 1.0 ppb. Long-term stability under steady-state conditions appeared excellent. The manufacturer recommends that the diffusion tubing (silicone rubber) in the chloride monitor be replaced on a biweekly basis, owing to short-term degradation from external contact with formic acid; the same tubing which is used in the sodium monitor has a quoted longevity of 6 months.

The range of the received chloride monitor was 0 to 50 ppb (linear scale). This was contradictory to the range specified on the purchase order (0 to 250 ppb). Orion has agreed to retrofit the electronics to give us the desired range.

Response time for the chloride monitor is excellent. Full range upscale response is 10 sec at a flow rate of 40 mℓ/min; downscale response is about 30 sec. The sodium monitor is somewhat worse (10 min full downscale response for complete recovery, equivalent upscale response time). On both, a lag time of 45 sec is observed from the time the sample first enters the system at a flow rate of 40 mℓ/min.

A second series of calibration data for the chloride monitor was generated in the following manner: A stock solution (2325 ppb $C\ell^-$) was injected into the polished dilutant (0 ppb $C\ell^-$) at four constant flow rates (0.35, 0.43, 0.52, 0.70 m /min). When the dilutant flow rate was 40 m /min, the corresponding concentrations were 20, 25, 30, and 40 ppb $C\ell^-$, respectively. Increasing/decreasing the flow rate of the dilutant would therefore decrease/increase the

chloride concentration when the injection rate is held constant. The theoretical concentrations for these experiments can be derived from the following equation.

$$\frac{f_d C_d + f_i C_i}{f_d + f_i} = C_{Cl^-}$$

where

f is flow rate

C is concentration

Subscript i is injectant

Subscript d is diluent

The manufacturers recommended diluent (sample) flow rate is 40 mℓ/min. The results for various NaCl concentrations and sample flow rates are given in Table 3-27 and Figure 3-20.

In most cases, the agreement between the observed and calculated values is reasonable when the flow rate is maintained close to the manufacturer's recommended value. Deviations are, however, substantially greater when the flow rate and/or concentration is lower. This was confirmed with another experiment. The monitor was calibrated, and the concentration of laboratory demineralized water measured as a function of sample flow rate. Readings were recorded 5 min after adjustment. The data are shown in Figure 3-20 with the data from the sodium monitor. While the sodium analyzer showed negligible (if any) response to changes in flow rate from 35 to 50 mℓ/min, the chloride monitor gave large variations depicting an inverse parabolic correlation between the two parameters. A significant improvement on the flow regulation system is sorely needed if meaningful data are to be obtained in the vicinity of 0 to 5 ppb.

Table 3-27

CHLORIDE MONITOR PERFORMANCE

Flow Rate Injectant	Diluent mℓ/min	Chloride Concentration (ppb) Calculated	Measured
0.70	45	36	36
0.70	40	40	40
0.70	36	44	42
0.70	30	53	off scale
0.52	45	26	26
0.52	40	30	30
0.52	36	33	33
0.52	30	40	39
0.43	50	20	20
0.43	45	22	23
0.43	40	25	25
0.43	35	28	36
0.43	30	33	38
0.43	25	40	off scale
0.43	20	49	off scale
0.35	45	18	14
0.35	40	20	20
0.35	36	22	16
0.35	30	27	29

Various substances were injected into the analyzer inlets to observe chemical transient responses at base line levels. While 2 mℓ of concentrated ammonia caused the chloride monitor to go off scale high (chloride impurity or OH^- response), the sodium monitor remained unchanged. This is important in that the condenser leak can be detected during a major ammonia transient. The injection of 2 mℓ 1M HNO_3 caused the sodium monitor to go off scale high, while the chloride monitor drifted slightly upward. Air injections caused the flow rate in both systems to decrease, yielding the expected positive response in the chloride monitor. The sodium analyzer was not affected.

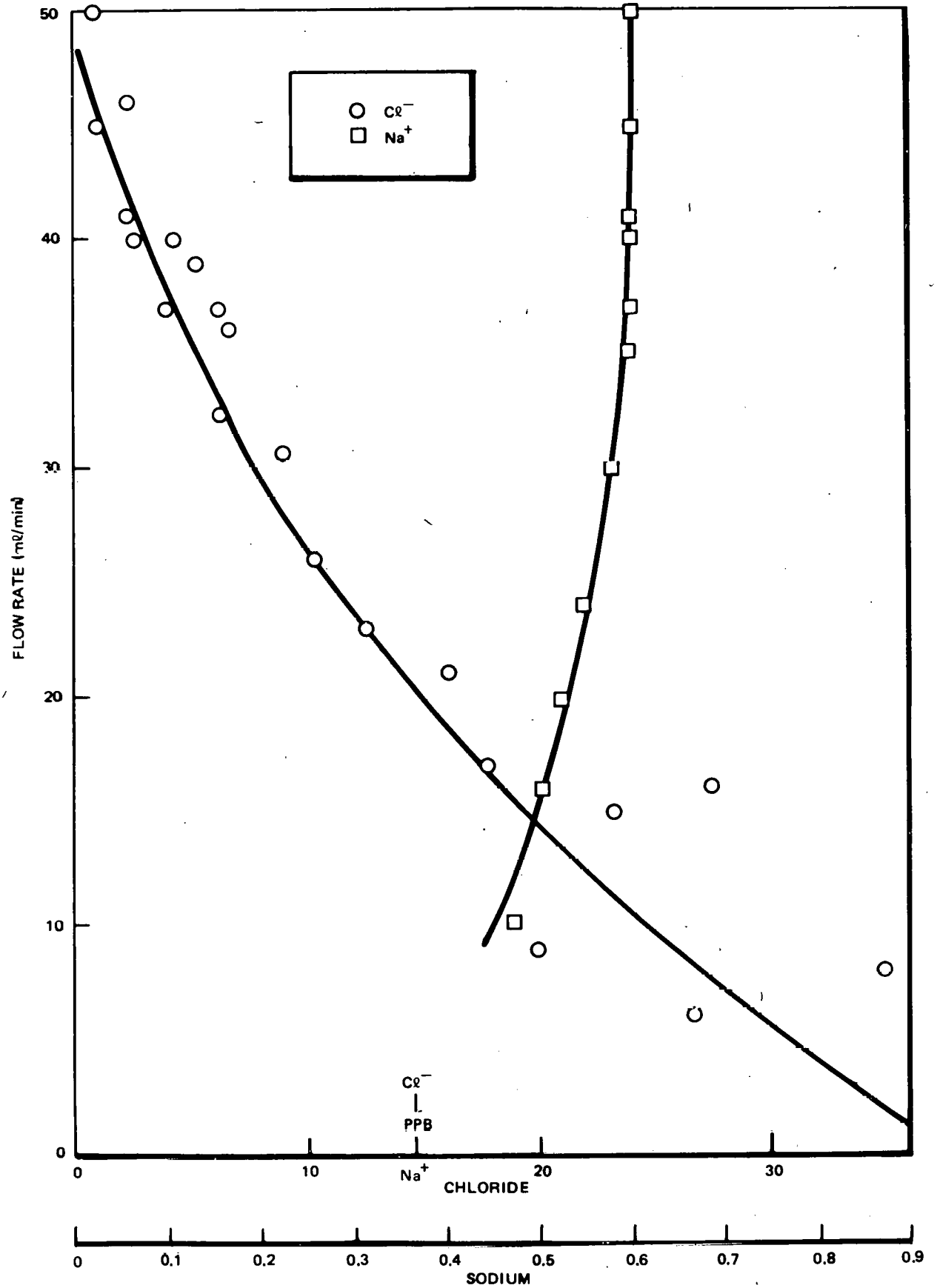

Figure 3-20. Chloride and Sodium Monitor Variation With Sample Flow Rate

3.4.4 System Modifications

In addition to improvement of the flow regulation system on the chloride monitor a transparent cooling water housing which jackets the electrode chamber should be added. The unit does not permit an inspection for entrapped air/steam bubbles in the vicinity of the electrode tip without complete disassembly. Since bubbles can only be unfavorable to the system, this retrofit is essential.

The maximum sample temperature the sodium monitor can tolerate is 50°C. Above this temperature, the compensation circuitry is not linear. The cooling water bath for the chloride monitor does not have sufficient capacity to handle an incoming stream whose temperature is greater than 45°C. Thus, larger sample coolers, similar to those employed for corrosion product sampling, are required for both systems. If and when the units are on line in a power plant, strict attention must be given to the cooling water supply. If cooling water is shut off, inadvertently or otherwise, the electrodes may be irretrievably damaged.

The chloride analyzer evaluation cannot be completed until an electronic retrofit which yields 0 to 250 ppb full scale is obtained. The sodium monitor appears to be ready for use in a power plant if the following minor design changes (which are also recommended for the chloride monitor) are made:

a. Improve the sample rotameter,

b. Improve the pressure regulator,

c. Replace the flow control valve,

d. Introduce a flow transducer upstream of the rotameter,

e. Have a multipoint recorder or data acquisition system available to monitor concentration, temperature and flow rate,

f. Filter and process stream prior to the sodium or chloride monitor inlet, and

g. Introduce a thermistor in the analyzer drain lines.

3.5 TASK B-4. PLANT MATERIALS COMPATIBILITY (B. M. Gordon)

Objective. A primary concern in the application of an AWC to the BWR is the possibility of materials-coolant incompatibilities which might be introduced. This task, in addition to evaluating the necessary and limiting additive and oxygen concentrations necessary to mitigate stress-corrosion cracking tendencies in the primary coolant loops, will investigate the general corrosion behavior of normally encountered BWR materials in the proposed additive chemistry environment.

The tests in the program are specifically designed to not only demonstrate that the various AWC's do indeed prevent stress-corrosion cracking of typical BWR structural materials, but also do not in themselves produce any detrimental or unacceptable corrosion problems.

3.5.1 Constant Extension Rate Tests (F. P. Ford, Corporate Research and Development Center, Schenectady, N.Y.)

The effect on the stress-corrosion susceptibility of sensitized Type-304 stainless steel of adding 20 ppm ammonia to BWR quality water at 288°C has been evaluated for various oxygen-levels in the water.

The evaluation was made by the CERT technique at a strain rate of 1.3×10^{-4} $minute^{-1}$, the cracking response being measured in terms of a "maximum" crack-propagation rate defined by [maximum observed crack penetration/test time], as discussed previously.[1] This method of evaluation and presentation is preferred over the standard technique of comparison of ductility parameters (elongation, reduction in area etc.), especially when attempting to distinguish between small differences in stress-corrosion susceptibility.

The results are tabulated in Table 3-28 and are shown in Figure 3-21 for initially smooth specimens and in Figure 3-22 for notched specimens.

Table 3-28

EFFECT OF AMMONIA ON STRESS CORROSION CRACKING OF TYPE-304 STAINLESS STEEL AT 288°C

Specimen	YS (ksi)	UTS (ksi)	% RA	Maximum Crack Penetration (in.)	O_2 (ppm)	NH_4^+ (ppm)	Test Time (hr)	Velocity (mils/day)
(a) Smooth Specimens								
Argon								
1A1	22.25	73.00	67	--	--	--	--	--
0.2 ppm O_2 Nominal								
1A3	20.00	69.00	36	0.033 I/G-T/G	0.2 /0.25		53.5	14.8
1B2	19.39	73.10		0.006 T/G	/0.25		77.1	1.85
1B3	21.44	70.86	55	0.020 I/G-T/G	0.16 /0.17	20.7	61.0	7.86
0.01 ppm O_2 Nominal								
1A4	19.50	71.00	54.0	0.017 T/G	0.02 /0.025	--	70.5	6.0
1A18	19.00	70.40	59.0	0.018 T/G	0.001/0.005	--	71.1	6.1
1B1	19.04	71.17	57.0	0.009 T/G	0.003	--	72.9	2.9
1B4	17.10	71.60	55.0	0.012 T/G	0.003/0.036	21.1	75.0	3.8
(b) Notched (0.013 in. depth) Specimens								
Argon								
1A5	23.10	80.0	46	--	--	--	--	--
0.2 ppm O_2 Nominal								
1A7	23.71	66.87	27	0.029 I/G-T/G	0.15 /0.2	--	30.41	23.0
1B10	22.36	72.27	34	0.029 I/G-T/G	0.2	--	35.58	19.59
1B7	20.54	62.60	26	0.047 I/G	0.16 /0.17	22.0	28.3	39.8
0.05 ppm O_2 Nominal								
1B9	29.18	77.64	29	0.021 I/G-T/G	0.074	--	32.25	15.56
1B6	22.6	76.46	-	0.030 I/G-T/G	0.07	22.3	38.7	18.60
0.01 ppm O_2 Nominal								
1A8	23.10	77.94	38	0.005 T/G	0.025	--	42.2	2.8
1B8	18.11	66.04	37	0.011 T/G	0.009	--	44.1	5.9
1B5	22.10	74.40	35/41	0.009 T/G	0.004/0.006	21.3	44.3	4.87

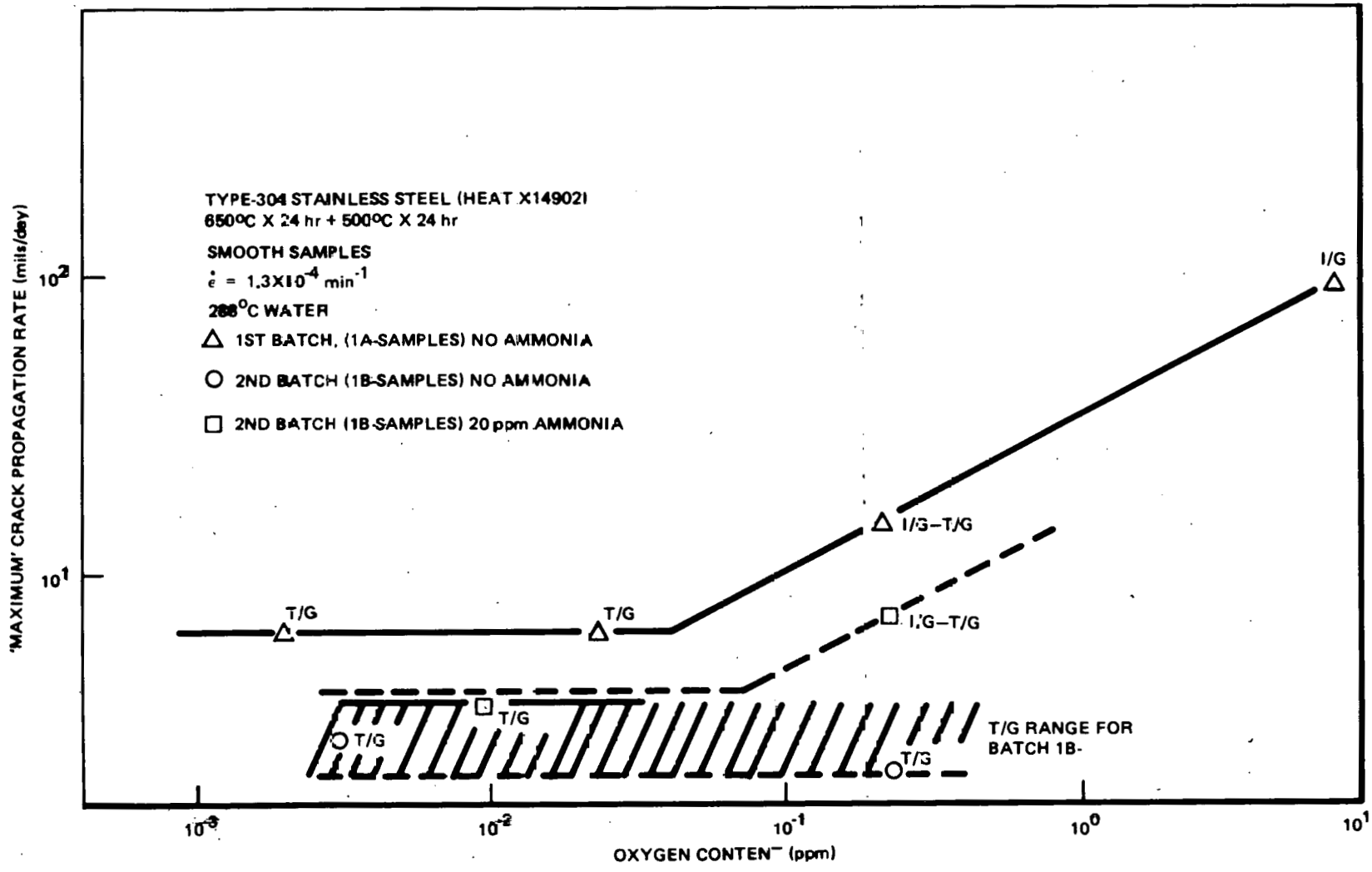

Figure 3-21. Crack Propagation Rate versus Oxygen Content for Smooth Samples

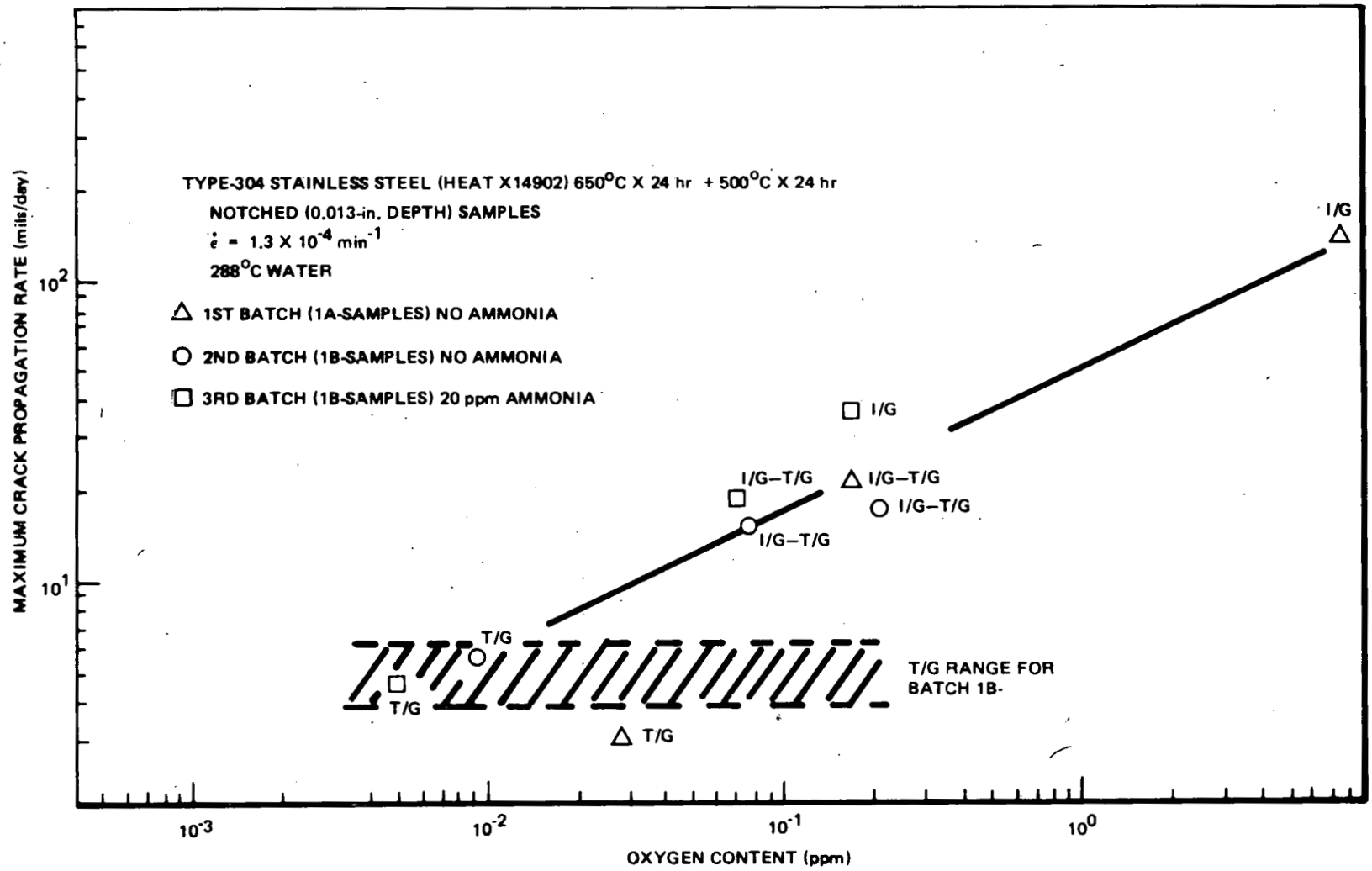

Figure 3-22. Crack Propagation Rate versus Oxygen Content for Notched Samples

The conclusions are:

a. There is a difference in results, for those tests without ammonia addition, between those specimens prefixed 1A and those prefixed 1B. (These batches were heat-treated, nominally under the same conditions, but at different times.) This difference in results in most marked on the initially smooth specimens (Figure 1) and is most likely related to an alteration in the ease of crack nucleation; note, for instance, that in the 0.2 ppm oxygen solution I/G cracking was not initiated in the 1B series (Specimen 1B2), whereas it was in the 1A series (Specimen 1A3). As expected, there was not such a marked difference in behavior between the two batches using prenotched samples (Figure 3-22), when chemical crack nucleation modes (which could be dependent on minor variations in heat treatment) are superseded by mechanical crack nucleation modes.

b. The maximum I/G crack propagation rate decreases with decreasing oxygen content, the crack morphology changing from I/G to T/G. As noted above, however, there is a considerable oxygen range over which this morphology change takes place, and this may also be a function of minor variations in heat treatment. The T/G crack propagation rate is essentially independent of oxygen content. At a given oxygen content, the ease of T/G crack nucleation is easier (see second quarterly report) than I/G cracking, but the crack propagation rates are considerably lower (c.f. 1B2 with 1B3).

c. The effect of ammonia was investigated using the 1B series of samples. There is not a major effect of ammonia content (20 ppm) on crack-propagation rate for a given crack morphology, e.g., compare 1B4 with 1B1 and 1B2 for T/G cracking on smooth specimens, and 1B5 with 1B8 for prenotched specimens. Any difference detected in the mixed-mode cracking range circa 0.2 ppm O_2 can be related to the different amounts of slow T/G and fast I/G cracking. For instance, the higher propagation rates for 1B7 (20 ppm NH_4^+) compared

with 1B10 (no ammonia) can be related to the higher percentage of I/G cracking in the former case; a similar explanation can be given for the higher propagation rate of 1B3 with respect to 1B2. It is unclear at this stage whether ammonia really promotes the faster I/G cracking mode (i.e., there are insufficient data to make such a positive claim), but in the situation where only I/G SCC is observed in practice (e.g., BWR operations), it would be reasonable to conclude that ammonia additions do not have a significant effect on crack propagation rates.

3.5.2 Hydrogen Addition Tests

Work is presently concentrated on Tests 1B11 - 1B13, i.e., the effect of 0.2 ppm H_2 addition to various oxygen-containing solutions on the SCC of sensitized Type-304. Difficulties persist in the attempt to satisfactorily analyze the dissolved hydrogen content; the present problem being the continual mechanical breakdown of the gas-sampling recirculation pump.

3.5.3 Straining Electrode Tests (M. Indig)

A series of SET to determine the effects of dissolved oxygen and hydrogen (potential) on the IGSCC susceptibility of an extremely susceptible heat of Type-304 (Heat No. M7616) has been completed. A detailed description of the test has been discussed previously,[1,18] and thus only a brief summary of the test background is presented here.

The SET as presented in Figure 3-23, is a CERT of an electrically insulated tensile specimen which is maintained at a fixed electrochemical potential. In all but one of the test environments the test electrolyte was a nitrogen deaerated 0.01 N Na_2SO_4 solution. The tests were conducted at 274°C (525°F) where the SET was initiated by first applying a constant extension rate of 0.0025 cm/h (0.01 in/h) and then by fixing the potential of the tensile specimen. The above strain rate is approximately 2×10^{-5} min^{-1}. The autoclave system is illustrated in Figure 3-24.

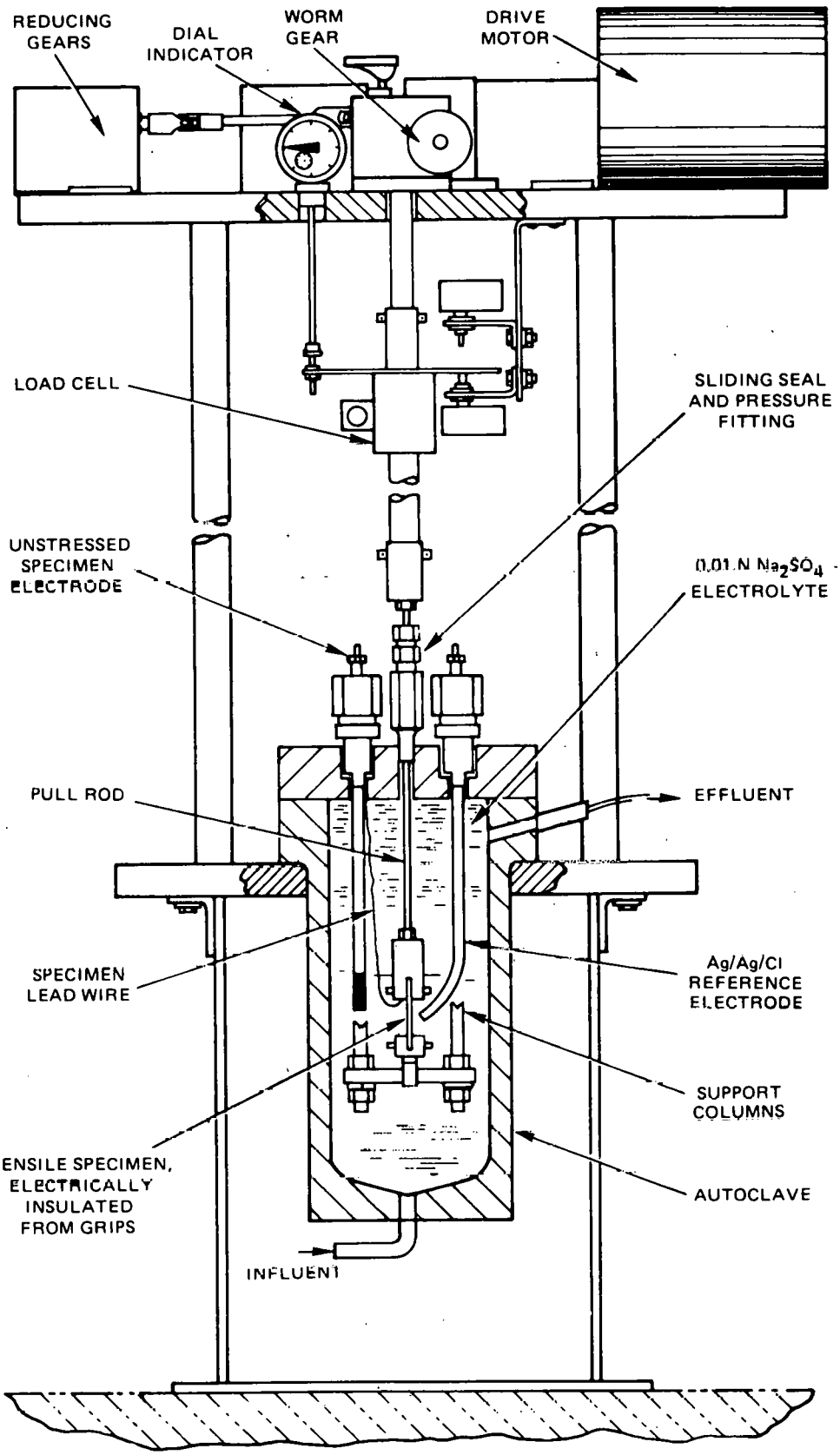

Figure 3-23. Straining Electrode Apparatus

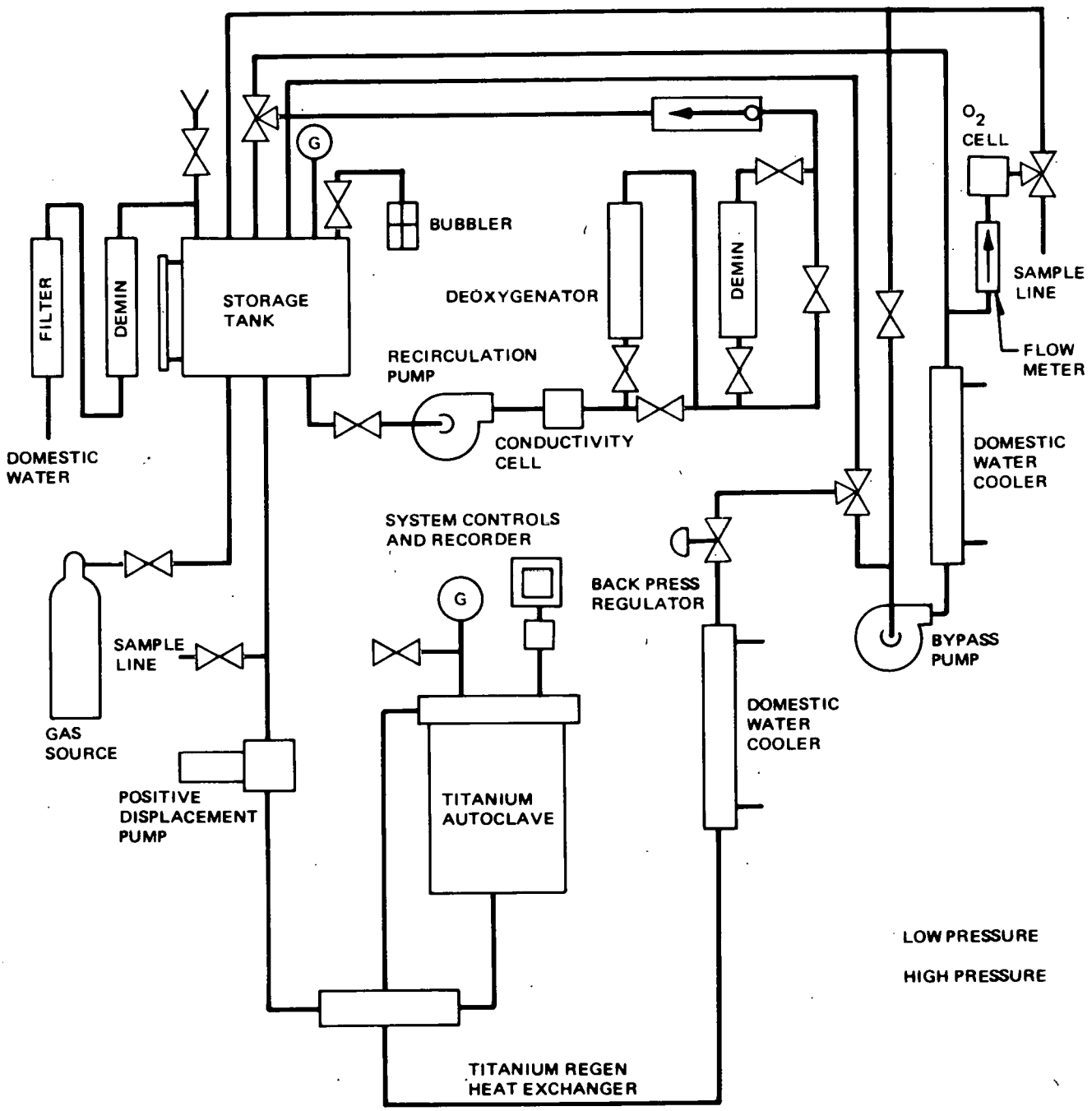

Figure 3-24. Refreshed Water Loop for Electrochemical Studies

The resistance of a highly susceptible heat of material was evaluated in SET's at 274°C and (with the exception of one run) in 0.01 N Na_2SO_4. "As-welded (w) and "as-welded-plus-low-temperature-sensitized" (W+LTS) conditions were tested at varying potential and with and without hydrogen addition.

The results are presented in Table 3-29. They are ranked according to increasing resistance to IGSCC with the hydrogen gas studies at the bottom (most resistant). The parameters used in ranking the specimens resistance to IGSCC are typical mechanical factors such as time to failure, reduction of area, percent elongation and mode of failure.

Table 3-29 shows that as the potential of welded stainless steel is reduced, the susceptibility to IGSCC decreases. An electrochemical potential of -0.400 V_{SHE} appears to mitigate IGSCC of as-welded Type-304. When the specimen receives an additional LTS treatment, severe IGSCC occurred at -0.400 V_{SHE}. Dropping the potential an additional 0.050 V_{SHE} produced only a slight improvement in the IGSCC response. However, when the potential is reduced to a level which simulates the presence of hydrogen (-0.750 V_{SHE}) the results are dramatically different. The cathodic potential is the electrochemical equivalent of approximately 4 ppm dissolved hydrogen at 274°C and produced ductile failure with only minor amounts of transgranular cracking. Since annealed stainless steel exhibits some TGSCC under the same test conditions, TGSCC, per se, does not warrant particular engineering consideration.

A similar experiment was conducted in the same 0.01 N Na_2SO_4 electrolyte where the potential was controlled by the direct addition of hydrogen to the system rather than electrochemical control with a potentiostat. The results of this study were characterized by similar mechanical property values as produced in the prior test where hydrogen was only simulated. The time to failure (206 versus 216 hr), reduction of area (28.6 versus 26.6%) and elongation valves (14.9 versus 13.6%) are essentially the same for the hydrogen gas and hydrogen simulation studies, respectively. The specimen in the hydrogen gas test was characterized by a fracture morphology of severe surface TGSCC with some minor IGSCC penetrations at the tips of the microfissures. The specimen overall failure mode was over 90% ductile.

Table 3-29

STRAINING ELECTRODE RESULTS FOR WELDED TYPE-304 STAINLESS STEEL (HEAT NO. 1) AT 274°C in 0.1 N Na_2SO_4
(Strain Rate of 2x10-5 min^{-1})

Process Code	Potential (SHE)	Fracture Stress MPa[a]	(ksi)	UTS[b] MPa	(ksi)	T_f[c] (H)	R.A.[d] (%)	Elong[e] (%)	Failure Morphology
W	-0.100	421	(61)	372	(54)	78	11.5	4.1	IGSCC
W	-0.300	614	(89)	448	(65)	161	26.7	10.4	0.7 IGSCC[f], 0.3 Ductile
W	-0.400	862	(125)	483	(70)	262	44.2	14.7	Ductile
W	-0.400	814	(118)	531	(77)	255	38.9	15.6	Ductile
W+grd+LTS	-0.100	317	(46)	276	(40)	39	5.0	1.6	IGSCC
W+LTS	-0.400	310	(45)	303	(44)	64	2.5	4.5	IGSCC
W+LTS	-0.450	545	(79)	455	(66)	234	26.7	7.9	IGSCC, Some Ductile
W+LTS	-0.750	669	(97)	489	(71)	216	26.6	13.6	Ductile, minor TGSCC
W+LTS	-0.65(H_2)[g]	620	(90)	448	(65)	206	28.6	11.7	Severe surface TGSCC some IGSCC penetration >90% ductile failure
W+LTS	-0.55(H_2)[g]	586	(85)	448	(65)	153[i]	23.0	12.3	general surface TGSCC >90% ductile failure

[a] Maximum load/failure cross section
[b] Ultimate tensile strength - maximum load/original cross-section
[c] Time to failure
[d] Reduction in area
[e] Elongation
[f] Initiated by short transgranular crack on I.D. machined surface.
[g] Potential controlled by H_2 addition (100 ppb)
[h] No reference electrode, no Na_2SO_4.
[i] Specimen failed at notch.

A third hydrogen experiment was performed in pure water, without Na_2SO_4, so that the effect of this substance, if any, could be evaluated. Also, no reference electrode was used to discount any effect of this item in the test series. Here again the mechanical properties were similar to the two other hydrogen experiments with the exception of a slight premature failure of the specimen due to a small unintensional notch along the gauge length. As expected, the failure which was also characterized by over 90% ductile failure occurred at this surface irregularity.

Therefore, the post-test examination of these three hydrogen SET tests (one simulated, two actual hydrogen additions) reveal that the specimens failed by ductile rupture, coalescence of microvoids, with only minor indications of IGSCC penetrations on one specimen. Transgranular cracks did occur on all surfaces and were often associated with surface discontinuties and cold worked areas, such as machining grooves on the i.d. section of the pipe from which specimens were fabricated. Previous studies in several laboratories have indicated that these transgranular cracks can be expected to occur in CERT or SET testing techniques. These cracks require considerable strain to initiate (approximately 10%) and have no engineering significance.[18]

3.6 TASK B-5. DEMINERALIZER PERFORMANCE (W. L. Lewis, L. L. Sundberg)

Objective. Current BWR practice is to use hydrogen form (i.e., acid regenerated) cation exchange resins for the bypass clean-up system and the full-flow condensate demineralizers. This practice can be continued when using hydrogen as the oxygen-suppressing additive. The use of dissociating additives such as ammonia or hydrazine however, dictates the use of an ammonia-based cation resin. Use of such ammonia-form resins instead of the acid form causes significant deterioration of all aspects of resin performance.

This task is designed to define the ion-exchange systems necessary to permit operation with the ammonia additive and to determine exactly what performance penalties will be incurred with such a system.

3.6.1 Performance Predictions

A series of calculations has been performed[18] to determine the effects of additives upon the BWR water treatment systems. The only additive with no apparent deleterious effects upon the ion-exchange resins is hydrogen. The other two additives considered, ammonia and hydrazine, affected the Condensate and Reactor Water Clean-Up Treatment Systems to such a degree that satisfactory operation with other than minor condenser seepage is highly unlikely. The latter two additives increase the pH of the feedwater and reactor water and reduce the exchange capabilities and capacities of the cation and anion resin beds. Of particular concern is the decreased sodium exchange capability of the cation resin in the condensate treatment system with high concentrations of ammonia. Additional effects of operation with hydrazine or ammonia which must be considered are the exacting physical separation requirements of the resins in deep bed regeneration systems and, the necessity for an increased volume of chemicals for regeneration. Of interest, also, is the requirement for high purity in the regeneration chemicals. Due to the alkaline properties of the condensate stream, a high level of regenerated sites is required for the ion-exchange resins, and a minimum amount of impurities in the regenerating stream can be tolerated.

In short, the penalties associated with the use of ammonia or amine additives are so severe they may well preclude further consideration of these additives as viable alternatives.

3.6.2 Resin Testing

Because of the critical impact the use of ammonia-based resins at high pH has on the ultimate additive selection, preparations are being made to actually test and compare resin performance in a San Jose test facility.

A schematic diagram of the test loop is presented in Figure 3-25. The suction side of the 10 horsepower feed pump is connected to a 150-gal, cylindrical, covered storage tank. The pump will discharge 51 gpm at 60 psig. This feed stream may be partitioned between three deep-bed columns or two filter-demineralizers or combinations of the five vessels providing total flow does not exceed the 51 gpm limitation.

Demineralizer inlet and return lines are 2-in. Schedule-40 polyvinyl chloride (PVC) pipe. The inlet header and each vessel outlet line contain taps for 1/4-in. sample lines.

Make-up into the surge tank is regulated by high and low level control switches with a vertical differential of about 1 in. Make-up demineralized water from the building supply is polished in a 3-in.-diam x 36-in. high chemically equivalent ion-exchange bed before entering the surge tank. The surge tank is cooled by a heat exchange coil containing 80 ft of 1/2-in. stainless steel tubing using building service water to maintain the surge tank temperature at 80°F.

Two tanks of 50ℓ each are used for additive injection--one for NH_3, the other for NaCl-Fe_2O_3. Two methods for additive addition were used. In the first, a Milton-Roy Mini Pump® was employed on each addition tank. The injection rate was typically 10 mℓ/min. One-eighth-inch stainless steel lines were run from the injection pump discharge to the top of the surge tank. The second method used two relays to control the open and closed times of a solenoid valve

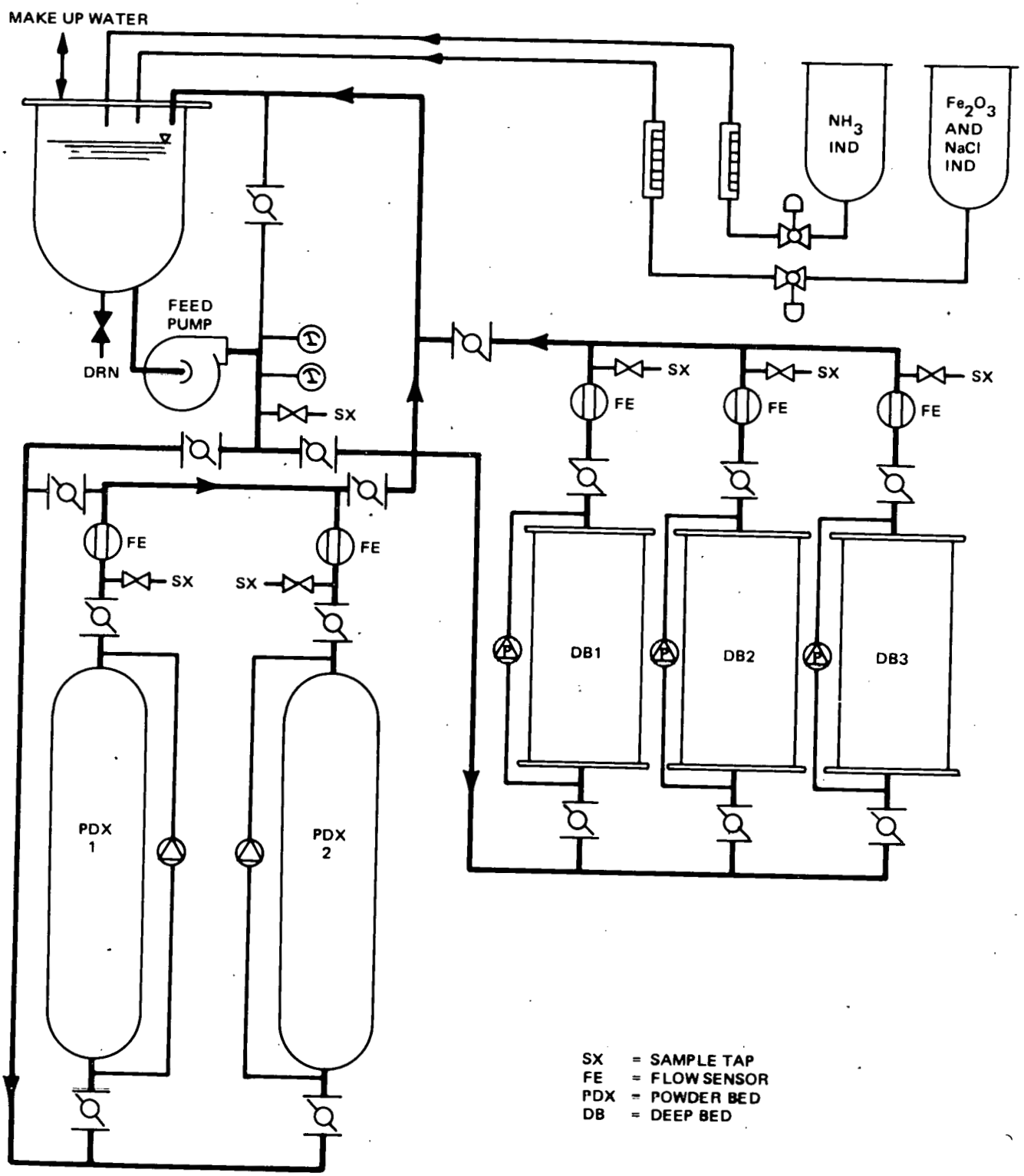

Figure 3-25. Resin Test System

between the addition and surge tanks. The addition tanks were pressurized to 5 psig with helium in this system to force the liquid into the surge tank.

The deep bed resin columns are 8-in. Schedule-40 PVC pipe. The nominal bed height is 3 ft, yielding an active resin volume of roughly 9ℓ. A 100-mesh stainless steel underscreen is clamped between the bottom flange sections of each vessel.

Bead resins were obtained from Bio Rad Laboratories, Richmond, California, and were ordered under the acceptance criteria of GE Purchase Specification 21A8844.

Prior to the test runs, these resins were washed with 5 column volumes of demineralized water through 100-mesh screen. This practice removed the leachable organics and resin fines. Without the wash the fines plugged the resin underdrains. The columns were loaded in 5-liter increments with the appropriate cation/anion ratio to minimize bed stratification. When all the resin was loaded, the columns were gently backwashed to remove air pockets. Column flow rates are measured upstream of the return header with Fisher-Porter Model 10A1027 flow meters with stainless steel floats.

3.6.3 Analytical Systems

3.6.3.1 Conductivity

Balsbaugh Series 910 conductivity monitors and cells will be used throughout this investigation. Cell constants are 0.01 or 0.1 CM^{-1} depending on the magnitude of the conductivity. Readings will be taken from the inlet header and each vessel outlet (typically) on an hourly basis. The effluent from each cell flows to a 1 1/2-in. x 18 in. PVC column of cation exchange resin (Dowex 50 x 8, 20-50 mesh, H^+ form) and then to a second conductivity cell. Thus, yielding the "acid conductivity" of each stream. The flow rate through each conductivity cell is 300 mℓ/min. Each cell and accompanying meter is placed in series periodically with a common feed stream to ensure the same reading after cross-calibration with a Beckman Model BB-1 ip cell. Output data are recorded on a 30-channel Leeds and Northrup Speedomatic recorder.

3.6.3.2 Sodium

Sodium ion concentrations were monitored by ion-selective electrodes (Subsection 3.4) using an Orion Model 151102 "a/sled" (absolute sodium leak detector). In this system, sample water flows through 4 ft of silicone rubber tubing which is immersed in ammonia liquor. Gas phase diffusion of ammonia into the sample raises the solution pH, thereby decreasing the system response to hydrogen ion. The system exhibited Nernstian behavior from 0.1 to 1000 ppb Na^+. Sample flow rate will be 40 mℓ/min. Sample water is filtered with a 0.45 μm Millipore® filter to prevent the formation of Fe_2O_3 films on the electrodes. The system is calibrated on a weekly basis per the manufacturer's recommendations using a Sage Instruments Model 355 syringe pump with UBS SRM 2201 as a working standard. Since only one unit is available, it is only possible to monitor one stream at a time.

3.6.3.3 Chloride

Chloride ion will be monitored with the prototype instrument from Orion Laboratories described in Subsection 3.4. Again the measurement principle is based on selective ion electrodes. Here the sample water passes through silicon rubber diffusion tubing that is immersed in 88% formic acid. Gas phase diffusion of formic acid into the sample lowers the pH, thereby decreasing the electrode response to hydroxide ion. In addition, the sample is cooled to 4°C to attain the desired sensitivity of the determination (0 to 50 ppb $Cℓ^-$). Cooling was accomplished with a Neslab TE-8 refrigerated bath circulator. Calibration procedures are identical to those for the sodium analyzer. Filtered sample flow rates are 40 mℓ/min, again with the restriction of analyzing only one stream at a time.

3.6.4 Test Plan

When the loop instrumentation is completed the following runs will be made:

Test 1

		Cation Resin	Resin Ratio	Flow, Gpm/ft^2
Resin Beds:	Deep Bed 1	NH_4	2:1	50
	Deep Bed 2	NH_4	1:1.3	50
	Deep Bed 3	H^+	1:1.3	50

Feed Solution: Na^+ - 200 ppb

Cl - 300 ppb

Fe_2O_3 - 200 ppb

NH_3: Test 1 Zero (pH $\sim$ 7)

Test 2

Repeat test except with 20 ppm ammonia added to feed (pH $\sim$ 10).

Test 3

		Cation Resin	Resin Ratio	Flow, gpm/ft^2
Resin Beds:	Filter/ Demineralizer 1	NH_4^+	1/1 w/o	4
	Filter/ Demineralizer 2	NH_4^+	2/1 w/o	4
	Deep Bed 1	NH_4^+	5/1 v/o	50

After test 3 is complete additional tests may be scheduled depending on the time and resources available and the insights gained in the first three runs.

3.7 TASK B-6. RADWASTE SYSTEM IMPACT (E. L. Burley)

Objective. Predict the radwaste inputs (amount and composition) accompanying the potential changes in water chemistry. Evaluate the effect of these loads on equipment capacity, construction materials, processing sequence, etc. Determine the cost of the resulting, modified radwaste system.

3.7.1 System Changes

The impact of an ammonia additive on the radwaste system is twofold: more and stronger chemical regenerants must be used to achieve the high degree of regeneration required, and the lowered ionic capacity of the resins requires more frequent regenerations.

The increased chemical consumption and resultant increased radwaste volume are illustrated in Table 3-30. The dramatic decrease in bed life at the high pH operating condition is also shown.

Even at the current [H^+ - OH^-] cycle regeneration frequency, chemical waste input to the radwaste system and final stored waste volumes therefrom are increased by factors of 4.6 and 5.2, respectively. If the decreased bed life is also considered, this increase becomes about 200-fold: clearly intolerable, both from the standpoint of system processing capacity and final waste volume.

3.7.2 Alternatives

If the amounts of sodium and chloride in the condensate were limited to 2.4 and 3.7 ppb, respectively (at the price of jeopardized plant availability) these elements would very rapidly establish an equilibrium with the ammonia based condensate treatment system resins and pass through them with no concentration change. Then, in a 7% clean-up system plant all sodium and chloride removal would take place in the lower pH clean-up system where resin capacities are much higher.

Table 3-30

RESIN REGENERATION WASTE

	Standard BWR	NH_3 Flow Sheet	NH_3 Flow Sheet +5/1 Resin Ratio
Resin Ratio (By Volume)	2/1	2/1	5/1
Chemical Requirements, lb/ft^3 Resin			
H_2SO_4 (cation resin)	8	20	20
NaOH (anion resin)	6	15	15
NH_3 (all resins)	--	8	8
Pounds of Neutralized Chemicals/ Regeneration			
Na_2SO_4	1400	1600	800
$(NH_4)_2 SO_4$	--	5600	5600
Volume of Chemical Waste per Regeneration (gal)			
Na_2SO_4 Soln	5300	6300	3000
$(NH_4)_2SO_4$ Soln	--	21000	25000
Operating Resin Capacity			
Cation Resin, meq/mℓ	0.55	0.0023	0.0023
Anion Resin, meq/mℓ	0.28	0.025	0.025
Single Bed Life With 12 gpm Cooling Water Leak, hr			
Cation Resin	2400	10	13
Anion Resin	600	54	27

Under these conditions clean-up bed life would be extended so that one clean-up bed regeneration was required each 35 hr opposed to one condensate bed regeneration every 2 hr. However, in a 1% (current standard) clean-up system, reactor water chloride concentration and conductivity would exceed established reactor water quality limits. Also, the radwaste system activity levels would be significantly and perhaps intolerably increased by having to handle clean-up resins and/or spent regenerants rather than those from the condensate system which is isolated from reactor water activities. In any case operation at "zero" condenser leakage represents a minimum radwaste volume increase of about six times that for the current non-additive flow sheet, increased operating problems notwithstanding. It is not considered a feasible alternative.

3.8 TASK B-7. INJECTION AND CONTROL EQUIPMENT (J. D. Seymour, N. A. Fedrick)

Objective. Identify the proper system locations at which to inject the additives and select the proper equipment for this purpose. Select the position at which to obtain a representative sample and the type of control instrumentations to use to monitor and control additive addition rate.

3.8.1 Hydrogen Injection System Selection

Studies performed at the Humboldt Bay reactor site and the General Electric Company showed[19] that hydrogen, when injected directly into reactor feedwater does not readily dissolve because bubble coalescence causes stratification of the gas. To preclude gas-phase stratification, it was decided to inject the hydrogen into a gas-liquid contacting device in a side-stream which would then be mixed with the main feedwater flow.

3.8.1.1 Design Basis

Design of the hydrogen injection system was based on the criteria listed in Table 3-31.

Table 3-31

RECOMMENDED DESIGN CRITERIA

Location of injection point	Suction of reactor feedwater pumps
Hydrogen gas flowrate	System should be capable of injecting 2 to 30 lb/hr
Space limitation	Small as practical
Control requirements	System should be designed to inject hydrogen into the feedwater in direct proportion to feedwater flow
Degree of Automation	System should be automated in such a manner as to maintain a constant injection flow in proportion to feedwater flow. The system should be capable of operating unattended with only weekly maintenance.

These criteria were met with the exception of the location of the injection point. The feedwater pumps (Dresden 2) are not capable of accommodating the additional flow as a result of recirculation through the side stream. A point immediately downstream of the pumps was chosen because it was near the recommended location, it has a higher pressure which provided a more favorable gas-to-liquid driving force, and it eliminated the potential problem of bubbles cavitating the pumps.

A 10% (of feedwater) or one million lb/hr flowrate was chosen for the side stream because with the maximum amount of hydrogen being dissolved (30 lb/hr) in this volume of water, the concentration of the gas (~30 ppm) is sufficiently far removed from the equilibrium concentration (~185 ppm) as to maintain a satisfactory gas-to-liquid driving force.

The side stream inlet temperature was taken as 300°F. The side stream inlet pressure was taken as 1250 psig although it could increase to 1650 psig (pump shutoff discharge head) at low feedwater flow rates. Pressure integrity design was based on the maximum possible system pressure. Gas absorber design, however, was based on minimum system pressure, and maximum hydrogen gas flow.

3.8.1.2 Types of Gas-Liquid Contractors Studied

Four gas-liquid contacting devices were considered: a packed column operated in the conventional manner, i.e., countercurrent flow with a continuous gas phase; a packed column operated in cocurrent flow with a discontinuous gas phase; a bubble column; and a bubble column containing a motionless (static) mixing element to promote gas bubble dispersion and gas-liquid contact.

These contacting devices were compared qualitatively on the basis of interfacial area, mass transfer coefficient, operating range, size, and cost. This comparison is summarized in Table 3-32.

Data on interfacial area were obtained from the study performed by Wang and Fan[20], who compared the interfacial area for gas-liquid contacting in a

Table 3-32

A COMPARISON OF FOUR GAS-LIQUID CONTACTING DEVICES

Basis for Comparison (Worst = 1 Best = 4)	Countercurrent Packed Tower	Cocurrent Packed Tower	Bubble Column	Bubble Column with Static Mixers
Interfacial Area	1	2-3	2-3	4
Mass Transfer Coefficient	1	2-3	2-3	4
Operating Range	Narrow	Variable	Variable	Variable
Size	1	1	3	4
Cost	1	2	4	3.5

tower with conventional packing, e.g., Raschig rings, in a bubble column, and in a bubble column with static mixing elements. They found the interfacial area for the Koch static mixers to be highest. The advantage of the mixing element over the conventional tower packing is that the former occupies a smaller percentage of vessel volume for a given contact area.

Contacting devices for insoluble gases are often compared on the basis of their $K_L a$, the product of the liquid-phase mass transfer coefficient and the gas-liquid interfacial area. The data of Houghton, et al.[21] indicate that the bubble column is superior to the packed column for the absorption of carbon dioxide at low gas flows. Their results are shown in Figure 3-26. Wang and Fan compared the $K_L a$ of bubble columns with the $K_L a$ of the Koch static mixer and found the Koch device to be superior at low gas flow rates (Figures 3-27).

In terms of operating ranges for the various contactors, it was postulated that the countercurrent packed tower would probably have a limited operating range due to the low gas absorption at high water flows, necessitating a hydrogen atmosphere (continuous gas phase) in the vessel with recycle or make-up gas streams. At low water flows, on the other hand, the hydrogen

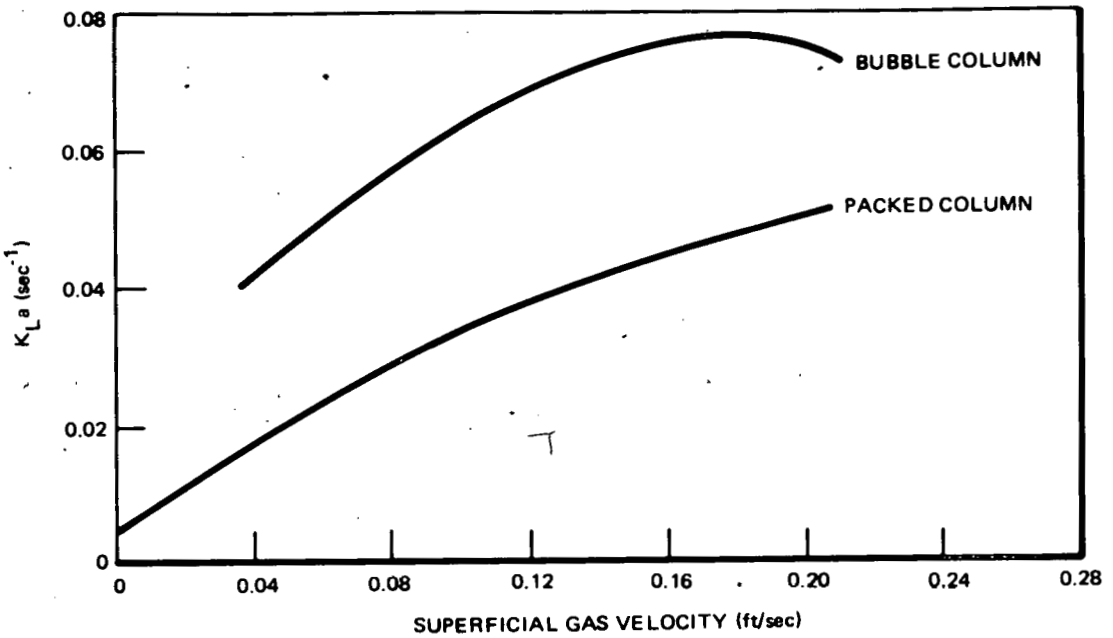

Figure 3-26. Column Efficiency versus Superficial Gas Velocity

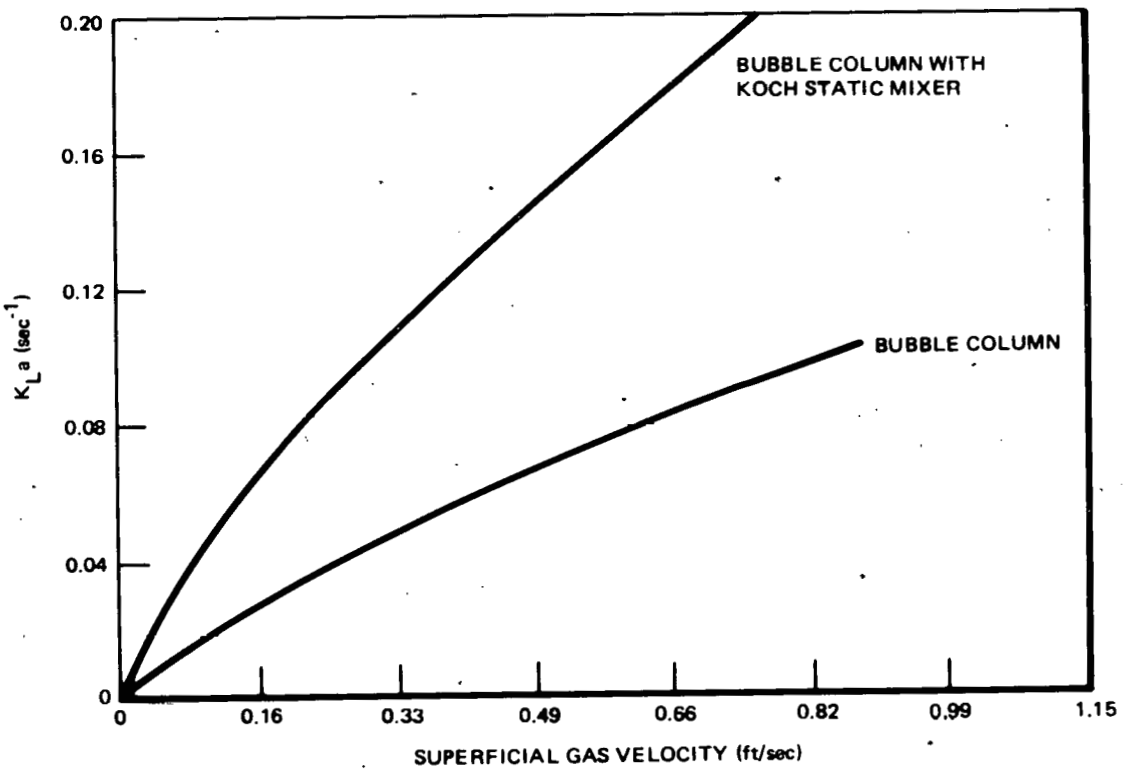

Figure 3-27. Comparison of Liquid-Phase Mass Transfer Coefficients

atmosphere would result in greater-than-desired hydrogen absorption and difficult process control -- a definite negative aspect of this device. Operating ranges for the other contactors would be variable and a specific comparison was not attempted.

With respect to size, a packed tower (either countercurrent or cocurrent) could pose a definite location and installation problem. Based on a maximum allowable mass flow capacity of the tower of 20,000 to 30,000 lb/hr-ft^2, the vessel diameter would be on the order of 7 to 9 ft, with a projected height of approximately 10 to 15 ft. The bubble column (with or without static mixers), however, would be simply a length of pipe with a diameter of about 12 in. In addition, this device is most flexible in terms of physical arrangement: it may be installed vertically or horizontally; it may be formed into a helix if installation space is limited; elements may be added or deleted as system requirements change.

Because of the large size and the necessity that the absorber be a pressure vessel, the cost of a packed tower was estimated to be approximately 5 to 10 times greater than for a bubble column. The difference in cost between the two bubble columns could be the cost in procuring and installing the mixing elements -- a relatively low cost differential.

Based on the above information the bubble column with the static mixing elements was chosen as the most effective gas-liquid contactor.

3.8.2 Design

The design is dependent primarily on the mass transfer coefficient. The mechanism for mass transfer, in general, is complicated and not fully understood. When the mechanics of bubble action and turbulence are included, it becomes exceedingly complex. For this reason a purely theoretical prediction of a mass transfer coefficient is not possible.[20] It is necessary, therefore, to employ correlations based on experimental data.

Researchers at Koch, Inc. have derived a design equation empirically. It is based on an oxygen-water system at ambient temperature and atmospheric pressure. In applying this equation to the injection of hydrogen gas several assumptions were made:

a. Hydrogen gas is a relatively insoluble substance; therefore, the resistance to mass transfer is wholly in the liquid phase.

   This was found to be generally true. However, there may be an added effect of gas-phase resistance if the ratio of liquid molal flow rate to gas molal flow rate is large, as is the case here. There was no information, however, for determining the extent of this effect.

b. The diffusivity of hydrogen gas in water is dependent on the liquid viscosity/temperature ratio and not directly on pressure.

   Although very little research has been done in this area, it seems that increased pressure decreases diffusivity by reducing the intramolecular spacing.[22] It is indicated that the effect of pressure on viscosity may be proportional to the effect of pressure on diffusivity. For water, though, pressure has little or no measurable effect on viscosity and probably no effect on diffusivity.[22]

c. The mechanism of mass transfer in a static mixer follows the two-film theory as opposed to the penetration theory.

   For this application the important difference in the two theories is the effect of diffusivity on the mass transfer coefficient. The two-film theory supposes that $K_L a$ is directly proportional to the diffusivity while the penetration theory assumes $K_L a$ to be proportional to the square root of the diffusivity. The two-film theory is supported by Koch researchers and by Wang and Fan for the Koch

static mixers. The penetration theory has been accepted by many investigators for devices such as the agitated bubble column and packed tower.

d. $K_L a$ is independent of liquid flow rate.

Although this is not true, this assumption leads to a very conservative design in this case.

e. Gas absorption is a logarithmic function.

This is a result of the Koch research.[23]

f. $K_L a$ values for the Koch type "LY" mixer are essentially the same as those for the type "AY" mixer.

The difference between the two types of mixers is the distance between the layers. The LY mixer has 1-in. layer separation, while the AY type has 0.5-in. layer separation.

3.8.2.1 Calculations

The empirical design equation derived at Koch research facilities is:[23]

$$L = \frac{Q}{K_L a \, A \, \bar{x}}$$

where

L = length of mixer, ft

Q = Gas absorbed in a section of pipe, moles/min

A = Cross sectional area of pipe, ft^2

$\bar{x}$ = Log mean driving force defined as[23]

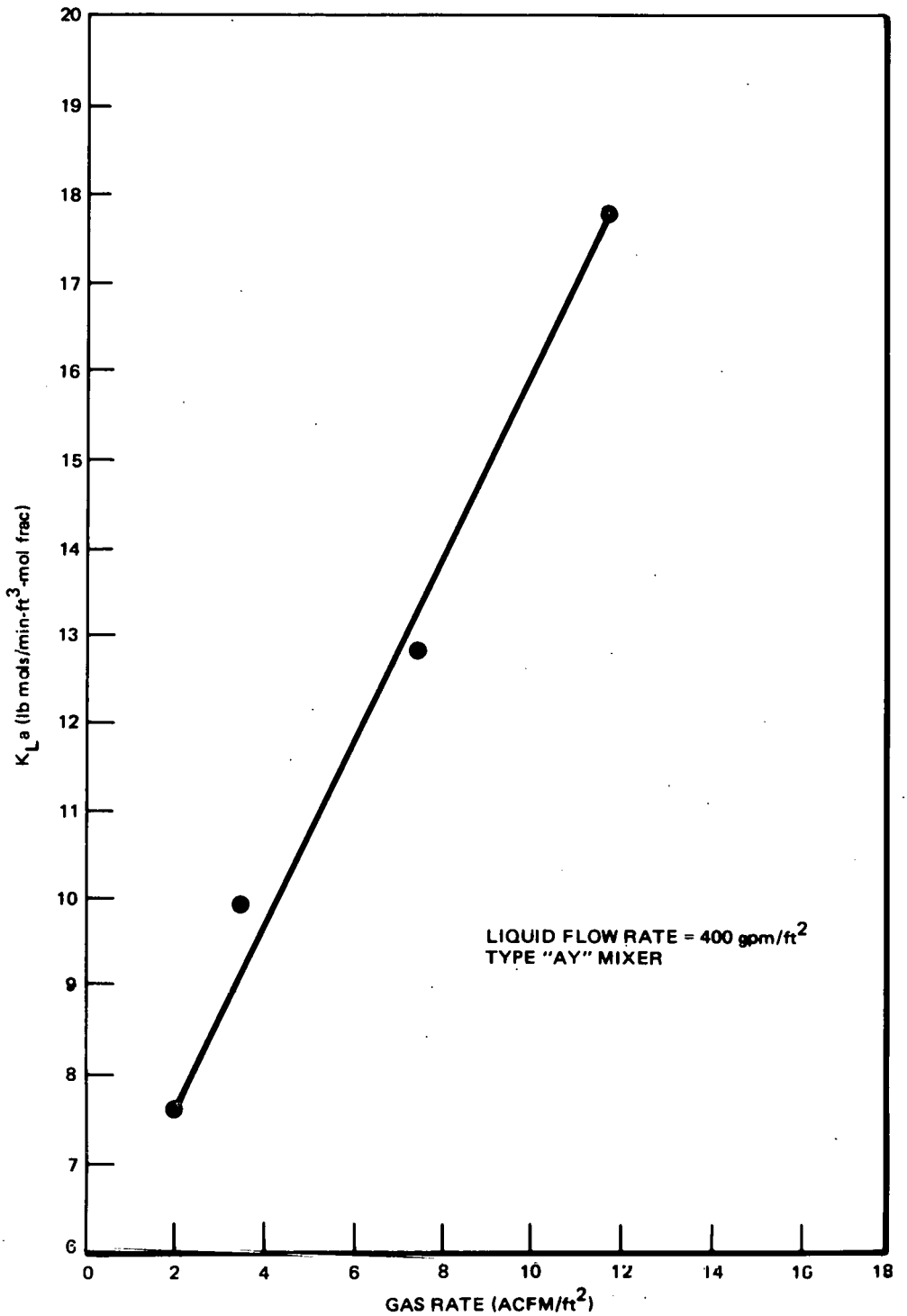

Figure 3-28. Correlation for $K_L a$ Based on O_2-H_2O System

$$\frac{(x^* - x_i) - (x^* - x_f)}{\ln\left(\frac{(x^* - x_i)}{(x^* - x_f)}\right)}$$

x_i, x_f = Mole fraction of gas dissolved in liquid at some initial and final point, respectively, dimensionless

x^* = Mole fraction of gas dissolved in liquid at equilibrium. This may be computed from Henry's Law.*

The value for $K_L a$ is obtained from a correlation provided by Koch (Figure 3-28). The $K_L a$ value from the graph must be corrected for the hydrogen-water system:[23]

$$K_L a\ (H_2 - H_2O) = K_L a\ (O_2 - H_2O) \times \left(\frac{D_{(H_2 - H_2O)}}{D_{(O_2 - H_2O)}}\right)$$

where

D = diffusivity, cm/sec

The range of $K_L a$ values that can be obtained from the graph is small because of the low gas flow rate. Koch suggested that a length for the mixing elements be determined by using the $K_L a$ for which there was a data point; then a logarithmic curve could be generated from the equation:

$$L = C \ln (1 - Abs)$$

---

*Henry's Law:[24] $p - Hx^*$

where p = partial pressure of the gas, atm

H = Henry's Law constant for the gas, atm/mol frac.

where

C = constant
Abs = fraction of gas absorbed

Using this method a hydrogen gas absorption curve was generated (Figure 3-29). Fourteen feet of mixing section was required to dissolve 99.95% of the hydrogen at an initial flow rate of 30 lb/hr. Sample calculations are given in Appendix B.

3.8.3 Results

The design of the gas-liquid mixing section consists of a 12-in.-diam pipe, 40 ft long, containing 14, 1-ft-long Koch static mixing elements. Empty pipe sections between the mixing elements extend the gas-liquid contact time without appreciably adding to the overall pressure drop. Hydrogen gas will be injected upstream of the first mixing element through a sparger or fritted disc. The mixing section is depicted in Figure 3-30.

The mixing section installation and arrangement is shown in the P&ID, Figure 3-31.

A screen downstream of the mixing section (not shown) will be included to prevent carryover of debris in the event of disintegration of any of the mixing elements. Hydrogen gas flow is controlled in direct proportion to the side stream flow rate which is, itself, controlled in direct proportion to the flow rate of the main feedwater stream.

3.8.4 Conclusions and Recommendations

The present design of the hydrogen injection system should be adequate to dissolve the required amounts of hydrogen gas at the prescribed conditions.

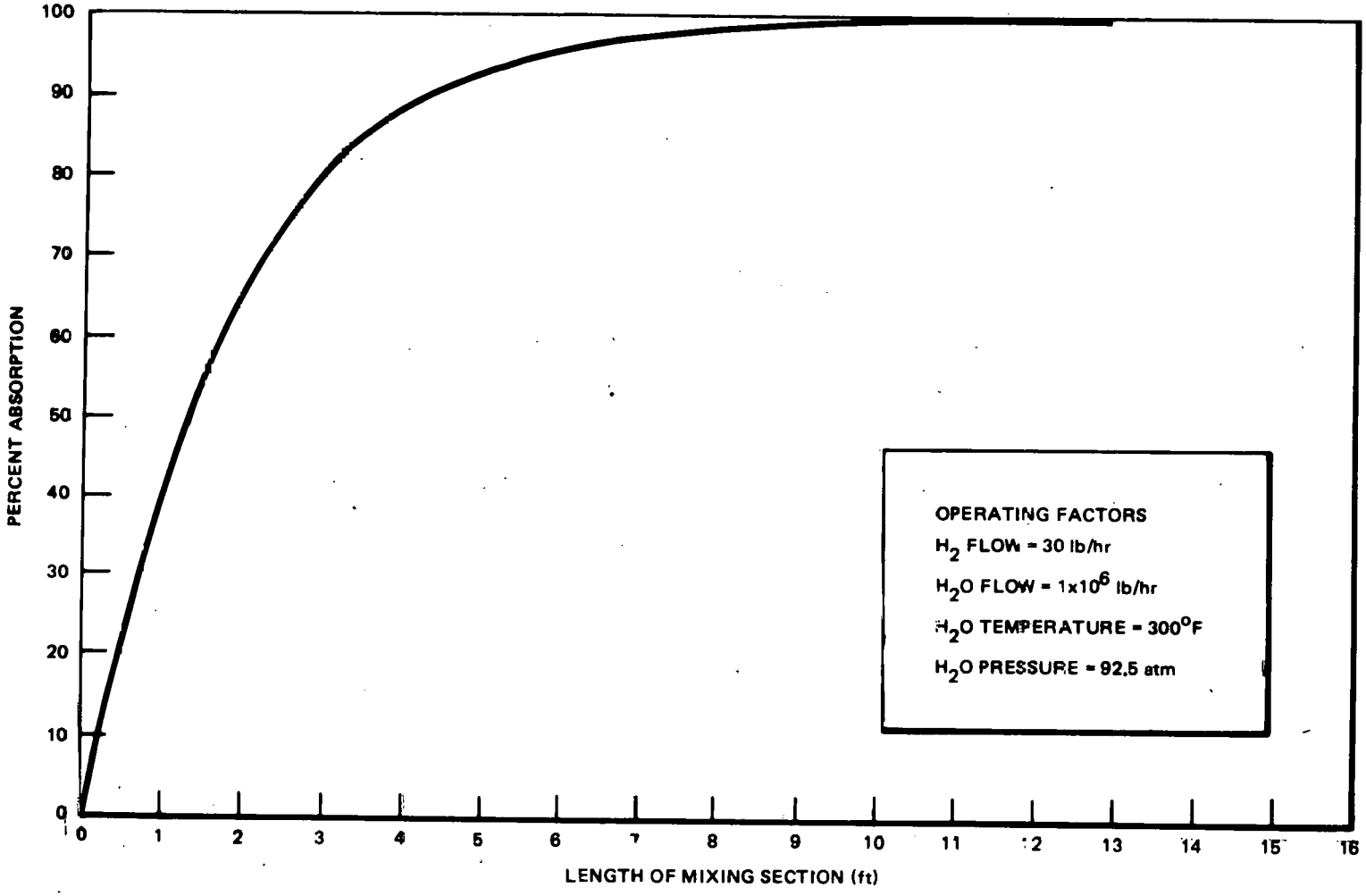

Figure 3-29. Absorption Curve for Hydrogen in Water

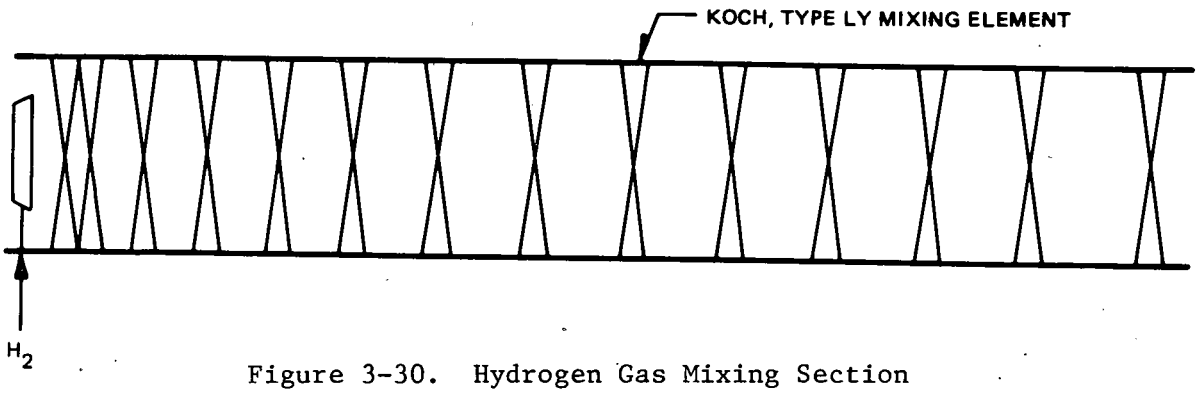

Figure 3-30. Hydrogen Gas Mixing Section

Although a very conservative approach has been taken in designing this system, there is still some uncertainty inherent in the design. The assumptions made in this case, (resistance to mass transfer is liquid-phase controlled, a $K_L a$ is proportional to the diffusivity (Two-Film Theory), etc.) if not strictly correct or applicable, could yield a less conservative design, resulting in a mixing section longer than presently specified. It should be noted, though, that the total length of mixing section may not necessarily increase as the mixing elements may be installed closer to each other than in the present design.

To obtain a precise design for the mixing section length laboratory testing is called for. It is recommended that laboratory testing be undertaken on hydrogen dissolution at high temperature and pressure to obtain a more accurate correlation for the mass transfer coefficient. In addition, horizontal and vertical performance testing should be carried out to determine if any advantages exist in operating the mixing section in one position rather than the other.

3.8.5 Cost Analysis

The estimated cost for the procurement and installation of such a hydrogen injection system is itemized in Table 3-33. The system was estimated on the basis of meeting ASME Boiler and Pressure Vessel Code, Section III, Subsection NB requirements when added to the feedwater line at an existing nuclear power plant. Equipment and hardware to be procured are given in Appendix A.

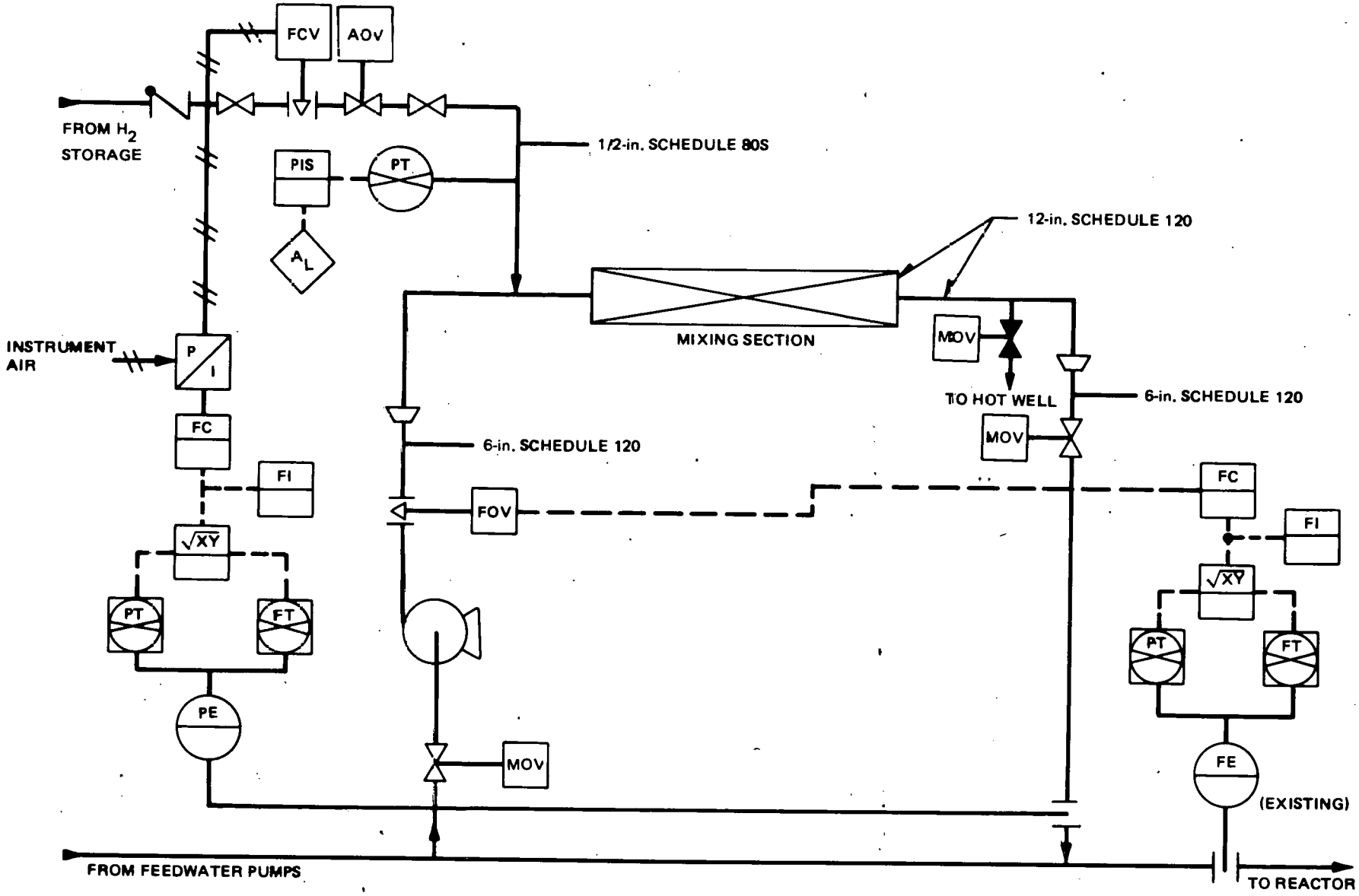

Figure 3-31. P&ID for Hydrogen Injection System

Table 3-33

COST ESTIMATE FOR HYDROGEN INJECTION SYSTEM

	1978 Dollars
Purchased Parts	257,000
Subcontracted Items (Including Installation)	166,500
Other/Raw Material	3,500
Direct Labor + Overhead	15,000
TOTAL COST	$ 442,000

3.9 TASK B-8. OPERATIONAL AND OTHER RELATED CONSIDERATIONS (R. J. Stevens, T. L. Wong, E. G. Leo, B. S. Shiralkar, J. D. Duncan, C. C. Lin, J. S. Wiley)

Objective. Consider and evaluate the effects of each additive on "normal" plant operation, e.g. manpower requirements, special safety or toxicity precautions, employee acceptance, licensing considerations and variations in radioactivity transport and deposition patterns.

3.9.1 Additive Surveillance Requirements

System surveillance must be maintained to monitor for process control, and to monitor additive handling areas for control of health and safety hazards.

The first category is covered under Task B7. For personnel health and safety however monitors should be used in enclosed areas such as the additive storage, distribution, and injection system areas.

The levels of concern for each proposed additive are shown in Table 3-34 as Threshold Limit Values (TLV), which are the maximum permissible levels in air related to toxicity/personnel health hazard, and Lower Explosive Limits(LEL) in air. These levels are in volumetric parts per million (vppm) or percent by volume in air.

Table 3-34

ADDITIVE CONCENTRATION LIMITS IN AIR

Additive	TLV	LEL (%)
Ammonia (NH_3)	50 ppm	15
Hydrazine (N_2H_4)	1 ppm	4.67
Hydrogen (H_2)	7%*	4.1

*The toxicity of hydrogen is only that related to displacement of oxygen by hydrogen. 19.5% oxygen is the recommended minimum content without self-contained breathing apparatus. This is equivalent to 7% hydrogen if H_2 is the only air diluent.

The normal practice for these types of monitoring systems is to set the alarm levels at approximately one half (1/2) of the above values to provide a sufficient margin for early remedial action. As a minimum the monitoring equipment should undergo daily operational checks.

Wherever possible, redundant monitoring equipment based on more than one measurement technique should be used.

3.9.2 Operational Guidelines

The start-up and normal mode operational considerations are, in part, a function of the injection and control system selected. The operational guidelines specific to the injection and control system are not covered in this task. However, the general considerations which apply in the three additive cases are as follows:

Addition systems shall be thoroughly purged with helium prior to the introduction of the additive, prior to any system repairs, and prior to restart of the system.

The reactor sub-system where the additive is introduced (i.e., containing the injection point), must be in operation prior to start-up of the addition system. The injection rate should be proportional to the flow rate of the reactor sub-system at the injection point.

Any plant or sub-system shutdown which isolates or stops flow at the injection location, should also automatically isolate and shut down the injection system.

Enclosed additive storage and usage areas should be monitored for leakage. Detection of the additive above one half the lower explosive limit (LEL) in air should automatically isolate the additive supply. The distribution/injection system should be immediately purged with helium, and the leak source should be repaired prior to restart of the additive system.

During such emergencies, personnel entering the area should use gas masks or self contained breathing apparatus until the area can be ventilated and brought below one-half the threshold limit value (TLV) for ammonia and hydrazine.

When ammonia or hydrazine levels above one-half the TLV but below one-half the LEL are detected, personnel with gas masks and other protective clothing may investigate for leakage without system shutdown. Shutdown and thorough purging of the system are required prior to initiation of repair work, however.

3.9.3 Special Training

Ammonia and hydrazine are highly caustic substances. Therefore, personnel working in the additive system area should be alerted to their hazards and they should also be trained in the proper use of protective clothing and breathing apparatus (gas masks, self contained air supplies, etc.).

Hydrogen's primary hazard is its highly flammable nature. Personnel working with hydrogen or in areas where hydrogen is present should be trained in proper procedures for handling of hydrogen and working with equipment, in areas where hydrogen is stored.

Additionally, the additives must be dealt with carefully during a fire situation. An error in fire fighting techniques may result in greater hazards than the original fire. Therefore, personnel should be instructed in the proper techniques for fire fighting associated with each additive.

3.9.4 Special Equipment

Due to the caustic nature of ammonia and hydrazine, the following items should be available in the additive system area: Emergency eyewash and shower stations, protective clothing such as rubber gloves and aprons, goggles, and emergency breathing apparatus.

A liquid hydrogen supply system would require temperature and/or pressure monitoring of the storage vessels to detect potential over-pressurization of the vessel and attached piping.

Monitors are also required in additive usage areas. These monitors must have range capabilities to cover the TLV and LEL for the additive in use. (This may be accomplished by use of two different monitors to cover the required range.)

A brief review of some of the available types of monitors for each of the additives is given below. It is, however, recommended that the various monitoring techniques for the chosen additive be tested for operation at the representative conditions prior to final selection of a specific monitor.

3.9.5 Ammonia Detection Methods

3.9.5.1 Solid State Electrolyte Sensor

This sensor is a solid state semiconductor material sensitive to ammonia. In the presence of ammonia the conductivity of the sensor increases proportionately to the amount of ammonia. The sensor is capable of measurements at or below one-half the threshold limit value of ammonia, but at these concentration is subject to interference or masking from other trace substances. Systems of this type are offered by International Sensor Technology Co. of Santa Ana, California and the FnMet Corp. of Ann Arbor, Michigan.

3.9.5.2 Photoionization

An ultraviolet light is used to ionize a particular substance by bombarding the sample stream with photons having an energy level at or above the ionization potential of the substance, but below that required for the major components in air. This method is subject to interference from other trace elements when the species of interest is at a low concentration. This system is manufactured by HNU Systems, Inc., of Newton Upper Falls, Massachusetts.

3.9.5.3 Infrared Analyzers

The operation of this system is based on the wavelength absorption characteristics of the substance of interest. An infrared "beam" is passed through the sample gas to a receiver. The reduction of energy at a specific wave length is a function of the concentration of the substance of interest. This system is less susceptible to interference. An infrared system capable of monitoring ammonia is offered by the Wilkes Division of Foxboro Company, of Burlington, Massachusetts.

3.9.5.4 Specific Electrode

This sensing method requires that a batch sample of gas be bubbled through a liquid where the ammonia will go into solution and be detected by the "specific" electrode. The problems associated with this system are the designs of the calibration and batch cycling systems. The specific electrode is offered by Lazaar Research Labs of Los Angeles.

3.9.6 Hydrazine Detection Methods

With some modification the methods discussed above for ammonia may be used for monitoring hydrazine. The specific electrode system will not measure hydrazine directly but may be used if an iodate solution is used as the absorbent. The iodate is converted to ionic iodide by the hydrazine. Therefore, the iodine electrode response will then be proportional to the hydrazine content of the air.

3.9.7 Hydrogen Detection

3.9.7.1 Solid State Electrode Sensor

The sensor described above may also be used for hydrogen detection. At the monitoring levels for hydrogen (~2%) there is less interference due to other impurities.

3.9.7.2 Thermal Conductivity

Variations in the thermal conductivity of a gas mixture may be used to indicate changes in the make-up of the gas. If the base gas mixture is known and remains constant, the level of concentration of an additive such as hydrogen may be measured. The thermal conductivity of a gas is measured using a heated coil in the sample gas stream. The temperature of the coil will stabilize based on the thermal conductivity of the gas. The coil resistance then is monitored as a temperature indication. This system is most effective when used in a two-component stream. Monitoring of ambient air is difficult since the components are not constant in concentrations. Also, this type of monitor is highly sensitive to moisture in the air. Thermal conductivity type sensors are offered by Teledyne Analytical Instruments of San Gabriel, California.

3.9.7.3 Catalytic Bead Sensor

This type of sensor is often used for combustible materials such as hydrogen; a catalyst bead is used to "burn" the hydrogen, thus heating the bead element. Once again the resistance of the element is measured as an indication of the temperature and therefore the hydrogen concentration. One of the primary problems with catalytic type sensors is the potential of poisoning the catalyst, which reduces the efficiency of hydrogen conversion. The Catalytic Bead Sensor system is offered by vendors such as Teledyne Analytical Instruments of San Gabriel, California, Dictaphone of Mountain View, California, and others.

3.9.7.4 Color Indicator Tubes

A sensing method which may be considered for manual backup is based on indicator tubes such as those offered by Drager (National Mine Service Company). These tubes when used with a hand suction pump give an indication of the concentrations of a particular trace component by a color change in the tube. These tubes can be used to measure down to the levels of concern for all three of the additives.

3.9.8 Additional Procedure Requirements

The additive system will require specific start-up, shut-down, isolation and purging procedures. The reactor subsystem containing the injection system will require procedural changes for startup and shutdown.

Special fire fighting procedures for each additive have been discussed.[18] Unique elements of these procedures should be addressed in the site emergency/ fire fighting procedures.

3.9.9 Emergency Core Cooling System

The AWC additives and their resultant modification of the H_2 and O_2 levels in the reactor vessel will have no impact on the ECCS for there is no change in the suppression pool concentrations and this pool is the source of ECCS water.

3.9.10 Post-LOCA Hydrogen Concentrations

The potential for an increase of post-LOCA hydrogen concentration due to an AWC system was evaluated. The increased hydrogen concentration in the core coolant causes an increase of approximately 0.1% (by Volume) H_2 gas in the drywell for Mark I and III plants. This slight increase however does not result in a post-LOCA hydrogen concentration exceeding 4% (by volume), the lower explosive limit for hydrogen in air. Figure 3-32 shows the buildup of hydrogen in the drywell as a function of time, for normal water.

3.9.11 Crud and Radioactivity Transport and Build-up

The buildup of crud on fuel heat transfer surfaces after and during operation with hydrogen added to the BWR feedwater is an important consideration. A literature search failed to reveal any pertinent information. A trip to the AECL laboratories at Chalk River was made to review data from a boiling

loop that had operated with hydrogen addition. Experimental conditions are given in Table 3-35 and the results in Table 3-36. The crud levels of 10 to 35 ppb in the NRX reactor loop are typical of BWR operations although levels of 100 ppb are common at Brunswick 2.

Fuel crudding rates have been extensively studied for BWR fuel and Figure 3-33 compares the axial shape of the expected BWR values with the distribution shown in Table 3-36. Both cases have been arbitrarily normalized to unity at the bundle inlet. Deposit weights cannot be compared directly because the AECL test (684) ran for only about a month compared to BWR fuel residence times of years. Only relative comparisons of the observed deposits can be made. The 684 test revealed what appears to be a marked Reynolds number dependency and the deposits were distributed relatively more uniformly along the fuel bundle than the General Electric BWR. Undoubtedly the Reynolds number changes contributed to the alternating decrease and then increase in deposition rates within the bundle, probably due to changes in velocity.

A considerable amount of time was taken during the AECL meeting discussing crud morphology. AECL had run the NRX loop with neutral chemistry and with hydrogen added and in both cases reported the fuel crud to be Fe_2O_3. This is also the dominant corrosion product species found on the BWR fuel. The Fe_2O_3 was stable even when the boiling test fuel element was returned to the regular CANDU environment. They were questioned as to their expectation of crud bursts upon start of hydrogen injection into an old plant and no such crud bursts were anticipated, because of the observed stability of the Fe_2O_3 and Fe_3O_4 structures.

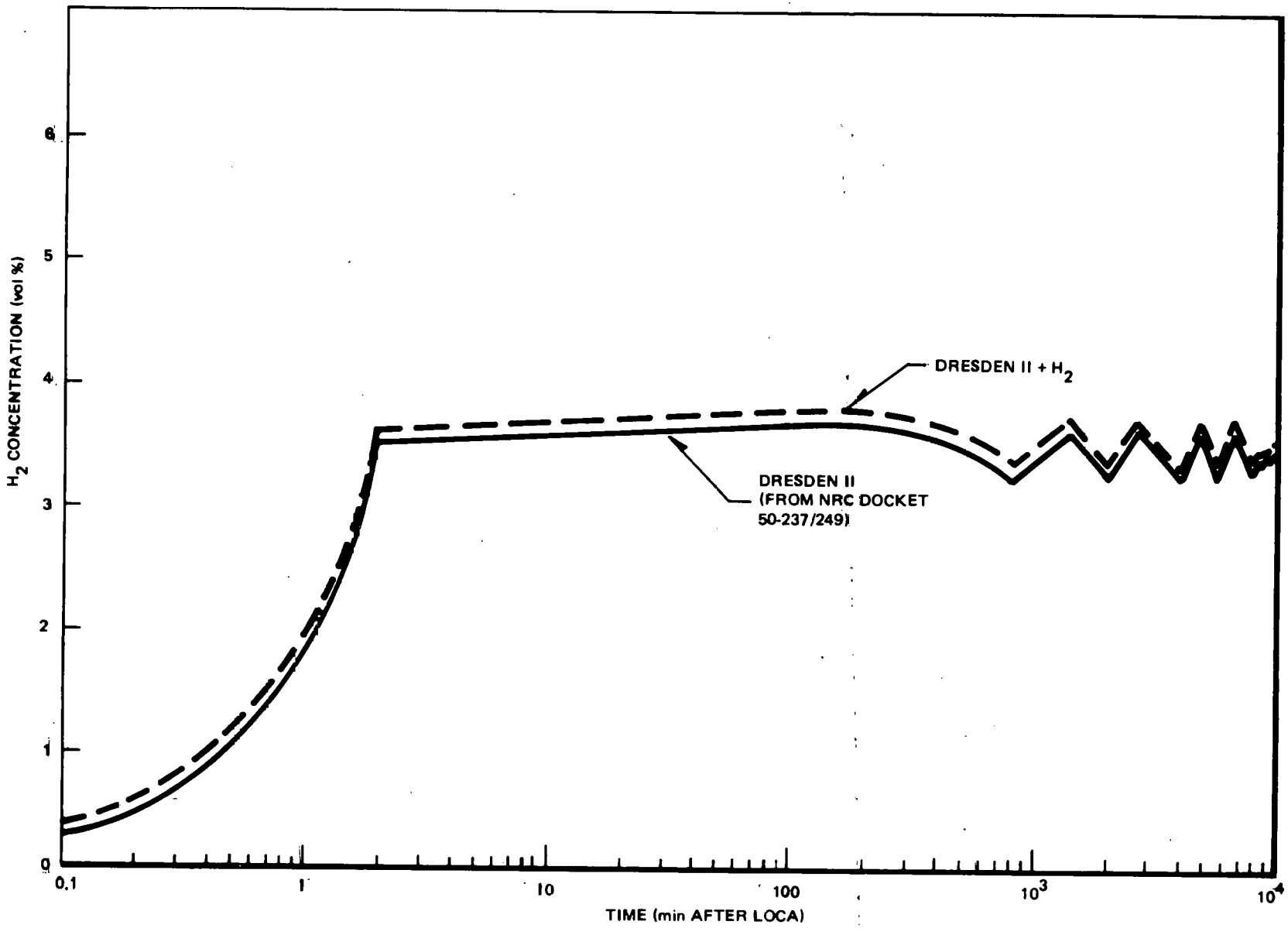

Figure 3-32. Drywell Hydrogen Concentration versus Time After LOCA

Table 3-35

OPERATING CONDITIONS OF NEUTRAL, BOILING WATER LOOP TEST FROM AECL, SEPTEMBER 1978

Exposure Time	44.5 Effective Full Power Days
Water Flow Rate	0.75 kg/s (1.65 lbm/s)
Pressure - Test Section Inlet	7.93 MPa (1,150 psi)
Temperature - At Outlet of Mixing Tee	278°C (532°F)
- Test Section Inlet	288°C (550°F)
- Test Section Outlet	294°C (561°F)
Outlet Steam Quality	11.3 wt%
Water Chemistry - pH	7.3 ±0.3
- Dissolved Hydrogen	>0.5 cm^3/kg
- Crud Level	10 to 35 µg/kg
Neutron Flux - Thermal	7.85×10^{17} n/m^2
- Fast	3.90×10^{17} n/m^2
Fuel String Power - Gross	0.171 MW
- Net (allowing for heat loss to core surroundings)	0.149 MW
Surface Heat Flux, Maximum	1.09 MW/m^2
Average Reynolds Number	1.0×10^5 (in trefoil bundle)
In Fuel String	2.3×10^5 (in single element)

Table 3-36

FUEL DEPOSIT DATA FROM BOILING LOOP TEST

FROM AECL, SEPTEMBER 1978

Bundle		Element	Surface Heat Flux (MW/m^2)	Steam Quality (wt%)	Deposit Weight of Iron (mg/m^2)
Outlet					
	1	1	-	11.3	40
		2	-	11.3	38
		3	-	11.3	40
	2	1	0.65	11.3	420
		2	0.65	11.3	580
		3	0.65	11.3	*
Flow	3	1	0.99	7.9	270
	4	1	1.1	6.6	370
		2	1.1	6.6	330
		3	1.1	6.6	730
	5	1	0.85	1.0	250
	6	1	0.39	0.0	480
		2	0.39	0.0	580
		3	0.39	0.0	590
Inlet					

*Element cut up for examination.

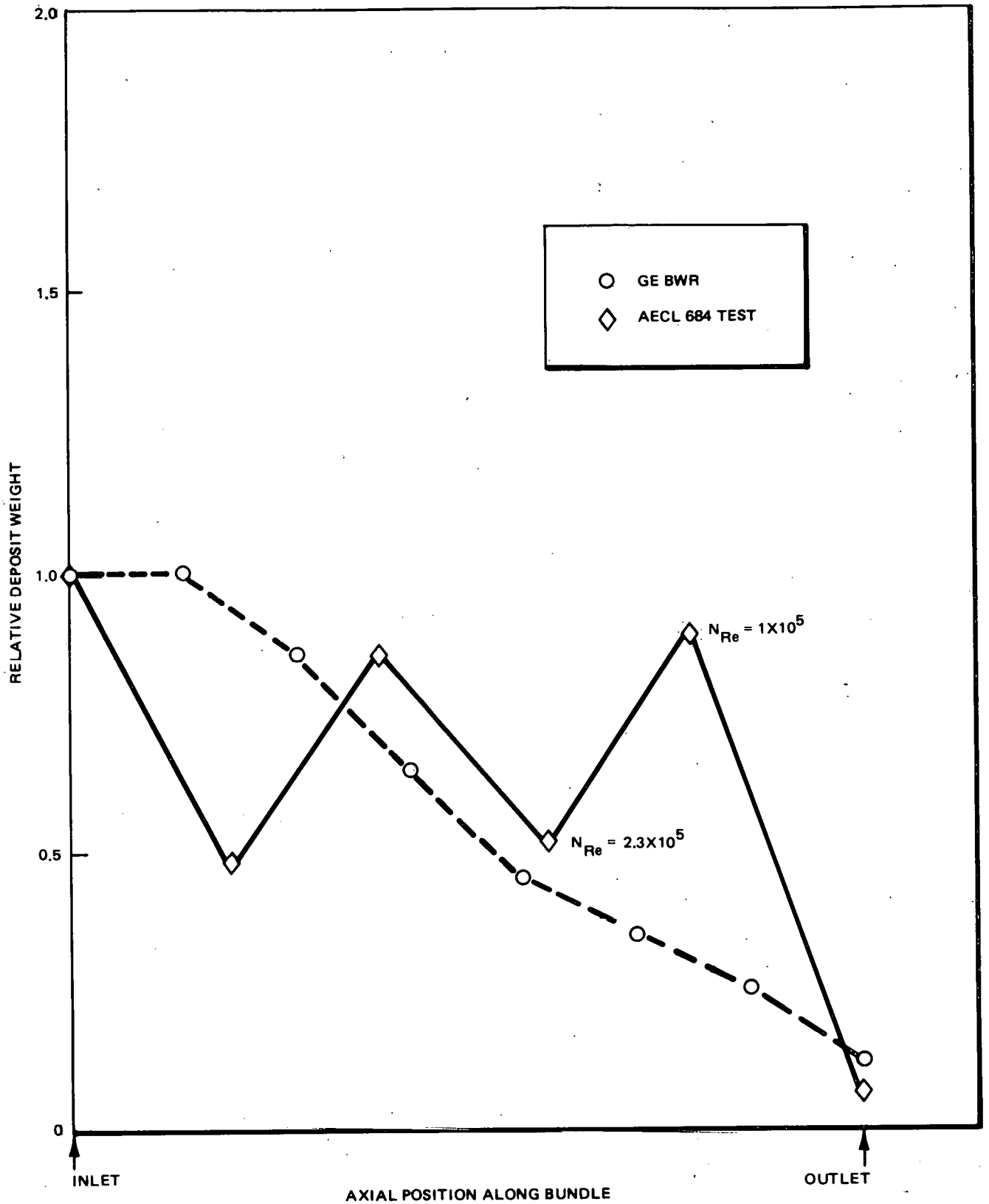

Figure 3-33. BWR Fuel Deposit Deposition

3.10 TASK B-9. ADDITIVE CONSUMPTION AND SOURCE (T. L. Wong)

Objective. Predict the consumption of each additive as a function of required coolant concentration and the consequent increase in plant operating cost from the use of each of the chemicals.

The effort on this task has been to obtain data on costs, recommended form and availability, and to determine whether any hydrogen recycle system should be further considered.

3.10.1 Hydrogen Recycle

The additive cost for hydrogen addition could be reduced by separating the hydrogen form the offgas stream at a location upstream of the recombiner and then recycling the fairly pure hydrogen back to the injection system. Based on available technology, several processes have the capability for separating hydrogen from the offgas. The swing-cycle adsorption process was discussed in a previous quarterly report.[8] Other potential hydrogen[18] separation processes are discussed in the subsequent section.

3.10.2 Membrane Separation Process

The membrane process for separating hydrogen from nitrogen is based upon the relative permeation of gases through a membrane barrier. The membrane separation process is a continuous process which operates at ambient temperature. The process operates with a differential pressure across the membrane. Generally, a membrane unit operates under pressure on one side and at atmospheric pressure on the low pressure side.

Figure 3-34 shows a schematic of a membrane separation unit. The feed gas consisting of nitrogen and hydrogen enters the unit at the high pressure side. The outlet gas from the unit is contained in two streams. One stream is hydrogen rich and the other stream is hydrogen-lean. The concentrations of hydrogen in the two streams are determined by the relative gas permeabilities and the available membrane area.

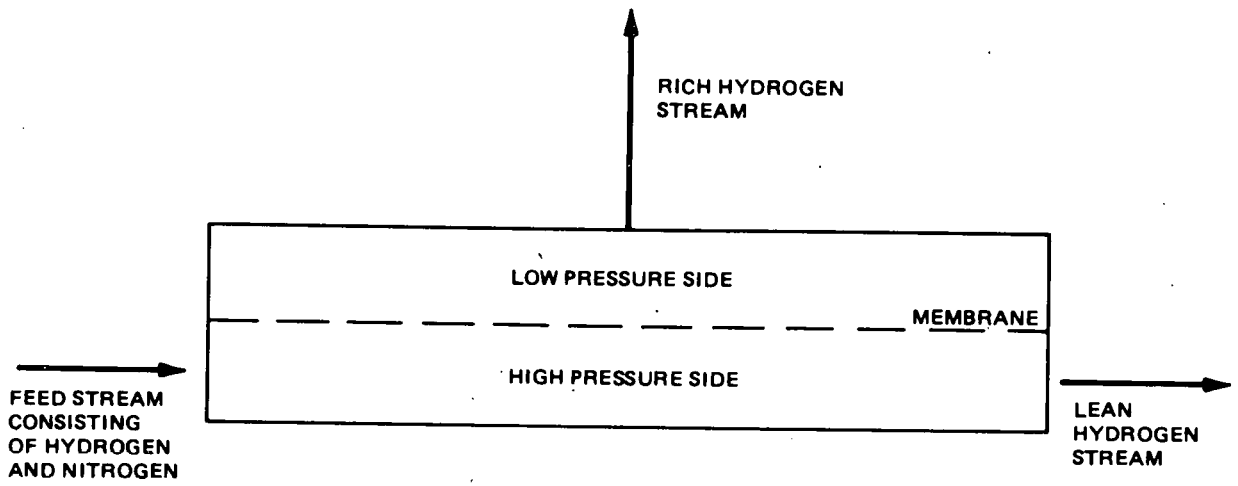

Figure 3-34. Membrane Separation Unit

In general, the large scale application of membrane separation had not materialized until recent years. This occurred after the development of technology for preparing hollow fibers. The utilization of hollow fibers permits the design and construction of membrane units with high effective membrane area to volume ratios and with the capability to withstand substantial pressure differentials.

For large-scale hydrogen separations, several membrane processes[25] exist. The Permasep Process developed by the DuPont Company consists of hollow fibers made of polymeric membrane. The hollow fibers are of the Dacron polyester type, 18 μ i.d. and 32 to 38 μ o.d. A module is constructed of millions of fibers encased in a steel shell rated at design pressure. A module is approximately 18 ft long by 12 in. i.d. A commercial unit has been operated for the recovery of hydrogen from refinery gases.

3.10.3 Metallic Membrane Processes

Other known large-scale hydrogen separation processes are the Union Carbide Hydrogen Purification and the Matthey Bishop Hydrogen Purification processes. These processes use metallic membranes made of palladium alloy. The Union Carbide process operates at a feed pressure of 500 psi and temperatures of 300 to 400°C or higher. Gas impurities such as CH_4, C_2H_6, CO and H_2S may have a deleterious effect on the membrane. Union Carbide operates their process to recover and purify hydrogen from olefins plants by-product fuel gas.

Matthey Bishop manufacturers and markets laboratory- and semi-scale hydrogen purification units made of Ag-Pd (10 to 50% silver) alloy membranes. Small units in the 10 to 50 scfh range are available commercially. Larger units such as a 1500 scfh unit are available only on a custom-made basis.

3.10.4 System Size

Calculations were made to size a hydrogen separation unit for concentrations and flow rates defined in the mass balance flow sheet for the 10 ppb oxygen reactor water case. The calculations were made by assuming that the feed stream is a binary gas mixture consisting of hydrogen and nitrogen. The DuPont hollow fiber gas permeabilities[20] of 165 and 3.1 [(cc) (cm) x 10^{-12}/ (sec) (cm^2) (cmHg)] for hydrogen and nitrogen respectively were used for these calculations. The concentrations of the effluent streams and the total membrane area requirements were estimated with a one-side mixing model. This model assumes plug flow for the feed stream which is introduced to the inside of the hollow fibers and complete mixing for the permeate phase. The mass balance flow sheet estimated with the minimum hydrogen reject concentration is shown Figure 3-35 for the membrane unit. The membrane area requirement for a high pressure side of 1.0 atm and a low pressure side of 0.1 atm was estimated to be 8.9 x 10^6 ft^2.

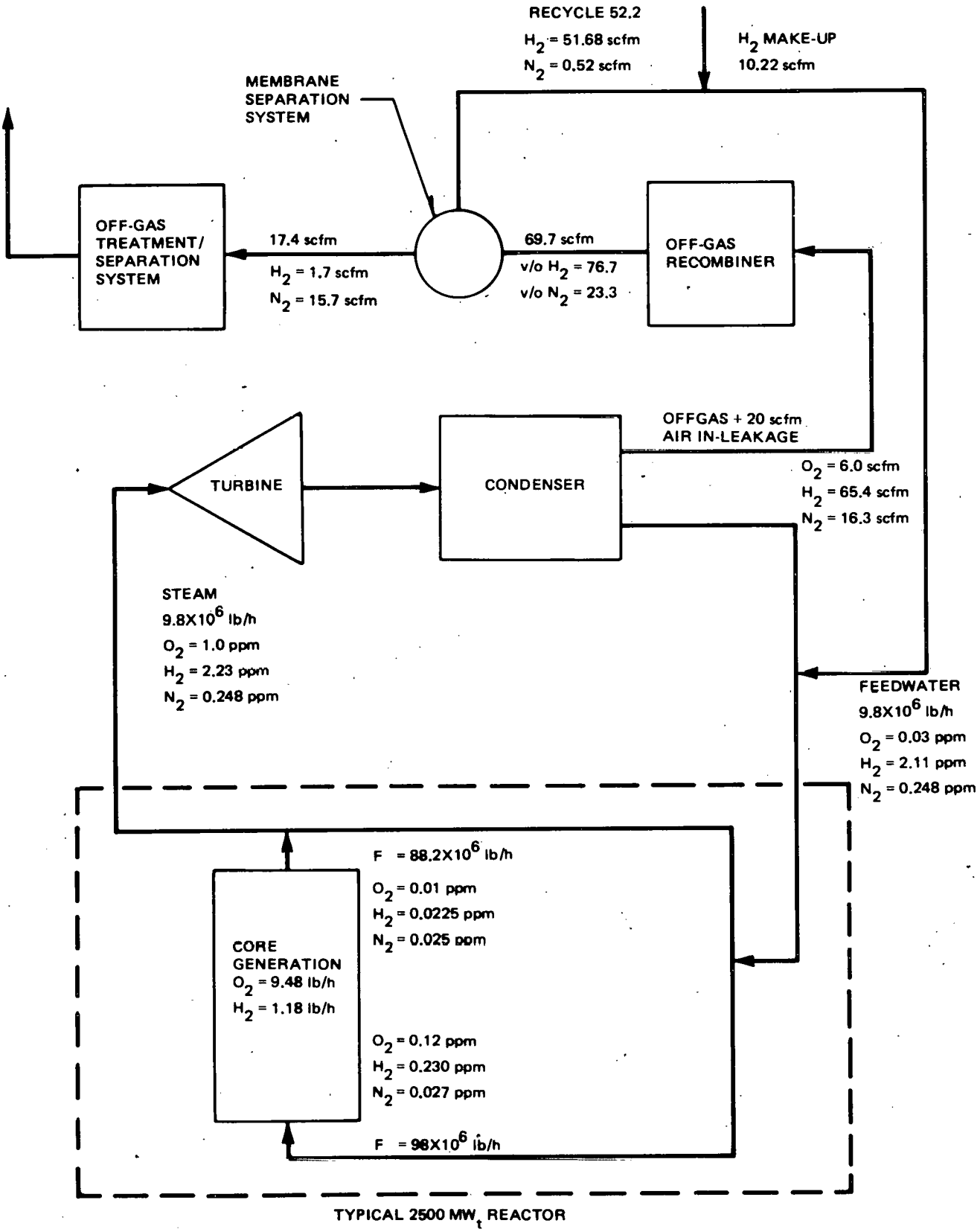

Figure 3-35. Mass Balance Flow Sheet with Hydrogen Separation

3.10.5 Sponge Alloy Separations

The use of metal hydrides for hydrogen storage has been a subject of research and development in recent years. Molycorp, Inc. proposes the use of rare-earth-based materials such as lanthanum-nickel alloys to store hydrogen. These alloys at a given temperature and pressure will adsorb hydrogen deep into their atomic structures to form hydrides. The process is entirely reversible since at a lower pressure, hydrogen will be liberated as a gas. A lanthanum-nickel alloy[26] has the capacity to store approximately 125 cc of hydrogen per gram of alloy at 2 to 3 atm of pressure and 0°C. Heat dissipation at the rate of approximately 13,000 Btu per lb mole of hydrogen adsorbed must be provided in the design of this type of hydrogen purification process. Based on available information large scale application of this process has not yet materialized.

4. REFERENCES

1. E. L. Burley "Oxygen Suppression in Boiling Water Reactors - Quarterly Report No. 2" October 1978, NEDC-23856-1.

2. E. L. Burley "Oxygen Suppression in Boiling Water Reactors - Quarterly Report No. 1", August 1978, NEDC-23856.

3. T. Mizuno, T. Kurosawa and M. Miyakawa, "Possibility of Reduction of Dissolved Oxygen with N_2H_4", unpublished paper.

4. Unpublished Communication, Roland Ivars of ASEA-ATOM to E. L. Burley (8/28/78)

5. D. R. Rogers "BWR Turbine Equipment N-16 Radiation Shielding Studies" General Electric Co. NEDO-20206.

6. Breden, C. R., "Boiling Water Reactor Technology Status of the Art Report. Volume II, Water Chemistry and Corrosion", ANL-6502 (Feb., 1963).

7. Whitham, G. K. and R. R. Smith, "Water Chemistry in a Direct-Cycle Boiling Water Reactor", Proc. of 2nd U.N. International Conference, Peaceful Uses of Atomic Energy, 7, 430-444 (1958).

8. Mihl, R. L. and M. H. Theys, "Radioactivity Buildup - N-16 Concentration in EBWR", Nucleonics, 19, 81-83 (1961).

9. Hammer, L., et. al., "Water Chemistry Research at the Halden Boiling Heavy Water Reactor (HPWR)", HPR-55 (June, 1958).

10. Carlson, F., "Experiment R2-5519, Radiochemical Studies Concerning the Cooling Medium Under BWR Conditions", Report AE-MK-592 (1972).

11. Stenström, T., "On the Chemical Fate of Nascent ^{11}C Atoms Introduced by Irradiation of Water and Aqueous Solutions with 185 MeV Protons", Ph.D. Thesis, Gustaf Werner Institute, Univ. of Uppsala, Uppsala, Sweden, 1970.

12. The chemical fate of C-15 and C-14 is expected to be identical to that observed by Stenstrom for C-11.

13. Kolba, V., "EBWR Test Reports", ANL-6229 (Nov., 1960).

14. Bromberg, S. J. and C. E. Kent, "Boiling Water Reactor Process Environment", NEDE-12577, Class III, Sept., 1975.

15. Kunz, C. O., W. E. Mohoney, and T. W. Miller, "Carbon-14 Gaseous Effluents from Boiling Water Reactors," ANS Transactions 21, 91 (1975).

16. Cobble, J. W., "Chemical Thermodynamic Studies of Aqueous Trace Components in Light Water Reactors at High Temperature and Pressure, Part 1", Three Year Summary, EPRI Contract No. RP 311-2; San Diego State Univ. Foundation, March 15, 1978.

17. Sweeton, F. H., R. E. Mesmer, and C. F. Baes Jr., "Acidity Measurements at Elevated Temperatures, VII Dissociation of Water", J. Soln. Chem., 3, 191 (1974).

18. E. L. Burley, "Oxygen Suppression In Boiling Water Reactors - Quarterly Report No. 3" March 1979 NEDC-23856-2.

19. Letter, S. G. Sawochka and D. T. Synder to W. L. Pearl, September 17, 1968.

20. Wang, K. B. and Fan, L. T. Chemical Engineering Science. (1978) 33, pp. 945-952.

21. Houghton, G., et. al. Chemical Engineering Science. (1957) 7, pp. 26-29.

22. Reed, R. C. and Sherwood, T. K. Properties of Gases and Liquids, 2nd Ed., McGraw-Hill. 1966, pp. 18-20, 382, 520-556, 571.

23. Nyberg, Paul. Private Communication, August 23, 1978.

24. Presberry, C. Solubility of Ideal Gases in Water, Y1002E101, BWR Chemical Technology Handbook. General Electric Co., 1977.

25. Hwang, S. T. and Kammermeyer, K., "Membranes in Separations", Techniques of Chemistry, Vol. VII, John Wiley & Sons (1975).

26. Molycorp Bulletin - Overview 45, Hydrogen Energy Storage, Molycorp, Inc., 6 Corporate Park Drive, White Plains, N.Y.

Appendix A

EQUIPMENT LIST — HYDROGEN INJECTION SYSTEM

Equipment	Size	Design Temperature/ Pressure	Material	Other Requirements
Flow control valve	6x8	300°F / 2000 psig	Carbon Steel (CS)	Motor operated 900# ANSI
Gate valve	6 in.	300 / 2000	CS	Motor operated No. of valves - 2
Pump and Driver		300 / 2000	CS	Water flow rate - 2175 gpm Inlet pressure - 1218 psig TDH - 406 ft. of water at design conditions
Orifice plate	6 in.	300 / 2000	316 Stainless Steel (SS)	Diameter orifice / Diameter pipe = 0.85
Mixing units	12 in.	300 / 2000	CS	Type - Koch LY No. of units - 14
Piping	6 in.	300 / 2000	CS	Schedule 120 No. of feet - 27
	12 in.	300 / 2000	CS	Schedule 120 No. of feet - 40
HYDROGEN SYSTEM				
Flow control valve	1/2 in.	70 / 3000	316 SS	Air operated
Gate valve	1/2 in.	70 / 3000	316 SS	1 Air operated valve 2 Manual valves
Check valve	1/2 in.	70 / 3000	316 SS	
Piping	1/2 in.	70 / 3000	316 SS	Schedule 80S No. of feet - 1200

Appendix B
SAMPLE CALCULATIONS

The following is a listing of the various computations that were performed in the course of the design of the hydrogen injection system. The actual calculations were programmed into and completed on a Texas Instruments, Inc. TI-59, Programmable Calculator. Program listings are available on request.

Physical Properties of Hydrogen and Water

1. Density of Hydrogen at T = 300°F; P = 1200 psig

$$\rho = 0.285 \text{ lb/ft}^3 \qquad \text{(Reference B-1)}$$

2. Density of Water at T = 300°F; P = 1200 psig

$$\rho = 57.31 \text{ lb/ft}^3 \qquad \text{(Reference B-2, Appendix 14)}$$

3. Viscosity of water at T = 300°F; P = 1200 psig

$$\mu = 0.185 \text{ cp} \qquad \text{(Reference B-2, Appendix 14)}$$

Calculation of Hydrogen-Water Diffusion Coefficient

1. For gas dissolved in a liquid

$$\frac{D_{ij} \times \mu_1}{T_{abs}} = \text{constant} \qquad \text{(Reference B-3)}$$

2. Diffusion of hydrogen into an aqueous solution at infinite dilution at T = 25°C; P = 1 atm.

$$D_{ij} = 4.8 \times 10^{-5} \text{ cm}^2/\text{sec} \qquad \text{(Reference B-4, experimental)}$$

3. μ_1 at 25°C = 0.9147 cp (Reference B-5)

4. Evaluation of the "constant"

$$\text{constant} = 4.8\text{x}10^{-5} \text{ x } 0.9147\text{x}10^{-2} / 298$$

$$= 1.473\text{x}10^{9} \text{ gm-cm/sec}^2\text{-°K}$$

5. Diffusion coefficient at T = 300°F; p = 1200 psig

$$D_{ij} = \text{constant x Tabs} / \mu_1$$

$$\mu_1 = 0.185\text{x}10^{-2} \text{ gm/cm-sec} \quad \text{(Reference B-2, Appendix 14)}$$

$$\rightarrow D_{ij} = 1.473\text{x}10^{-9} \text{ x } 422 / 0.185\text{x}10^{-2}$$

$$= 3.36\text{x}10^{-4} \text{ cm}^2/\text{sec}$$

Calculation of Length of Mixing Section for a Given Amount of Absorption

1. Design parameters

a. 23% of gas absorbed

b. Initial hydrogen flow is 30 lb/hr

c. Pipe: 12-in. Schedule 120, i.d. = 10.75 in.

d. $\rho_{H_2} = 0.285 \text{ lb/ft}^3$

e. $\rho_{H_2O} = 57.3 \text{ lb/ft}^3$

f. P = 92.5 atm

2. Calculation of Q

$$Q = 0.23 \times 30 / 60 \times 2 = 0.0575 \text{ lb mol/min}$$

3. Calculation of A

$$A = (10.75/12)^2 \times \pi / 4 = 0.6303 \text{ ft}^3$$

4. Calculation of $\bar{x}$

a. $x^* = P/H = 92.5/4.9\times10^4 = 1.888\times10^{-3}$

b. $X_i = 0$

c. $x_f = 30 \times 0.23 \times 18 / 9.77\times10^5 \times 2 = 6.356\times10^{-5}$

d. $$\bar{x} = \frac{(1.888\times10^{-3} - 0) - (1.888\times10^{-3} - 6.356\times10^{-5})}{\ln(1.888\times10^{3}/1.888\times10^{-3} - 6.356\times10^{-5})} = 1.856\times10^{-3}$$

5. Calculation of K_La

a. $V_{gas} = (30 - (30 \times 0.23))/60 \times 0.285 \times 0.6303$

$= 2.1 \text{ ACFM/ft}^2$

b. K_La for O_2-H_2O = 7.5 (Figure 3-28 of main report)

c. $$K_La \text{ for } H_2\text{-}H_2O = K_La_{(O_2\text{-}H_2O)} \times \frac{D_{(H_2\text{-}H_2O)}}{D_{(O_2\text{-}H_2O)}}$$

$$= 7.5 \times \frac{3.36\times10^{-4}}{2.51\times10^{-5}}$$

$$= 100.5$$

6. Calculation of Length, $L = Q/K_L a A \bar{x}$

$$L = 0.0575/100.5 \times 0.6303 \times 1.856\times10^{-3}$$

$$= 0.488 \text{ ft}$$

Generation of Hydrogen Absorption Curve for Koch Static Mixers

1. Determine value of constant from L = 0.488 ft for 23% absorption

$$C = L/\ln(1 - abs) = 0.488/\ln(1 - 0.23) = 1.8$$

2. Computation of hydrogen adsorption curve

$$L = C \ln(1 - abs)$$

Table B-1 summarizes the results for L versus various values for abs.

Calculation of Pressure Drop Through Hydrogen Injection Side Stream Loop

1. ΔP for entrance and exit piping

$$\Delta P/L = 0.00000336 \times \frac{f \times W^2}{d^5 \times \rho} \text{ (Reference B-6, p. 3-2)}$$

$$\Delta P/L \text{ (6 in. Schedule 120)} = 3.36\times10^{-6} \times \frac{0.0165 \times (9.77\times10^5)^2}{5037 \times 57.3}$$

$$= 0.1833 \text{ psi/ft}$$

$$\Delta P/L \text{ (12-in. Schedule 120)} = 0.00546 \text{ psi/ft}$$

Table B-1

MIXING LENGTH VERSUS HYDROGEN ABSORPTION

Abs	L (ft)
0.02	0.0036
0.04	0.073
0.06	0.111
0.08	0.15
0.1	0.19
0.12	0.23
0.14	0.27
0.16	0.31
0.18	0.36
0.2	0.41
0.3	0.64
0.4	0.92
0.5	1.25
0.6	1.65
0.7	2.17
0.8	2.9
0.9	4.1
0.99	8.3
0.999	12.
0.9995	14.

2. ΔP for 90° long radius elbows

$$\Delta P = 0.00000028 \times \frac{K \times W^2}{d^4 \times \rho}$$ (Reference B-6, p 3-4)

but $K = f\ L/D$

and $L/D = 20$ (Reference B-6, p. A-30)

so

$$\Delta P = 2.8 \times 10^{-7} \times 20 \times f \times W^2/d^4 \times \rho$$

$$\Delta P\ (6") = 2.8 \times 10^{-7} \times 20 \times \frac{0.0165 \times (9.77 \times 10^5)^2}{915.7 \times 57.3}$$

$$= 1.68 \text{ psi}$$

$$\Delta P\ (12") = 0.0978 \text{ psi}$$

3. ΔP for gate valves

with L/D = 13 (Reference B-6, p. A-30)

$$\Delta P = 2.8 \times 10^{-7} \times 13 \times f \times W^2/d^4 \times \rho$$

$$= 1.09 \text{ psi (ft 6-in. valve)}$$

4. ΔP for entrance and exit effects

with K = 0.04 for well-rounded entrance and
K = 1.00 for well-rounded exit (Reference B-6, p. A-26)

$$\Delta P = 2.8 \times 10^{-7} \times 1.04 \times W^2/d^4 \times \rho$$

$$= 5.30 \text{ psi (for 6-in. Schedule 120 pipe)}$$

5. ΔP for expansion and contraction effects

with K = 0.545 for a 6"x12" expansion and
K = 0.33 for a 6"x12" contraction (Reference B-6, p. A-26)

$$\Delta P = 2.8 \times 10^{-7} \times 0.875 \times W^2/d^4 \times \rho$$

$$= 4.46 \text{ psi}$$

6. ΔP for flow measuring orifice

$$\Delta P = (W/1891 \times d_o^2 \times C)^2 \times 1/\rho$$ (Reference B-6, p. 3-5)

with d_o = 4.676", d_o/d_1 = 4.676/5.501 = 0.85

and C = 0.83 (Reference B-6, p. A-20)

$$\Delta P = (9.77 \times 10^5 / 1891 \times 4.676^2 \times 0.83)^2 / 57.3$$

$$= 14.1 \text{ psi}$$

but actual pressure drop is 34% of this value (Reference B-7, p. 12)

$\Delta P = 14.1 \times 0.34 = 4.8$ psi

7. ΔP for mixing section

$$\Delta P/L = 3.6 \times 10^{-5} \times f \times \rho \times v^2/d_H \quad \text{(Reference B-8)}$$

$$= 3.6 \times 10^{-5} \times 0.19 \times 57.3 \times 94.96^2/1.19$$

$$= 2.97 \text{ psi/ft}$$

The above pressure drops are summarized in the following table.

Table B-2

SYSTEM PRESSURE DROPS

	Entrance Piping	Mixing Section	Exit Piping
Empty Pipe	(15 ft) 2.75	(26 ft) 0.14	(12 ft) 2.20
Elbows (2/sect)	3.36	0.20	3.36
Gate Valve	1.09		1.09
Ent/Exit Effects	5.30 total		
Mixing Section		(14 ft) 41.58	
Exp/Contr. Effects	4.46 total		
Orifice plate			4.80
Flow Control Valve	25 allowed		
Total by Section	41.96	41.92	11.45
Total Pressure Drop	95.33 psi		

Calculation of Side Stream Pump Size

1. Water horsepower

$$P_{wat} = Q \times P/1714 \qquad \text{(Reference B-6, p. B-9)}$$

$$= 2126 \times 162/1714$$

$$= 201 \text{ hp}$$

2. Brake horsepower

$$BHP = P_{wat}/\text{efficiency}$$

$$= 201/0.6$$

$$= 335 \text{ hp}$$

References - Appendix B

B-1. Properties of Principal Cryogenics, 3rd. Part., 1966, pp. 111-2.

B-2. McCabe, W. L. and Smith, J. C. Unit Operations of Chemical Engineering, 3rd Ed., McGraw-Hill. 1976, pp. 732, 697.

B-3. McCarty, T. D. Hydrogen Technological Survey - Thermophysical Properties. NASA SP-3089, 1975, pp. 102-103.

B-4. Reed, R. C. and Sherwood, T. K. Properties of Gases and Liquids, 2nd Ed., McGraw-Hill. 1966, pp. 18-20, 382, 520-556, 571.

B-5. Bird, R. B., Stweard, W. E., and Lightfoot, E. N. Transport Phenomena. John Wiley & Sons. 1970, pp. 8.

B-6. Crane Technical Paper No. 410, 1969.

B-7. American Society of Mechanical Engineers, Power Test Code, 19.5; 4-1959. Flow Measurement - Part 5, Measurement of Quantity of Materials.

B-8. Pluess, R. C. Pressure Drop Calculations on Koch Static Mixing Units, Revision 1. Koch Engineering Co. 1977.

GENERAL ELECTRIC